Spring 5-2016

Temporally and spatially resolved quantification of hemodynamic forces and endothelial mechanics

Lori M. Lambert
University of Nebraska-Lincoln, lorimaylambert@gmail.com

TEMPORALLY AND SPATIALLY RESOLVED QUANTIFICATION OF HEMODYNAMIC FORCES AND ENDOTHELIAL MECHANICS

by

Lori M. Lambert

A DISSERTATION

Presented to the Faculty of

The Graduate College at the University of Nebraska

In Partial Fulfillment of Requirements

For the Degree of Doctor of Philosophy

Major: Mechanical Engineering & Applied Mechanics

(Fluid Mechanics)

Under the Supervision of Professor Timothy Wei

Lincoln, Nebraska

May, 2016

TEMPORALLY AND SPATIALLY RESOLVED QUANTIFICATION OF HEMODYNAMIC FORCES AND ENDOTHELIAL MECHANICS

Lori M. Lambert, Ph.D.

University of Nebraska, 2016

Adviser: Timothy Wei

The endothelium is a thin layer of endothelial cells that line the interior surface of an artery. Due to their direct contact with blood flow, endothelial cells experience varying hemodynamic forces and respond to these forces by altering their morphology. When plaque and other substances accumulate in the walls of arteries, *i.e.*, atherosclerosis, endothelial cells have abnormal responses to blood flow. Studying atherosclerosis progression is, therefore, a two-fold investigation into 1) the hemodynamic forces that cause endothelial responses, and 2) the biological and mechanical responses of endothelial cells. The ultimate goal of this study was to develop an experimental method that was able to temporally and spatially quantify hemodynamic forces and endothelial mechanics.

The current study cultured bovine aortic endothelial cell monolayers in microchannels and used micro-particle tracking velocimetry (μPTV) techniques and fluid mechanics principles to quantify fluid forces and cell morphology for monolayers subjected to steady shear rates of 5, 10 and 20 dyne/cm^2. Cell topography, shear stress, and pressure distributions were calculated from sets of velocity fields made in planes parallel to the microchannel wall. For each experiment, measurements were made in three-hour intervals for 18 hours. Endothelial cell conditions varied between normal and necrotic and the cell culture surface varied between untreated glass and fibronectin-

coated glass. This study demonstrated the ability to make *in-situ* quantifications of fluid forces and endothelial mechanics using μPTV techniques and fluid mechanics principles. It was found that there is a three-dimensional change in cell morphology as a result of applied shear stress. In addition, cell morphology is directly related to local variations in fluid loading, *i.e.*, shear stress and pressure.

ACKNOWLEDGEMENTS

First and foremost, I would like to thank my parents who have encouraged me since I first stepped foot into a classroom. My academic career would not have been possible without their continual inspiration and unyielding support. I am incredibly grateful for the sacrifices they have made over the years so I can pursue my dreams. They are truly my heroes.

I would also like to thank my adviser, Dr. Timothy Wei, for not only graciously giving me the opportunity to pursue my doctorate but for inspiring and encouraging me to reach my potential as an engineer. It was truly a blessing to have an advisor that I could call my friend. I will forever be grateful for his mentorship and friendship throughout my graduate career.

I would also like to acknowledge my doctoral committee members, Dr. Linxia Gu, Dr. George Karniadakis, Dr. Iraklis Pipinos, and Dr. Sangjin Ryu, for their invaluable insight and helpful suggestions during my doctoral research and the writing of this dissertation.

I would like to thank my labmate, Erica, and my UNMC collaborators, Derek and Nick, for their support, assistance, and insight while processing data and conducting experiments. This research would not have been possible without the generous assistance and equipment provided by the many collaborators at UNMC.

I would also like to thank my sisters, Kimberly and Valerie, and all of my friends and family for their support. When research was difficult, I was grateful to have their enthusiasm, encouragement, and cheerfulness.

Last but certainly not least, I would like to thank my husband, Andy, whom which I am forever grateful for his positivity, encouragement, and reassurance during my time in graduate school. I would not have made it through the late-nights of data processing and 24-hour experiments without his unconditional love and support.

CONTENTS

LIST OF TABLES

LIST OF FIGURES

CHAPTER 1

INTRODUCTION

The main purpose of the cardiovascular system is to supply nutrients and blood to different regions of the body. The heart, which acts as the pump for the cardiovascular system, is connected to the rest of the body through a complex network of blood vessels including capillaries, veins, and arteries. The arteries dilate and contract while blood is pumped through them to accommodate to the varying hemodynamic conditions (*i.e.* blood flow and pressure).

Cardiovascular diseases (CVD) affect over 84 million people in the United States and abnormal blood flow in arteries has been associated with these diseases [1]. The hemodynamics related to both healthy and diseased arterial conditions is of high importance when studying CVD due to this association. The subsequent sections discuss the hemodynamics related to both healthy and diseased arteries. The role the arterial wall, and specifically endothelial cells, play in the development of CVD will be described. In addition, previous studies investigating the hemodynamic forces on endothelial cells will be detailed as well as the objectives for this study.

1.1 Healthy arterial function and background

The nature of the heart is to pump blood throughout the body in a cyclic pattern which creates pulsatile flow conditions within the arteries. In this regard, blood flow and pressure conditions within arteries are unsteady by nature. During a cardiac cycle, the heart contracts and drives blood out of the heart during systole and then refills with blood during diastole. Due to the contraction and relaxation of systole and diastole,

respectively, blood pressure is at its maximum during systole and at its minimum during diastole. In contrast, blood flow can vary depending on the distal resistance of arteries. In other words, the blood flow and pressure in arteries, although pulsatile, may exhibit different flow properties throughout the arterial network.

1.1.1 Steady flow

While blood flow through arteries is unsteady by nature, numerous, computational, theoretical, and experimental investigations still utilize steady flow conditions for simplicity. For steady flow investigations, fully-developed, laminar flow through a rigid blood vessel is generally assumed. The volumetric flow rate, Q, from Poiseuille's equation is,

$$Q = \frac{\pi d^4 \Delta P}{128 \mu L} \tag{1.1}$$

where d is the blood vessel diameter, ΔP is the pressure drop across the length of the blood vessel, L, and μ is the dynamic viscosity of blood through the vessel.

In order to assume Poiseuille flow for arterial circulation applications, a few hemodynamic conditions have to be taken into account. Specifically, for the Poiseuille equation, the fluid's viscosity must be considered constant across all physiologic shear rates. While blood is a complex fluid, consisting of a 40% by volume suspension of red blood cells, previous literature has shown that blood behaves as a Newtonian fluid in blood vessels in which the diameter of the lumen of the vessel is large compared to the diameter of the red blood cells [2]. Therefore, in this study, blood can be considered to have homogenous properties including a viscosity that acts independently of the velocity gradient. However, blood has been shown to behave like a non-Newtonian fluid when the

lumen of the vessel is less than 0.5 mm, *e.g.* flow within capillaries, and this behavior is most common at low shear rates in which red blood cells tend to cluster into larger particles. Where the Newtonian flow assumption is valid, the viscosity of blood is approximately 4 centipoise (cP), or 4×10^{-3} Pa·s.

In addition to viscosity considerations, blood flow has to be steady when assuming steady Poiseuille flow. If the flow is subject to any acceleration or deceleration and the pressure gradient is used to transfer kinetic energy to the blood, Poiseuille flow cannot be assumed for the flow application.

1.2 Atherosclerosis background and diseased arterial function

Atherosclerosis is a subset of cardiovascular diseases that are responsible for over 26,000 deaths in the United States each year [3]. The word "atherosclerosis" originates from the Greek word "athero" meaning groats and "sclerosis" meaning hardening [4]. This reflects the fact that atherosclerosis is a progressive disease in which cholesterol, fat, and other substances accumulate in the walls of arteries. This accumulation results in hardening of the arterial wall and constriction of the flow passage.

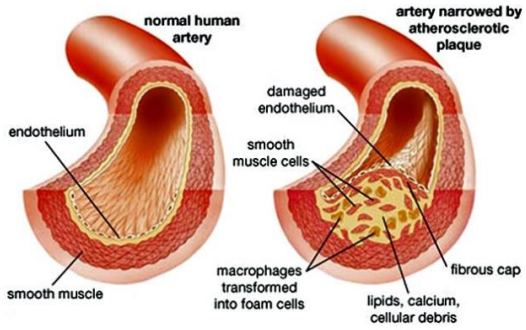

Figure 1.1: Illustration of a healthy, normal artery (left) and an atherosclerotic artery (right). The plaque and debris that collects underneath the endothelium causes the lumen of the atherosclerotic artery to narrow [5].

The accumulation of plaque and fatty deposit can significantly reduce blood flow in an artery. In addition, plaques that are unstable can rupture and cause blood clots that may block blood flow to other areas of the body. If plaque causes blockage in arteries that pump blood to the heart, a heart attack can occur. Also, arteries leading to the brain and legs that have blockage of blood flow can result in stroke or difficulties walking, respectively.

Atherosclerosis typically occurs in the carotid artery, femoral artery, coronary arteries, and the abdominal aorta [6]. These vessels have complex geometries that include bends and bifurcations, areas that have been associated with low mean wall shear stress. This is consistent with the findings of several studies demonstrating that atherosclerosis has a strong preference to arterial regions experiencing low shear stress [7-9]. Furthermore, areas of low shear stress also coincide with areas of high low-density lipoprotein (LDL) concentrations [9-14]. LDL is a glycoprotein that transports lipids (*i.e.* cholesterol) within blood vessels. Specifically, cholesterol-carrying LDL can transmigrate the endothelial layer as a result of endothelial layer disruption and the content within LDL can become oxidized leading to plaque growth in the arterial wall [8, 15, 16]. It is hypothesized that endothelium disruption is caused by a change in an endothelial cell's shape as it is subjected to different shear stresses, and the relationship between cell shape and shear stress can affect the localization of LDL transmigration, and therefore, atherosclerosis.

There are several procedures that exist to treat atherosclerosis. One minimally invasive procedure involves inserting a vascular stent at the atherosclerotic site during angioplasty. This procedure involves collapsing a vascular stent and inserting it over a

deflated balloon-tipped catheter so that it can be moved through the artery to the blockage site. The balloon is then inflated so that the stent expands into a scaffold that keeps the lumen of the artery open to allow blood flow. A more invasive surgery would involve bypass surgery in which blood flow is rerouted around the diseased site using a bypass graft to improve blood flow. The graft can be a vein or artery transplanted from another part of the body or may consist of a synthetic material like Dacron (PET) or polytetrafluoroethylene (PTFE) [17].

Despite these advancements in treatments, problems still exist. In stent procedures, restenosis can occur in which there is a reoccurrence of the vessel narrowing. In an effort to solve this problem, drug-eluting stents have been introduced in the artery. Despite efforts, angiographic restenosis occurred in 57% of stent patients after 6 months according to a study [18]. For bypass surgeries, there is a major concern with graft patency which is the chance a graft will remain open. Vascular grafts that have a diameter less than 6 mm have less than a 30% patency rate after 5 years [19]. In addition, hemodynamic conditions, like intimal hyperplasia, can develop after introducing a bypass graft.

Intimal hyperplasia is the abnormal proliferation of smooth muscle cells, or the intimal layer of the arterial wall, and is a CVD that results from post-surgical complications. Intimal hyperplasia leads to thickening of the intimal layer which causes the vessel to narrow. Also, regions of low shear stress have been associated with the development of intimal hyperplasia [20]. Studies have found that the average wall shear stress linked to intimal hyperplasia is less than 10 dyne/cm^2 compared to the normal wall

shear stress that ranges from 15 to 20 dyne/cm^2 for arteries considering several species [21-22].

Cardiovascular diseases, like atherosclerosis and intimal hyperplasia, are studied at several different scales. At the macro-scale level, CVD risk factors like smoking, diabetes, high levels of cholesterol, and high blood pressure are investigated; while at the meso-scale, complex structural attributes of arteries like bifurcations are linked to varying hemodynamic conditions. At the cellular and sub-cellular levels, the biological response of the cellular components of arterial walls, like endothelial cells, to CVD conditions are of highest interest. This dissertation focuses on the genesis of CVD on the cellular and sub-cellular levels.

1.3 Endothelium

The artery wall can be divided into three main layers: intima, media, and adventitia. Figure 1.2 shows the location of these layers. The intima is the layer closest to the lumen of the artery, the media is the middle layer, and the adventitia is the outermost layer of the artery. The intima, or tunica intima, consists of an endothelial cell layer which is surrounded by a "basement membrane" and the internal elastic lamina. The media, also referred to as the tunica media, consists of a layer of smooth muscle cells surround by the external elastic lamina. The adventitia, also referred to as the tunica externa, consists of collagens, fibroblasts, nerve cells, and elastin fibrils. The effects of atherosclerosis can be seen mainly in the intima of the arterial wall, or the layer in most direct contact with blood flow [23].

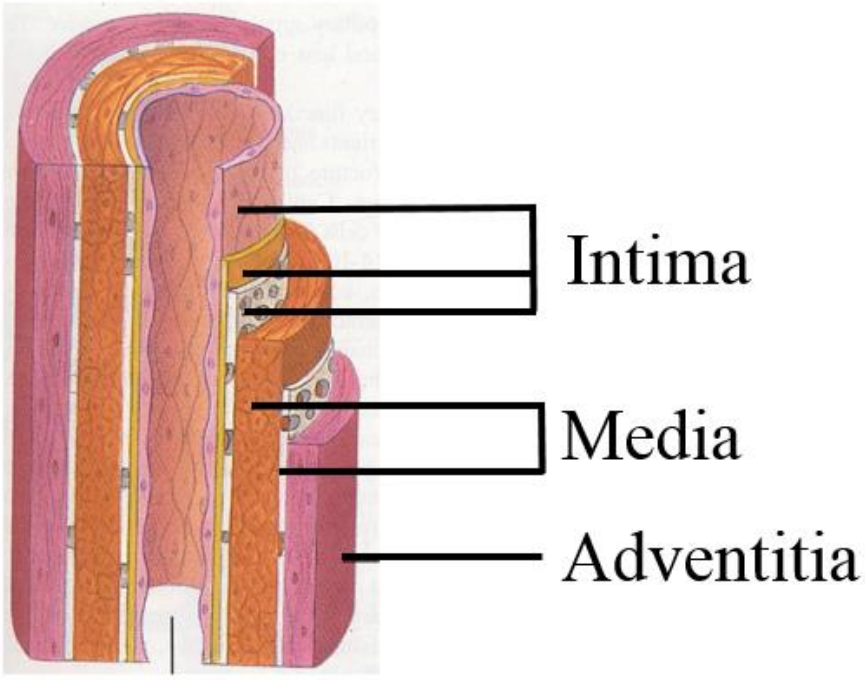

Figure 1.2: Illustration showing an arterial wall and the three main layers: intima, media, and adventitia [24].

The endothelial cells of the intima layer experience three main hemodynamic forces resulting from blood flow as shown in Figure 1.3. Hydrostatic pressure due to blood pressure in the artery acts normal to the cell surface, shear stress created by frictional forces due to viscous blood flow acts tangent to the cell surface, and dilation and constriction of the arterial wall cause circumferential tension and stretch. Each of these forces can cause a biological response in endothelial cells, like gene or protein expression. This process is called mechanotransduction and will be discussed in greater detail in the subsequent sections.

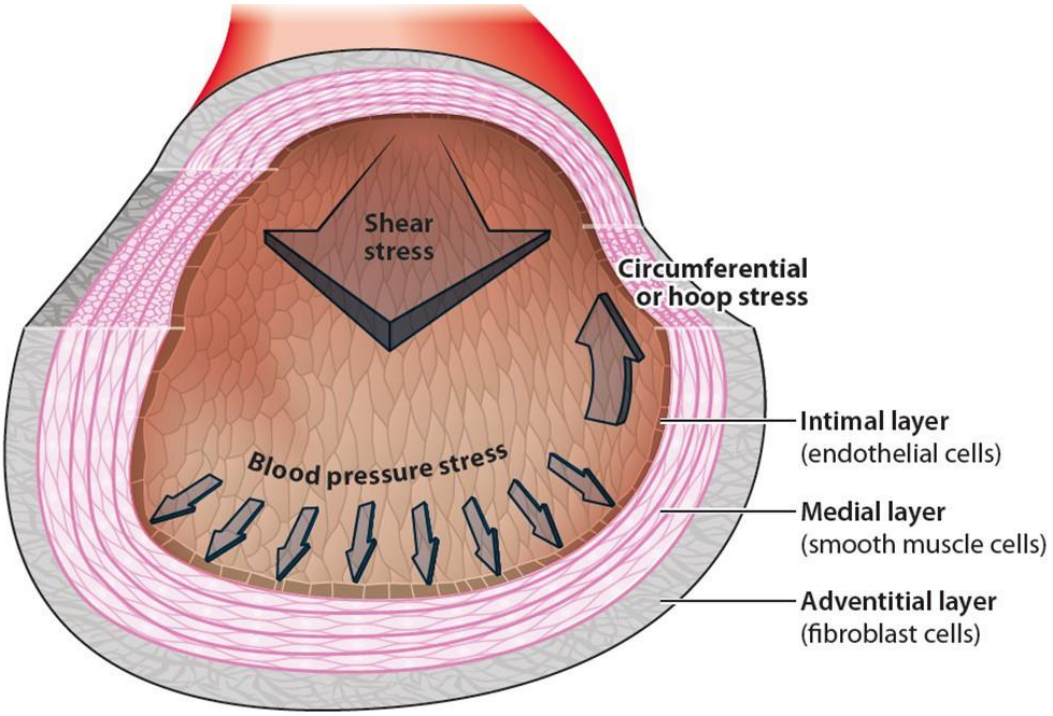

Figure 1.3: Illustration showing shear stress acting tangent to endothelial cells and blood pressure acting normal to endothelial cells. The three different layers of the arterial wall are also shown [23].

1.3.1 Quantifying hemodynamics

The heart acts like a fluid pump and helps distribute blood and nutrients to all parts of the cardiovascular system. Due to the unsteady nature of arterial flows, the endothelial cells that line the lumen of an artery experience temporally and spatially varying forces including pressure, shear stress, and circumferential stretch and tension, as mentioned in the previous section.

Blood pressure in the arteries of a human has a normal physiological range from 80 mmHg during diastole to 120 mmHg during systole. The pressure difference experienced in a cardiac cycle is 40 mmHg or 5.3×10^4 dyne/cm^2 [25]. In addition to

blood pressure which acts normal to the cell surface, wall shear stress which acts tangent to the cell surface is also important when considering pressure variations at the cellular and sub-cellular level. Wall shear stress is determined by blood viscosity and the shear rate at the cell surface and varies with the cardiac cycle. Normal wall shear stress has physiological ranges from 10 to 20 dyne/cm^2 [26]. For this study, the point-wise variations in pressure and shear stress due to flow are measured and analyzed. These values indicate the magnitude of shear stress and pressure at specific locations over the cells. As opposed to the bulk blood pressure exerted on the arterial wall measured using a blood pressure monitor, the pressure values in this study identify the flow induced pressure variations between and over endothelial cells. Although circumferential tension and stretch are present in addition to blood pressure and wall shear stress, they will not be considered in this study.

Since the length/width and height of endothelial cells are on the order of tens of microns and microns, respectively, the effects of hemodynamic forces on endothelial cells are critical at the micro-scale [27]. Specifically, cell surface height varies from cell to cell and over a single cell. Early studies investigating forces over endothelial cells computationally modeled the cell surface height of several adjoining endothelial cells as a sinusoidal function. This was done because accurate cell topography measurements were not yet attainable with the then-present technology [28]. This simplistic, computational approach utilizing a linear velocity gradient showed that wall shear stress increased with cell surface height and the maximum local shear stress was larger in magnitude than the applied shear stress. Also, this same study found that pressure was greater on the leading edge of a cell and lesser at the trailing edge of a cell. Although this study helped

demonstrate a relationship between cell topography and local shear stresses, the simplistic cell model limits the understanding of the cellular response to flow.

More recent *in vitro* studies investigating endothelial cell surface topography under applied shear flow utilized atomic force microscopy (AFM) measurements to map the cell surface topography [29]. Like the previous study mentioned, maximum wall shear stress was greater than the applied shear stress and corresponded to the location of maximum cell height. Although, pressure variations were roughly 80% of the applied shear stress for the AFM study while they were four to five orders of magnitude smaller than the applied shear stress for the sinusoidal model study. Similar to the AFM study, another numerical study took into account the deformability of the cell membrane and found that variations in pressure were large compared to the magnitude of the applied shear stress [30]. While both of these studies successfully identified variations in shear and pressure at the cellular level, the temporal resolution of the AFM study was limited by the time-consuming process of measurements; and the numerical study, although insightful, was physiologically limited due to numerical modeling.

More recently, studies utilized micro-particle imaging velocimetry (μPIV) techniques to compute hemodynamic information [31, 25]. These studies used the velocity information from μPIV to compute topography, wall shear stress, and pressure. They found that wall shear stress and pressure were on the same order of magnitude, and because of this, the magnitude and orientation of the resultant force on the cells was just as dependent on the shear stress force as the wall-normal pressure force.

1.3.2 Quantifying endothelial mechanics

Endothelial cells respond to the mechanical stimuli of hemodynamic forces through morphological and biological responses. Biological responses include elements of mechanotransduction including gene and protein expression while cell morphological responses include changes in cell orientation, shape, size, and height. Abnormal cell morphological and biological responses to mechanical stimuli have been associated with the localization of CVD.

Morphological responses associated with blood flow were first investigated in an *in vivo* canine artery [32]. The study found that cells were elongated and parallel to blood flow in straight sections of a vessel and more randomly oriented and less elongated in entrance regions of vessels. Furthermore, a slice of the canine thoracic aorta was rotated 90° to its original direction and then implanted in the aorta. After surgery, the cells of the implanted slice realigned in the flow direction. In another experiment, the endothelial cell morphology and orientation in a rabbit aorta was found to be a likely indicator of the direction and magnitude of blood flow [33]. These studies imply a strong relationship between blood flow characteristics, endothelial cell morphology, and the genesis of CVD.

Several *in vitro* experiments have been carried out to investigate the relationship between blood flow and cell morphology. Preliminary experiments showed that endothelial cells in quiescent flow are polygonal in shape and exhibit “cobblestone-like” growth patterns. When under steady, unidirectional shear stress, *in vitro* experiments found that bovine aortic endothelial cells aligned with the flow direction as well as elongated into ellipsoidal shapes [34]. In addition, several studies found that the cell morphological response to shear flow was dependent on the magnitude of the applied

shear stress and the length of shear stress exposure [35-37]. In contrast to the mentioned laminar flow studies, studies introducing turbulent flow over endothelial cells did not demonstrate cell realignment or elongation [38]. In addition to unidirectional *in vitro* experiments, pulsatile and oscillatory experiments, *i.e.,* no net flow, found that while pulsatile flow experiments showed cells alignment in the flow direction, oscillatory experiments did not show significant changes in cell morphology [39]. Each of the aforementioned experiments indicated that endothelial cells differentiate between different flow environments. Although, higher resolution experiments are needed to further investigate the sub-micron variations in flow around cells and clearly understand their relationship to endothelium realignment.

Although shear stress is most often considered the main hemodynamic force responsible for morphological and biological responses, the effects of pressure are not entirely clear. *In vivo* variations in local blood pressure have shown to cause remodeling in vessels where the change in pressure was proportional to the rate of the vessel remodeling [40]. In addition, endothelial cells that experienced increased normal forces acting on them due to osmotic pressure showed an increase in cell height with a reduction in external osmolarity [41]. Like studies mentioned previously, these experiments reiterate the need to investigate pressure, and moreover, perform investigations on the sub-cellular level in order to understand the complex relationship between cell remodeling and pressure.

The biological response of endothelial cells to hemodynamic forces will not be discussed within the context of this study, but reviews related to gene and protein

expression in response to mechanical stimuli of endothelial cells can be found in [27] and [42].

1.3.3 Quantification of hemodynamics and endothelial mechanics

Early studies on endothelial cells could not accurately determine cell surface topography due to limitations in experimental measurements on the cellular and sub-cellular level. Therefore, simultaneous measurement of cell morphology and local hemodynamic forces at the micro-scale were not able to be thoroughly investigated. For example, cell surface topography measurements were acquired for the first time using AFM [43]. Although AFM measurements are possible *in vitro* in quiescent environments on living cells, measurements are difficult in an applied flow environment. As mentioned previously, the time-consuming nature of AFM makes it difficult to simultaneously study hemodynamics and endothelial mechanics. For this reason, interference microscopy was implemented to measure cell heights in applied flow. Despite the ability to attain topographical information during a flow experiment, the shear stress distributions were not able to be calculated *in-situ*. Instead, topographical models from AFM and interference microscopy were used to calculate shear stress distributions using computational fluid dynamic (CFD) simulations [44-45]. As mentioned previously, although models can be insightful, this two-step approach does not allow *in-situ* measurement of both hemodynamics and endothelial mechanics.

Recently, μPIV techniques have been utilized to simultaneously calculate cell surface topography, shear stress, and pressure distributions at the micro-scale level using flow field information [25, 31]. These studies advanced endothelial cell research with their *in vitro*, non-invasive approach to study hemodynamic forces and endothelial

mechanics *in-situ*, but the experiments fell short on replicating the endothelium physiology, *i.e.*, non-confluent endothelial cell layers. With that said, this study aims to use a similar experimental technique to make *in-situ* measurements of hemodynamic forces and endothelial mechanics using *in vitro* confluent endothelial cells.

1.4 Research goals

When considering the research focuses in the previous sections, there are generally three main subject areas to consider during atherosclerosis progression: blood flow mechanics (local pressure and/or shear stress effects on the endothelium and LDL transmigration), endothelium mechanics (cell topography effects due to changes in fluid characteristics), and biochemical transport (rate of LDL transmigration due to changes of the endothelium or shear stress). Relating these three subject areas to the endothelium would be beneficial because the endothelium does not only experience the low-shear stresses associated with diseased arterial regions, but it is also the only barrier between cholesterol-carrying LDL and the intima, the arterial layer where atherosclerosis develops. For this reason, a comprehensive study investigating the relationship between endothelial mechanics, hemodynamics, and LDL transmigration is needed.

A research flowchart that incorporates the study of these subject areas is shown in Figure 1.4. The first two columns are *in vitro* endothelial cell experiments. The first experiment within the *in vitro* endothelial cell experiments is steady flow over a cultured endothelial cell layer without LDL. This initial experiment is the baseline experiment in which experimental techniques for measuring shear stress, pressure, and topography are validated. This initial experiment is the scope of this study, *i.e.*, steady flow experiments without LDL. The next experiment is steady flow over a cultured endothelial cell layer

with LDL. This experiment will validate experimental techniques for tracking LDL transmigration.

After the steady flow *in vitro* endothelial cell experiments, research can proceed in two ways: introduce pulsatile flow to the *in vitro* endothelial cell experiments as shown by the dotted lines in Figure 1.4 or proceed to co-culturing experiments. Introducing pulsatility to the *in vitro* endothelial cell model allows physiologic flow conditions to be studied. The *in vitro* co-culture section of the flowchart involves the co-culture of smooth muscle cells and endothelial cells. The co-culture not only more closely replicates the structure of an arterial wall, but also enables the study of the mechanotransduction of smooth muscle cells and endothelial cells. The co-culture experiments would also be subdivided into no LDL/LDL and pulsatile/steady flow experiments similar to the *in vitro* endothelial cell experiments.

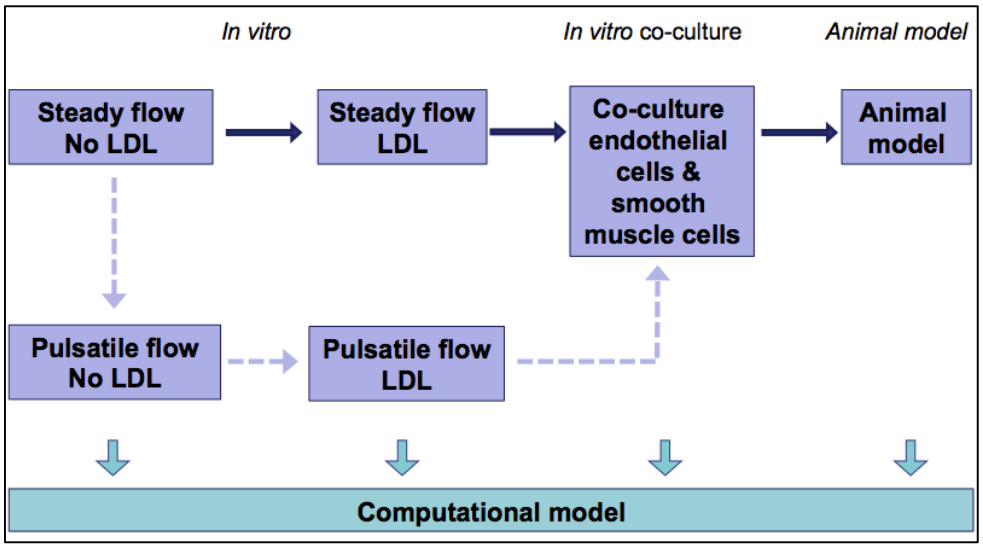

Figure 1.4: Research flowchart including *in vitro*, *in vitro* co-culture, and animal model experiments.

After the *in vitro* co-culture section, the next section of the flow chart is the development of an animal model in which we would study flow over a punch-out of the arterial wall of a pig. Lastly and as seen on the bottom of Figure 1.4, each experiment of the flowchart will assist in developing a multi-scaled computational model for predicting atherosclerosis progression.

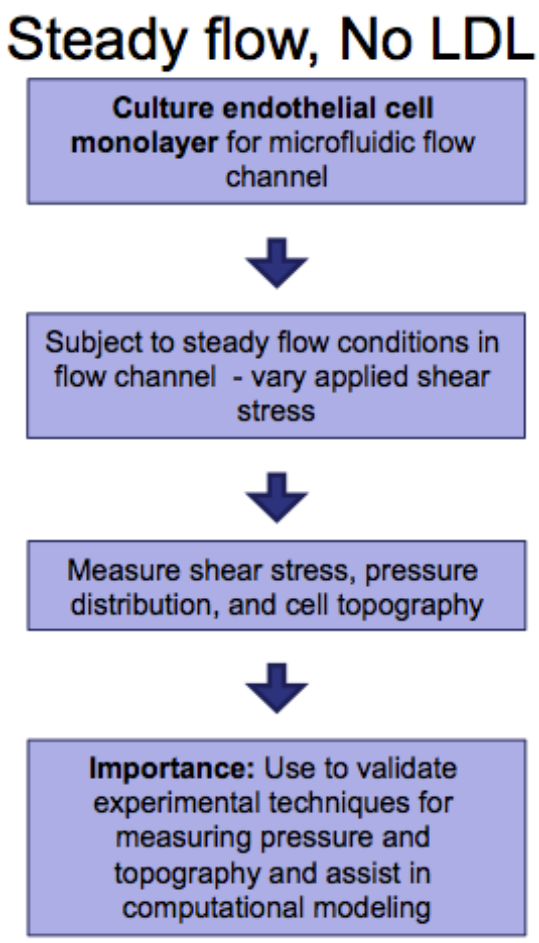

Figure 1.5: Research flowchart outlining the specific objectives for *in vitro* steady flow endothelial cell experiments without LDL.

Specifically, this study investigates *in vitro* endothelial cell experiments subjected to steady flow without LDL, or the first step in Figure 1.4. The specific objectives for this study are shown in further detail in Figure 1.5. By isolating the endothelium to a microchannel flow system, we can simultaneously and non-invasively study hemodynamics and endothelial mechanics on a cellular and subcellular level. In addition, varying arterial conditions and culture substrates can also be studied; including, normal functioning endothelial cells, necrotic endothelial cells, and extracellular matrix glycoproteins. Thus, the ultimate goal of this study is to develop an experimental method capable of measuring cell surface topography and hemodynamic forces over endothelial cells with the sensitivity to make these measurements while different environmental and cellular conditions related to atherosclerosis are present. The specific experimental tasks include,

1. Culture confluent layers of normal and necrotic bovine aortic endothelial cells *in vitro* on untreated glass
2. Culture confluent layers of normal bovine aortic endothelial cells *in vitro* with an extracellular matrix glycoprotein, *i.e.,* fibronectin coating
3. Quantify cell surface topography, wall shear stress, and wall pressure over the aforementioned confluent endothelial cell conditions

1.5 Coordinate system

All experimental measurements and computations are with respect to a Cartesian coordinate system. Figure 1.6 shows the coordinate system relative to the flow direction, microchannel bottom wall, and endothelial cell location. The *x*-axis is parallel to the flow

direction, or streamwise direction. The *y*-axis is referred to as the transverse (spanwise) direction, and the *z*-axis is perpendicular to the flow direction and the microchannel bottom wall and is referred to as the wall-normal (bi-normal) direction.

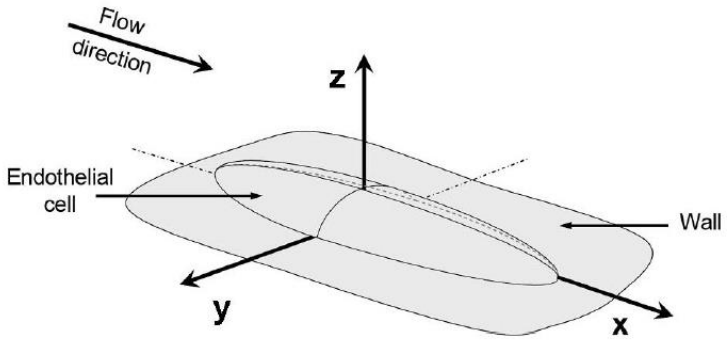

Figure 1.6: Cartesian coordinate system in reference to endothelial cell and flow direction [25].

CHAPTER 2

EXPERIMENTAL MATERIALS AND APPARATUS

In order to study the mechanotransduction of endothelial cells on the cellular and subcellular levels, confluent layers of bovine aortic endothelial cells were subjected to a series of flow experiments. An extensive culturing protocol was implemented to culture the endothelial cells for *in vitro* measurements. A micro-flow control system and micro-particle tracking velocimetry (μPTV) equipment were used to control flow conditions and acquire images for analysis. The apparatus and materials used for the experiments are described in the following sections.

2.1 Cell culturing before cell insertion

Bovine Aortic Endothelial Cells (BAOECs) (Lonza Walkersville Inc., Walkersville, MD) were cultured at the University of Nebraska Medical Center. The initial aliquot of cells was thawed and divided equally into 8 x 2 mL cryovials upon arrival. The cryovials were stored at -70 °C for future use. One 2 mL cryovial of endothelial cells was needed for each flow experiment. The cells from the cryovial were subcultured onto 3 x 100 mm tissue culture dishes (CytoOne) using Endothelial Cell Basal Media (EBM) including growth factors, cytokines, and supplements from the SingleQuots™ Kit (Lonza Walkersville Inc., Walkersville, MD). The cells in the tissue culture dishes were grown in an incubator at 37°C supplemented with 5% CO_2. Cells were passaged three times and each passage was subcultured onto 3 x 100 mm tissue culture dishes. The third passage of cells was grown to 100% confluency before inserting the cells into the Fluxion BioFlux™ microchannels. The cells were then grown to confluency in the microchannels which usually took around 6-10 days. The detailed

instructions for culturing the endothelial cells from the initial aliquot to cell insertion are detailed in Appendix A.

2.2 Micro-flow control system

The BioFlux™ 1000z (Fluxion Biosciences Inc., San Francisco, CA) was used to perform the live endothelial cell analyses under controlled shear flows. The micro-flow control system utilized 24-well plates with embedded microchannels for *in vitro* flow assays, a pressure pump to control shear flow, an automated microscope stage to control three-dimensional acquisition location, and PC software for systematic control.

The 24-well BioFlux™ plates allowed multiple steady flow assays to be performed simultaneously at applied shear stresses ranging from 0 - 20 dyne/cm^2. Figure 2.1 illustrates the layout of each plate in which there are six columns of four wells. Columns 1 and 2 are input wells that have an associated output well in column 3, and columns 4 and 5 are input wells that have an associated output well in column 6. For a given row on the plate, two input wells are connected to the adjoining output well through a microchannel where the endothelial cells are cultured for assays. The microchannels are depicted in the viewing window of Figure 2.1. A different level of shear stress could be specified for each of the two columns of inlet wells on either side of the plate which allowed the system to operate two different applied shear rates during a given flow assay.

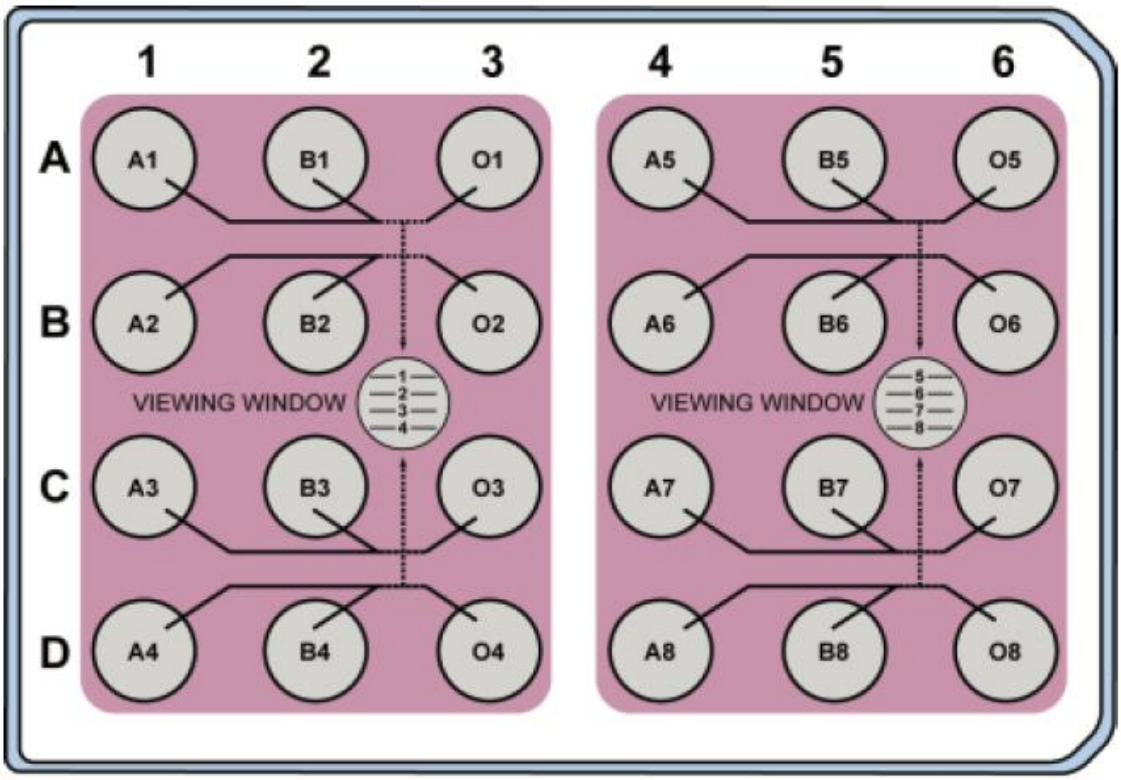

Figure 2.1: Illustration of 24-well BioFlux™ plate showing four rows and six columns of wells. Microchannels are shown within each "Viewing Window" [46].

The microchannels were pre-fabricated within the BioFlux™ 24-well plates through Fluxion Biosciences. Inlet and outlet wells each had a volume of 3 mL which was used to contain the working fluid used in experiments. In order to induce flow from the inlet wells containing media to the outlet well, the shear rate and microchannel selection was specified in the BioFlux™ PC software. The software triggers the BioFlux™ pneumatic pump to apply the corresponding amount of pressure to each set of inlet wells which created a pressure difference across the microchannels connected to the outlet wells. The pressure difference drove the working fluid from the inlet wells through the microchannels for the flow assay experiments. The microchannels had a rectangular

cross-section which was 350 µm in width (*y*-direction) by 70 micrometers in height (*z*-direction). The side and upper walls of the microchannels were constructed using PDMS and permanently adhered to glass, or the bottom surface of the microchannel. Figure 2.2 shows the 24-well BioFlux™ plate positioned on the microscope stage.

The BioFlux™ PC software also contained an automated stage with three-dimensional movement abilities. The stage also included a heating element that kept the temperature of the BioFlux™ plate and media at 37°C as required for endothelial cell viability. Although automated control was not used for experiments in this study, the location of data acquisition was solely controlled using the BioFlux™ PC software. The basic components of the BioFlux™ system including the BioFlux™ software and positioning stage are shown in Figure 2.3.

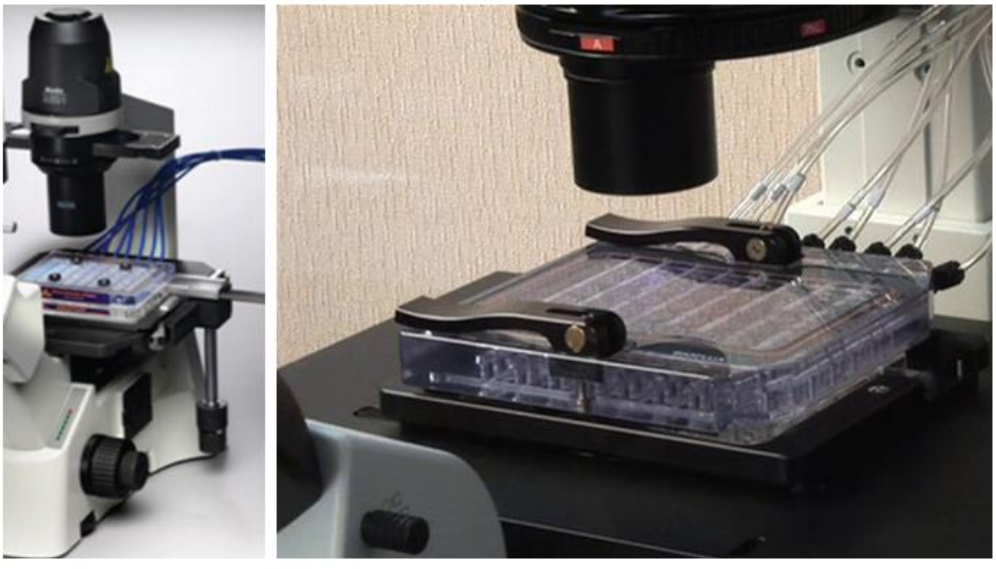

Figure 2.2: Microscope system setup (a) with 24-well BioFlux™ plate and microscope positioning stage (b) [46].

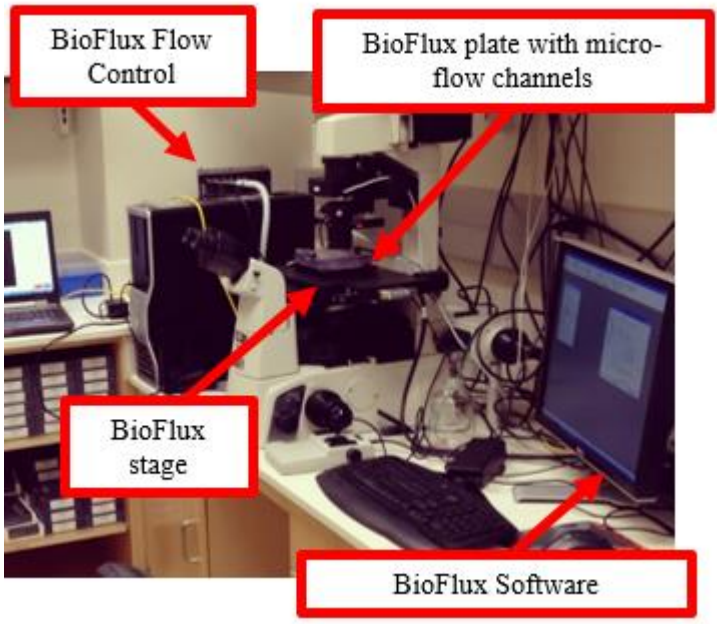

Figure 2.3: Basic components of the BioFlux™ flow system used to control flow over endothelial cells. Cells were cultured *in vitro* in the microchannels of the 24-well BioFlux™ plate.

2.3 Micro-particle tracking velocimetry

Experimental measurements were made using micro-particle tracking velocimetry (µPTV). The technique is derived from 'PTV' which is an image-based experimental technique that measures velocity by tracking individual particles in a flow. The prefix 'micro' refers to the ability to measure micro-scale particle displacements in the flow. Micro-particle tracking velocimetry uses particle recognition and tracking algorithms to measure the particle movement and then compute particle velocity. The following subsections will provide an introduction to µPTV and discuss the basic components in a µPTV system.

2.3.1 Introduction

In a typical PTV experiment, the fluid of interest is pre-seeded with small neutrally buoyant particles. The particles act as flow tracers when illuminated by a two-dimensional plane of light, and the illumination plane defines the measurement plane for the PTV system. As the particles travel with the flow, a high-speed camera records successive images with a very short time between images to track the motion of the particles illuminated by the plane of light. The velocity of each illuminated particle can be determined from the displacement of the particle from a recorded image to the next successive recorded image and the time elapsed between the two corresponding images. The velocity field for the two-dimensional measurement plane is then calculated using a spatial averaging technique. Figure 2.4 shows the setup of the microscope components of µPTV system used for the experiments in this study.

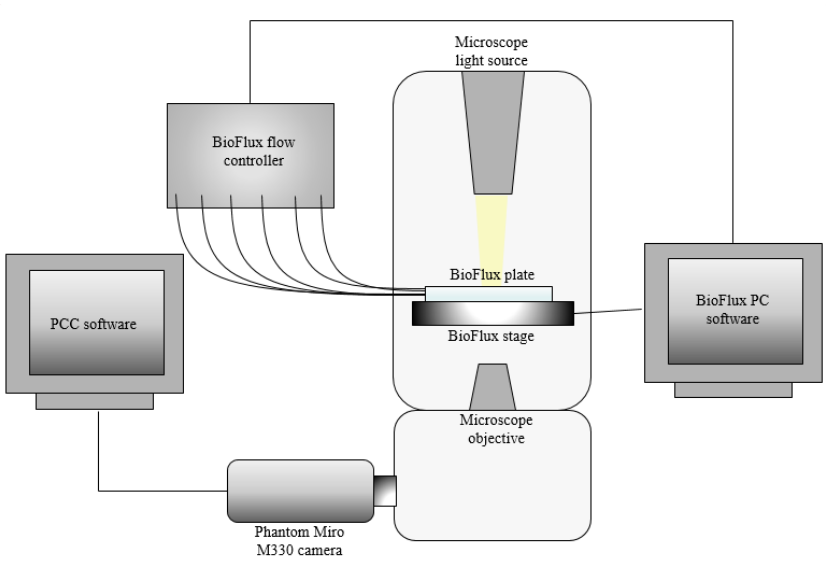

Figure 2.4: Schematic of the basic components of the experimental setup including the components of the µPTV system and the BioFlux™ flow system.

For µPTV experiments, the plane of light used to illuminate particles is considered optically thick compared to the scale of interest and therefore, a three-dimensional volume is illuminated compared to a two-dimensional plane. In this regard, the depth-of-focus of the microscope's objective is used to define and limit the thickness of the measurement plane. It is important to note that the plane that defines the particles for the µPTV algorithm is a different thickness than the measurement plane, but the position of the measurement plane remains the same. Image processing techniques are implemented to limit particles in a µPTV input image to only those within $z = \pm 0.15$ µm, this spatial resolution is referred to as the particle plane. A particle plane is positioned at the same location as the measurement plane but has a thinner virtual depth. Further details on the process used to define the particle plane are discussed in the following paragraph.

2.3.2 Basic components

An in-house µPTV algorithm and system were used for this study. The system included a camera, microscope objective, microscope light source, and tracer particles. Figure 2.4 shows the basic components and their setup for the µPTV system.

The microscope objective was one component that determined the thickness of the measurement plane. The objective was selected based on the lateral resolution and the depth-of-focus desired for the experiments. The lateral resolution, usually just referred to as the resolution, is the shortest distance resolved between two objects using the objective. The lateral resolution of an objective, r, is defined as,

$$r = \frac{0.61\lambda}{NA} \tag{2.1}$$

where λ is the imaging wavelength and *NA* is the objective's numerical aperture. Depth-of-focus, *d*, is the thickness, or height, in which an imaging plane can provide an acceptably clear and/or shape image. This thickness is defined as,

$$d = \frac{\lambda n}{NA^2} + \frac{n}{M(NA)} r \tag{2.2}$$

where λ is the imaging wavelength, *n* is the index of refraction of the medium between the objective's lens and the specimen, *NA* is the numerical aperture of the objective, *M* is the objective's magnification, and *r* is the lateral resolution of the objective [47].

A CFI Super Plan Fluor ELWD 40× microscope objective (Nikon Instruments Inc., Melville, NY) was used for this study. The working distance of the objective was 2.8 – 3.6 mm which accounted for the thickness of the stage between the microchannel and the microscope objective. The correction ring on the objective was set to 0.18 to account for the thickness of the glass bottom of the microchannel, or 180 µm. The numerical aperture of the objective was 0.6 and the imaging wavelength was 550 nm (microscope lamp). Based on equations 2.1 and 2.2, the depth-of-focus was 1.5 µm and the lateral resolution was 0.55 µm. Although the lateral resolution of the objective was important, the sensor of the camera ultimately determined the resolution of the images acquired in this study. The image resolution was 2.06 pixels/µm which was found by using the known width of the channel in an image as a scale. The image resolution and depth-of-focus were important when considering the size of the seeding particles for µPTV.

The microscope objective was a part of a Nikon Eclipse Ti-S inverted microscope system used for brightfield imaging. Figure 2.4 shows the microscope assembly used for

this study. The assembly includes a side port which mounts the camera using a C-mount camera attachment. Illumination was provided by the microscope's LED lamp that was located at the top of the microscope system and directed downward in line with the objective. With this setup, the microscope lamp illuminated the seeding particles from above the microchannel while the microscope objective allowed the microchannel to be viewed from below. Köhler illumination was achieved prior to each experiment. It should be noted that this study did not use fluorescence microscopy.

The Phantom Miro M310 camera (Vision Research, Wayne, NJ) used for data acquisition had a thermoelectrically-cooled CMOS sensor with 1280 x 800 pixels resolution and 12-bit depth. This camera included Extreme Dynamic Range (EDR) exposure and burst mode capabilities for PTV applications. The camera was capable of exposure times as low as 1 µs which allowed the measurement of flows in excess of 1 m/s. The camera was controlled by Phantom Camera Control (PCC) software (Vision Research, Wayne, NJ).

Red Fluoro-Max Fluorescent particles (Thermo Scientific, Waltham, MA) were used as the seeding particles for the µPTV system. The particles had an average diameter of 1 µm and a density of 1.05 g/cm^3 which allowed the particles to be neutrally buoyant during the experiments. The particles were initially selected based on their size and excitation/emission wavelengths (542 nm/612 nm) but were ultimately used for their ability to scatter light from the LED microscope lamp.

Experiments were conducted to determine the final thickness of the particle plane using the seeding particles described above and the Fluxion Biosciences microscope

stage. The microscope stage holds the BioFlux™ plate and had the ability to make three-dimensional movements with 0.1 μm precision. With that said, seeding particles were suspended in Endothelial Cell Basal Media (EBM) and pumped through a microchannel in a 24-well BioFlux™ plate. The flow was turned off and particles were allowed to settle on the bottom surface of the microchannel. The seeding density was very low at 1 particle/50 μm^2. The LED microscope lamp was turned on at a quarter of the maximum intensity allowed by the microscope, which is also the same intensity used for data acquisition in this study. This was the minimum intensity required for data acquisition without overexposing the cells to light. The focal plane was first positioned 2 μm beneath the microchannel and then moved upwards in the *z*-direction at 0.1 μm increments. After each increment, an image was acquired for calibration purposes. The images acquired at each *z*-position are shown in Figure 2.5 (a).

The thickness of the particle plane used to identify tracer particles for μPTV is established by tracking particles with a specific light intensity. Using the images taken for calibration shown previously in Figure 2.5 (a), a threshold was applied to the images using MATLAB so that only pixels with specific light intensities were shown in the resulting image. For this study, an imaging threshold value of 0.72 was used for images with a light intensity ranging from 0 to 1. This threshold value resulted in an image where only the pixels with a light intensity above 0.72 were kept in the image and they were converted to a pixel value of 1, *i.e.*, a binary image. Applying the threshold value mentioned, the corresponding processed images are shown in Figure 2.5 (b). Using this method, it can be seen that particles illuminate at a higher intensity value in a 0.3 μm

section within the initial 0.9 µm focal plane produced by the microscope objective.

Therefore, the depth of the particle plane is ± 0.15 µm when tracking particles for µPTV.

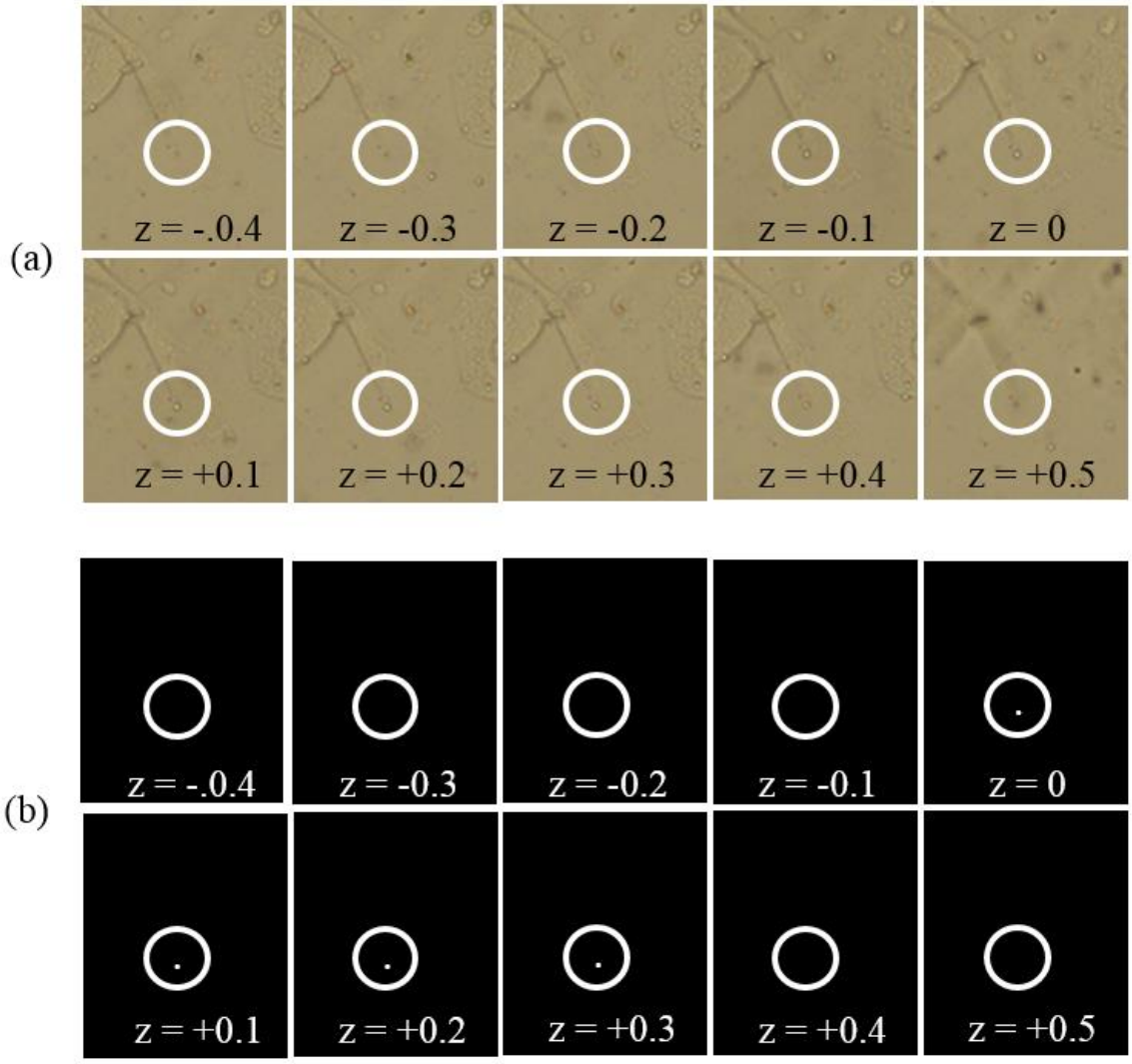

Figure 2.5: A series of brightfield images depicting the luminosity of a stationary seeding particle from z = -0.4 µm to z = +0.5 µm in increments of 0.1 µm (a), and the corresponding processed image after applying an intensity threshold (b).

CHAPTER 3

EXPERIMENTAL METHODS

Three types of experiments were performed in this study – (1) steady flow over confluent layers of normal endothelial cells cultured on untreated glass, (2) steady flow over confluent layers of normal endothelial cells cultured on fibronectin, and (3) steady flow over confluent layers of necrotic endothelial cells cultured on glass. The two main protocols required for each experiment involved culturing endothelial cells and setting up the μPTV and flow system. The following sections discuss the two main protocols in further detail and also the differences in each protocol for each type of experiment in this study.

3.1 Culturing endothelial cells

The main apparatuses used for culturing endothelial cells included bovine aortic endothelial cells, tissue culture dishes, BioFlux™ plates, culturing solutions, microscope, incubator, cell counter, culture substrates, and a laminar flow hood. The culturing substrate and media were the only culturing components adjusted for the different types of experiments mentioned previously. The basic components used for culturing endothelial cells are discussed in further detail in the succeeding sections.

3.1.1 Bovine Aortic Endothelial Cells

As previously discussed in subsection 2.1, bovine aortic endothelial cells (BAOECs) were first cultured in tissue culture dishes before seeding the cells into the microchannels of the 24-well BioFlux™ plate. After the third passage, the endothelial cells were counted using the Countess™ Automated Cell Counters (Invitrogen, Carlsbad, CA) and checked for viability. A high concentration of cells (>7.5 x 10^6 cells/mL) was

required for cell insertion in the microchannels. If the concentration was too low, cells were not able to grow to confluency. Once at least 330 µL of the desired concentration of cells was reached, the cells were inserted into the microchannels of a BioFlux™ plate.

For cell insertion, the solution of cells was divided evenly amongst the inlet wells of a 24-well BioFlux™ plate. The BioFlux™ 1000z pump was triggered for 2-3 seconds to pump the cell solution from the inlet wells to the outlet wells of the plate. After the pump was shut off, the suspended cell solution could be seen in the microchannels using the Nikon Eclipse Ti-S microscope. Figure 3.1 shows an image depicting the desired density of suspended endothelial cells in the microchannel just after cell insertion. After cell insertion, the BioFlux™ plate is placed in the incubator (37 °C supplemented with 5% CO_2) for two hours while the cells adhere to the bottom surface of the microchannels. As stated previously, the detailed instructions for culturing the endothelial cells from the initial aliquot to cell insertion are in Appendix A.

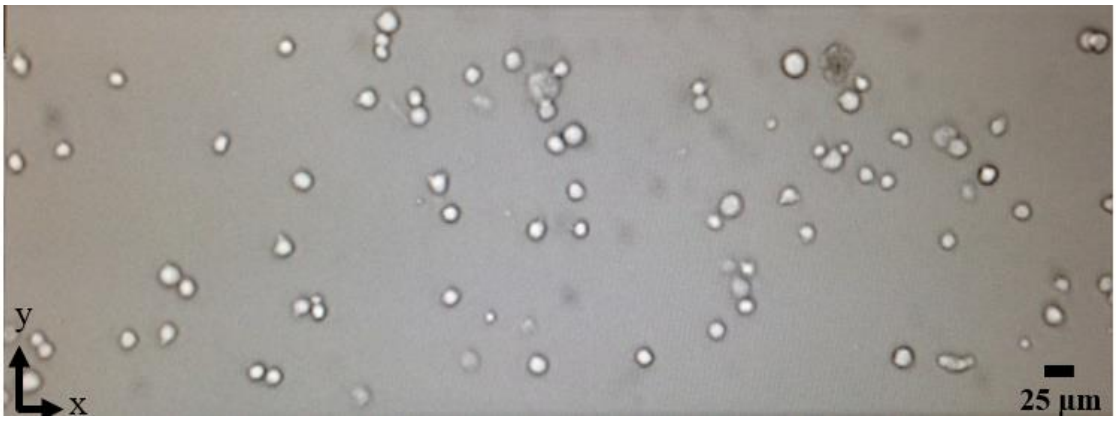

Figure 3.1: Trypsinized endothelial cells suspended in a microchannel right after cell insertion. The image shows the desired seeding cell density in order to culture a confluent layer of endothelial cells. Flow is from left to right in the image.

3.1.2 Culture substrates

Cell adhesion plays an important role in growth, migration, structure, and the normal function of cells. Specifically, cell adhesion helps maintain multicellular structure and can aid in signal transduction between cells. Cell substrates used in cell culture can provide different molecule and receptors for cell attachment [48]. For this reason, flow experiments were performed on endothelial cells cultured on a fibronectin substrate and endothelial cells cultured without a substrate, or on untreated glass.

Endothelial cell experiments including a culture substrate utilized fibronectin from bovine plasma (Sigma-Aldrich, St. Louis, MO) diluted in a deionized phosphate buffered solution (D-PBS) to a concentration of 100 µg/mL. Fibronectin from bovine plasma is a multifunctional glycoprotein that has been shown to promote cell attachment in endothelial cells [49].

Before cell insertion, microchannels were primed with D-PBS and then coated with the fibronectin solution. The BioFlux™ plate was placed in the incubator (37°C supplemented with 5% CO_2) for 1 hour while the coating adhered to the channel. After 1 hour, the microchannel was washed with D-PBS and then cells were inserted as described previously. Microchannels that did not include a substrate for experiments were only primed with D-PBS before cell insertion. Since the fibronectin-coated channels used a very low concentration of fibronectin to coat the channels, the optical clarity was not affected.

3.1.3 Growth media

To promote cell viability, different fluids were used for culturing the endothelial cells in the microchannels and for performing the flow experiments. After cells were inserted in the microchannels, each inlet well of the BioFlux™ plate was filled with 2 mL of a 50% EBM and 50% CO_2-independent media (GIBCO™) solution at 37 °C supplemented with L-glutamine and fetal bovine serum (FBS). CO_2-independent media was utilized in the solution because the high cell seeding concentration required extra buffering to maintain the pH at 7.2-7.4. The solution in the inlet wells was aspirated and replaced with fresh solution every 24 hours in order to constantly supply the endothelial cells with nutrients to ensure cell viability. Between media replacement, the BioFlux™ plate was kept in the incubator to ensure physiological conditions for the cells. After each 24 hour period, the cells were checked for confluency. Once the cells reached confluency, they were ready for the flow experiment. Figure 3.2 shows a brightfield image of a confluent layer of BAOECs in a BioFlux™ microchannel that is ready for experimentation.

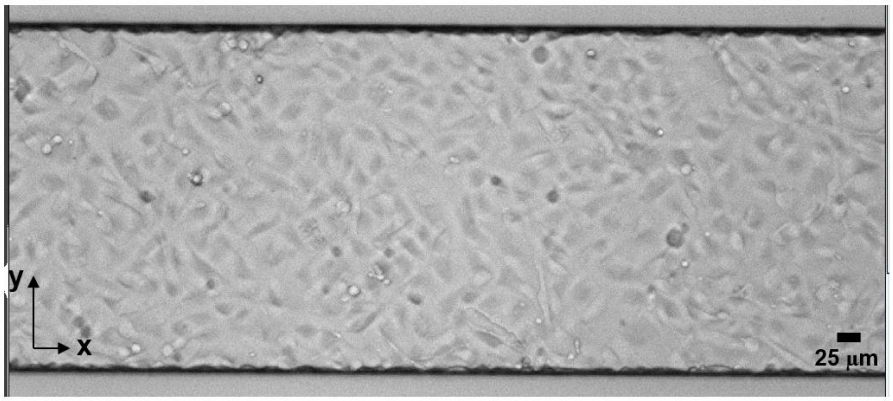

Figure 3.2: Confluent layer of endothelial cells cultured in a microchannel. The image shows the desired cell confluency for flow experiments. Flow is from left to right in the image.

3.2 Micro-PTV system and flow system

The main apparatus used for the μPTV and flow system included the camera, microscope system, Fluxion Biosciences flow system, seeding particles, and the working fluid. As described previously, the endothelial cells were cultured to confluency before the flow experiments. The camera, microscope system, and seeding particles were required for data acquisition and the working fluid and Fluxion Biosciences flow system were responsible for flow application. The basic components of the μPTV and flow system are discussed in further detail in subsequent sections.

3.2.1 Working fluid

The working fluid chosen for an experiment dictated whether the cells were normal or necrotic for the given flow experiment. For necrotic endothelial cell flow experiments, CO_2-independent media supplemented with L-glutamine and FBS was used as the working fluid. This media solution helped maintain a pH of 7.2-7.4 while the experiment was conducted outside of an incubator and in the absence of 5% CO_2 supplementation. For necrotic endothelial cell flow experiments, EBM was used as the working fluid. Since endothelial cells cultured in EBM required 5% CO_2 supplementation to remain healthy, the pH for these experiments was considerably lower which resulted in necrotic endothelial cells during the experiment. All media solutions used for flow experiments in this study were kept at 37 °C using the microscope stage heating element. Also, the solutions had a density and viscosity similar to water.

3.2.2 Seeding particles

As discussed in subsection 2.3.2, the seeding particles acted as flow tracers for the μPTV measurements. A fairly low particle-seeding density was needed per image for

μPTV measurements so that each individual particle can be tracked between images. The seeding density for μPTV experiments was determined by the particle displacement between successive images and the minimum distance between neighboring particles. In order for the μPTV algorithm to recognize and track individual particle movement, the average particle displacement between images must be less than the average distance between neighboring particles. In this regard, the particle density used for the μPTV measurements in this study was ~10 ppm. This was attained by combining 0.0005 mL seeding particles with 3 mL of the working fluid.

Seeding particles were pre-mixed in the working fluid prior to the flow experiments using a pipette. Previous experiments performed by Leong *et al.* found that similar particle densities had no adverse effects on cell growth and viability, and the low particle seeding densities did not affect the viscosity of the working fluid [25].

3.2.3 Applied flow rates

For this study, the BioFlux™ micro-flow control system used an electropneumatic pump with the 24-well BioFlux™ plates to conduct steady flow experiments at 5, 10, and 20 dyne/cm^2. These shear stresses corresponded to flow rates of 0.0245 mL/s, 0.049 mL/s, and 0.098 mL/s, respectively; and the Reynolds numbers of the channel were 2.66, 5.32, and 10.64, respectively. Both EBM and the CO_2-independent media solution utilized as the working fluid for experiments had a density of 993 kg/m^3 and dynamic viscosity of 0.72 x 10^{-3} N s/m^2.

3.3 Imaging system

The major components of the μPTV system including the imaging components were discussed in subsection 2.3.2. The following sections will describe the methodology used for data acquisition.

3.3.1 System setup

Before performing the flow experiments, equipment including the camera, imaging software, and the BioFlux™ software had to be setup and calibrated for data acquisition.

Once the camera and software were set up and calibrated as described in Appendix A, the BioFlux™ plate with a confluent layer of BAOECs was placed on the microscope stage. Using the BioFlux™ software, the stage was moved around and the BAOECs in the microchannels were inspected for confluency and cell health. Stage positions that corresponded to healthy BAOECs at 100% confluency within the field-of-view of the camera were saved in the BioFlux™ software. Since each three-dimensional stage location was saved, data acquisition was able to be taken at the exact same location in each microchannel during every time step in an experiment.

An important thing to note is that only one microchannel location on each side of the BioFlux™ plate could be measured for each flow experiment. As mentioned previously, each BioFlux™ plate has one column of four microchannels positioned on each side of the 24-well plate. When the microscope LED lamp is turned on for data acquisition, the entire column of microchannels on the side of the plate being viewed is exposed to the microscope's light. Since BAOECs are very sensitive to light exposure,

only one microchannel position from each side of the plate was selected for data acquisition.

3.3.2 Data acquisition

The field-of-view of the cells was in the *x*-*y* plane and measurements were acquired at 8 different *z*-positions starting at the bottom surface of the channel (z = 0 µm) and ending 10 µm upwards from the wall in the channel flow. The bottom of the microchannel was found by positioning the focal plane so that the very few seeding particles resting on the bottom of the channel came into focus. The 8 different *z*-planes measured were z = 0, 1, 2, 3, 4, 6, 8, and 10 µm and a depiction of the first several planes are shown in Figure 3.3. The location of each measurement plane was reached using the BioFlux™ software which had a sub-micron resolution.

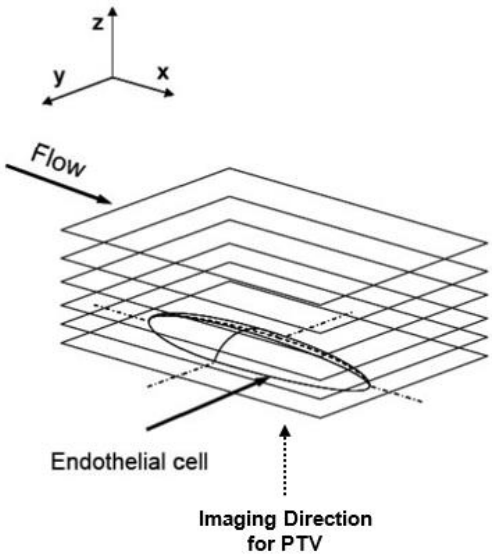

Figure 3.3: Schematic depicting the measurement plane locations with respect to the endothelial cells, imaging direction and flow. The schematic does not depict the actual number of measurement planes and is not drawn to scale [25].

Although the applied shear stress varied amongst the experiments, data acquired for µPTV was always acquired using an applied shear stress of 3 dyne/cm^2. Since the light intensity used for data acquisition was relatively low, the exposure time of the camera needed to be longer. The longer exposure times required a lower applied shear stress so that seeding particle movement, *i.e.* streaking, was not captured within an image. Although the flow rate was decreased every 3 hours, the integrity of the endothelial cell experiments was not compromised since the time required for data acquisition was only 7 minutes during each 3 hour time step. This length of time is too short for any morphological changes to occur. Details in section 4.3.7 and Figure 4.15 demonstrate that cell morphological changes occur over hours rather than minutes.

The camera's framing rate was 160 frames per second with 960 horizontal pixels by 720 vertical pixels resolution for all experiments. An image resolution of 2.06 pixels/µm resulted in a field-of-view that was 466 µm by 349 µm. The exposure time for all experiments was 250 µs. The PCC camera software was set to "Burst Mode" so that two successive images were captured at the given framing rate. The time between successive images is called the burst period. Since flow velocity can vary for a given *z*-distance from the channel's bottom, the burst period also varied depending on the location of the measurement plane. The burst periods for measurement planes at z = 0, 1, 2, 3, 4, 6, 8, and 10 µm were 3125 µs, 3125 µs, 2900 µs, 2600 µs, 2300 µs, 1900 µs, 1500 µs, and 1200 µs, respectively. The burst period chosen for each measurement was based on the desired particle displacement, 10-15 pixels, between successive images for µPTV measurements.

For all experiments, 3000 image pairs were acquired at each measurement plane and the microscope's LED lamp was set at 25% of maximum intensity during image acquisition. Since the particle seeding density was relatively low, a velocity field was computed by using all of the images for the given field-of-view. Measurements for μPTV were taken at the 0^{th}, 3^{rd}, 6^{th}, 9^{th}, 12^{th}, 15^{th}, and 18^{th} hours during the flow experiments. Measurements every 3 hours over the course of the 18-hour experiment allowed morphological cell changes and hemodynamic forces to be compared at each time step for the same group of cells. A detailed protocol for μPTV data acquisition can be found in Appendix A and details on the μPTV algorithm can be found in Chapter 4.

CHAPTER 4

DATA PROCESSING

The goal of data processing was to compute velocity, surface topography, shear stress, and pressure for confluent layers of endothelial cells at different applied shear stresses. Before this data could be computed, raw images from data acquisition had to be processed for the µPTV program. After image processing, the in-house µPTV algorithm computed velocity fields for each measurement plane. The velocity information was used to compute shear stress and pressure measurements over the endothelial cells. The following sections detail the data processing procedures, including steps for image processing, µPTV processing, and post-processing velocity information.

4.1 Image processing

Raw images acquired during µPTV measurements had to be pre-processed for the µPTV program. While images acquired were initially RGB color images, the µPTV program required binary images depicting white tracer particles (*pixel value* = 1) and a black background (*pixel value* = 0). To accomplish this, raw images were converted to grayscale and a threshold was then applied to the images. As previously discussed in subsection 2.3.2, the threshold value chosen decreases the thickness of the particle plane for µPTV. After thresholding the images, the resulting image was a binary image in which the tracer particles were white and the background was black. Figure 4.1 shows a raw image before and after image pre-processing. Note that the particles shown in the pre-processed image are slightly enhanced in size for clarity.

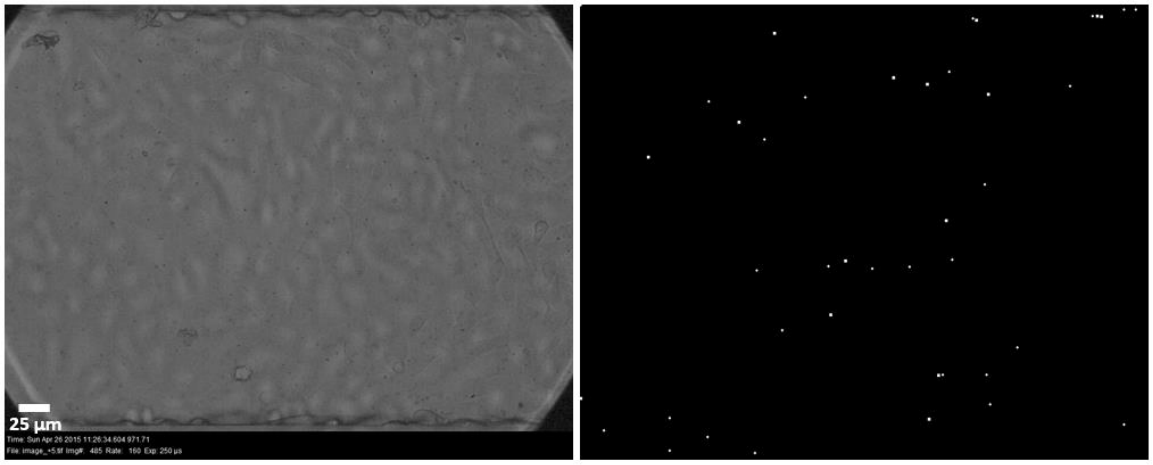

Figure 4.1: An unprocessed image (a) showing in-plane seeding particles with a slightly higher intensity than the background. After pre-processing, the resulting image (b) shows the seeding particles (enhanced in size to show clarity) in white and the background in black. The pre-processed image (b) is used as an input for the µPTV algorithm to track particle movement. Flow was from left to right and the images shown are for z = 4 µm.

4.2 Micro-PTV processing

After pre-processing images, the in-house µPTV program computed two-dimensional velocity fields for each measurement plane. As mentioned previously, 3000 image pairs were acquired at each measurement plane during each time step. There are two major steps in the in-house µPTV program - (1) particle displacement analysis for each image pair, and (2) composite velocity averaging.

For the first step, pre-processed image pairs are read through the µPTV program. The algorithm finds connected-components with a pixel value of one (white) with an area no greater than 5 pixels^2 in the first and second image of the pair. The area constraint ensures that only seeding particles are tracked for velocity measurements. Each sub-pixel centroid location found in the first image is compared with the sub-pixel centroid

locations found in the second image. For a given centroid location in the first image, the algorithm searches for any centroids in the second image that are located within a 30 pixels x 30 pixels window centered on the centroid in the first image. The pixel window size was determined by the distance particles moved between an image pair. If more than one centroid is found in the second image within the 30 pixels x 30 pixels window, the algorithm does not consider the centroid in the first image for velocity measurement. If there is only one centroid found in the second image within the window, the distance between the centroid of the first image and the centroid of the second image is calculated. If there are no centroids in the second image, the particle may have moved out of plane, and therefore, is not used for velocity measurements. The velocity of the centroid is computed by dividing the distance traveled between images by the burst period time. This velocity measurement is saved in a matrix which has the same size as the initial images, 960 pixels x 720 pixels. The coordinate location of the first image's centroid determines the coordinate location to save the computed velocity value in the matrix. The step described above is repeated for each centroid in an image pair. All 3000 image pairs are read through the program and each centroid's velocity measurement is recorded in the velocity matrix mentioned. There is only one velocity matrix for a given measurement plane.

The second step in the µPTV program computed a velocity field from the matrix mentioned previously. After the 3000 image pairs are read into the program and the velocities of each centroid are saved in the matrix, there is a velocity value assigned to ~85% of the pixel locations in the field-of-view. In order to increase the accuracy of the velocity measurements, the final matrix was spatially averaged using a 7 pixels x 7 pixels

kernel filter. After spatial averaging, the resulting matrix defined the velocity field for the given measurement plane with a vector spatial resolution of 3.3 μm. Figure 4.2(a) shows an example of a spatially averaged vector field overlaid on an image of BAOECs, and Figure 4.2(b) shows a zoomed-in area of the vector field which depicts the vector spacing around a single endothelial cell. Notice that there are no vectors located near the center of the endothelial cell because the vector field is for a *z*-plane intersecting the cell so there is no flow in that area. Also, the vector field shown is for streamwise velocity, *u*, because only the streamwise velocity vectors are used to make topography, shear stress, and pressure computations.

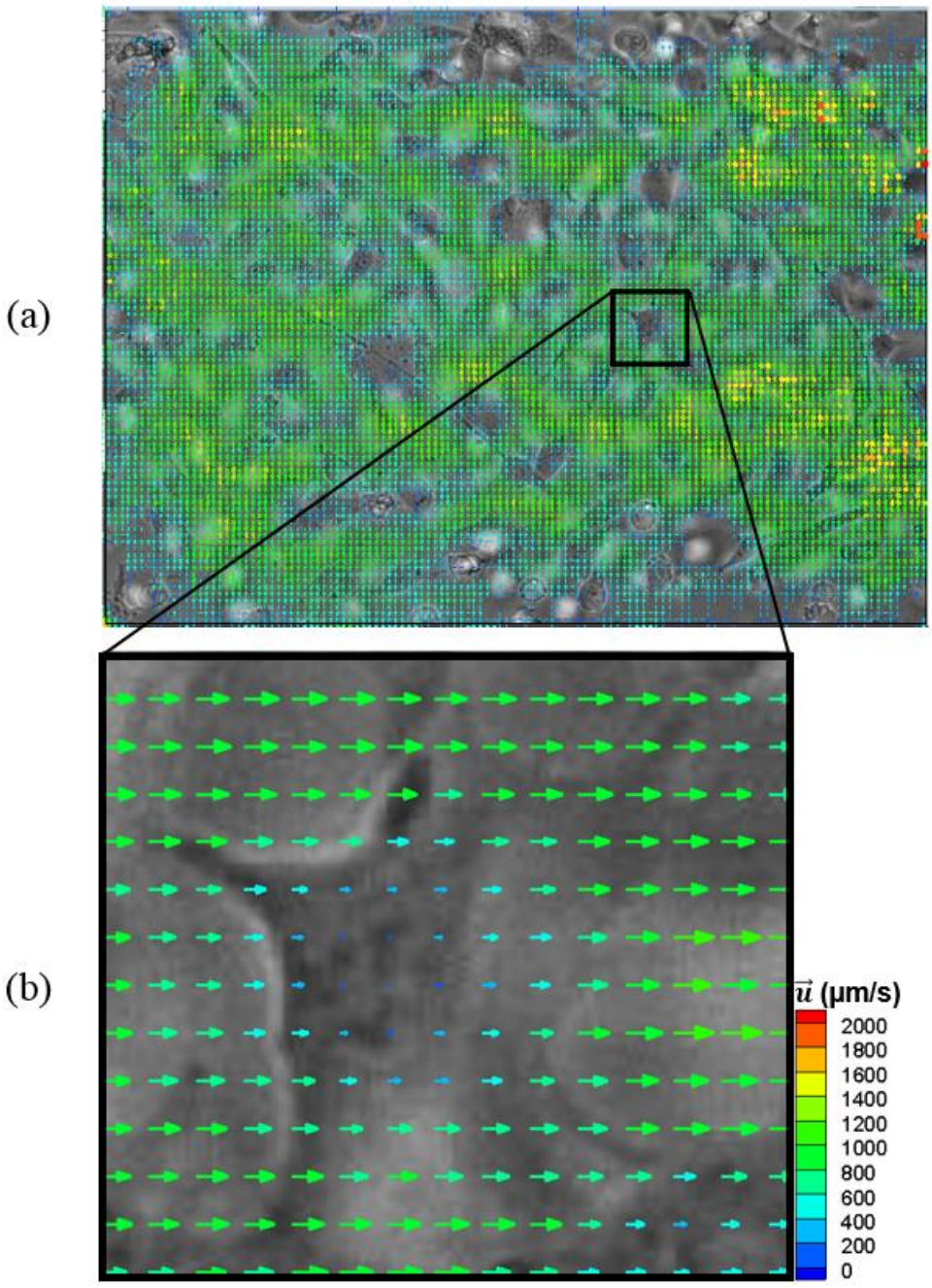

Figure 4.2: A streamwise velocity vector field overlaid on an image of endothelial cells for the field-of-view (a) and a zoomed-in area within the field-of-view depicting the streamwise velocity vector field spatial resolution around a single cell as shown in the underlying image (b). Flow is from left to right and the vector field is for z = 3 μm.

4.3 Post-processing velocity information

After velocity information was computed for each measurement plane and each time step, algorithms were constructed and applied to extract information including shear stress, cell surface topography, and pressure over the endothelial cells. The subsequent sections will discuss the algorithms implemented to perform these calculations.

The first algorithm implemented identified and replaced erroneous velocity information. Velocity vector fields computed using the μPTV program usually included a few velocity vectors that deviated in direction and magnitude when compared to their neighboring vectors. The majority of these vectors resulted from background noise introduced in the second image of the image pair. These erroneous vectors were found using a local median test [50]. A 6 x 6 kernel was used with a threshold value of 2 for the local median test. During the test, each vector value within the 6 x 6 area was compared to the value of the 35 neighboring vectors within the same area. If a velocity vector was larger than the product of the threshold and the standard deviation of the neighboring vectors or the sum of the median, it was considered erroneous. Also, the vector was considered erroneous if the difference between the median value and the product of the threshold and standard deviation of the neighboring vectors was smaller than the vector value. Each erroneous velocity vector was replaced with the average of its neighboring vectors.

4.3.1 Theoretical velocity profile versus experimental velocity profile

During experiments, planar measurements were taken from the bottom wall of the microchannel up to 10 μm away from the wall into flow. Since these measurement planes were so close to the wall, the velocity profile was considered linear in this region. To

verify this, µPTV measurements were compared against the Poiseuille profile for a two-dimensional flow. For the experimental data, media seeded with tracer particles was introduced in a BioFlux™ microchannel without cell culture at 3 dyne/cm^2. Average velocity measurements were taken parallel to the bottom of the microchannel at 1 µm increments from z = 0 µm to z = 10 µm. The theoretical velocity profile for the given flow rate and fluid viscosity was compared to the velocity profile found using the average velocity computed at each plane from z = 0 µm to z = 10 µm. This comparison is shown in Figure 4.3. The comparison shows that not only is the velocity profile linear within 10 µm from the microchannel bottom, but the accuracy of the measurement plane location accessed using the BioFlux™ stage is very high at a correlation coefficient of 0.98.

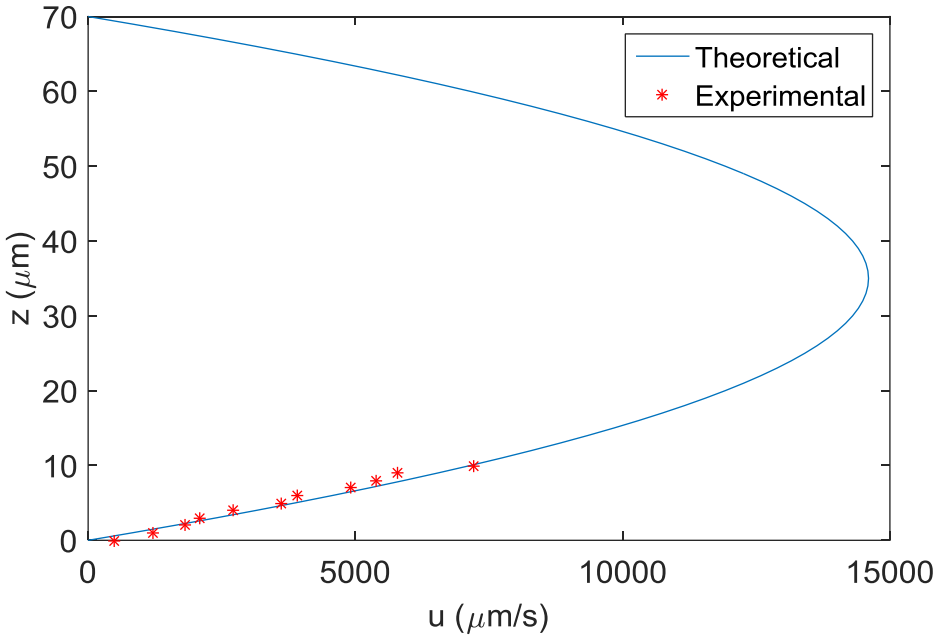

Figure 4.3: A comparison of the theoretical streamwise velocity (u) profile and the experimental velocity profile computed using average velocities for measurement planes ranging from z = 0 µm to z = 10 µm.

4.3.2 Accounting for channel tilt

In order to compute shear stress, topography, and pressure information, it was desired to position the measurement planes perfectly parallel to the bottom wall of the microchannel. Due to the inability to keep the microscope stage and the BioFlux™ plate perfectly parallel to each other, the measurement planes and the bottom wall of the microchannel were slightly tilted with respect to each other. The tilt resulted in a maximum height difference of 5 μm across the field-of-view in the *x*-*y* direction. Since measurements were taken with sub-micrometer resolution, variations in distance from the wall due to the tilt resulted in inaccurate shear stress, topography, and pressure calculations. Consequently, algorithms needed to be developed to account for the channel's tilt.

Although the microchannel bottom was technically confluent with endothelial cells, there were still micron-sized spaces between endothelial cells in which there was no cell coverage on the bottom of the microchannel - this is inevitable in cell culture. Since there were always areas between cells in which the channel bottom was present, an in-house algorithm was developed to account for tilt by analyzing the topography measurements for those areas.

The tilt-correcting algorithm utilized the original matrix of topography information for the entire field-of-view. To depict the routine of this algorithm, Figure 4.4 displays a 5 x 8 matrix of random values that serves as a condensed example of the original topography matrix (109 x 137). First, the algorithm calculated the minimum topography value for a 31 x 31 region of data (105 μm x 105 μm area) in the upper, left-hand corner of the topography matrix. In order to save space, this region is depicted as a

9 x 9 region outlined in dark black in the abbreviated example in Figure 4.4(a). Using our abbreviated example to continue explanation, the minimum height value for this square region was computed and then that value was assigned to the same 9 x 9 locations in an empty matrix depicting the running average of minimums as shown in Figure 4.4(b). Then, the 9 x 9 boxed region is moved one location to the right in the initial 5 x 8 matrix and the minimum for this new region is calculated as shown in Figure 4.4(c). This new minimum value calculated is then brought into the new 9 x 9 locations within the existing running average of minimums matrix and any data locations that possess minimum values are averaged with the new minimum value found as shown in Figure 4.4(d). This process is repeated across each column and each row of the topography matrix resulting in a running average of minimums matrix that's the same size as the topography matrix. Calculating an average minimum value ensures that any erroneous minimum values in the topography matrix are averaged out.

Once the running average of minimums matrix is calculated, it is subtracted from the topography matrix. Since the minimum topography value measured at any 105 μm x 105 μm area in the field-of-view represented the channel bottom between endothelial cells, then the final scale for topography measurements after subtraction is measured in reference to the channel bottom, and therefore, tilt is accounted for in the topography.

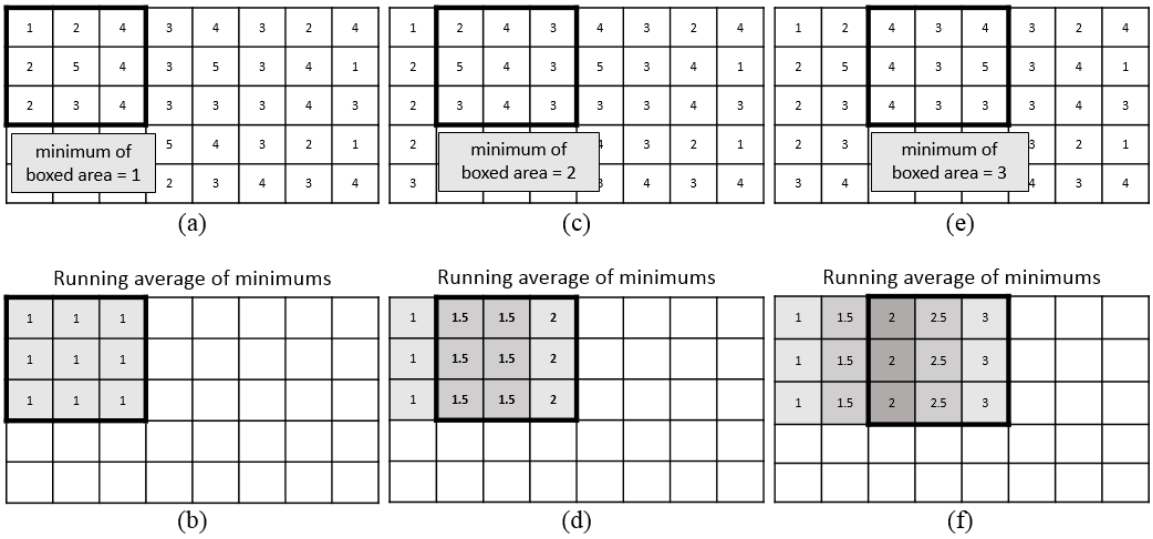

Figure 4.4: Depiction of the routine of the tilt-correcting algorithm used with topography measurements. Illustrations (a), (c), and (e) show how a minimum filter window moves across the topography matrix to calculate the running average of minimums as shown in (b), (d), and (f).

4.3.3 Shear stress and cell surface topography

The velocity profile at each *x* and *y* vector location was used to calculate the shear stress and cell surface topography for each time step. This was based on assuming a no-slip boundary condition, *i.e.*, zero velocity, at the cell and channel surface. This assumption does not take into account the effect of endothelial cilia on flow conditions at the cell surface. However, the assumption allows clear point of comparisons between different flow cases and different time points during flow experiments.

The local velocity profiles for each *x* and *y* location were found using the velocity profiles generated from multiple measurement planes from $z = 0$ μm to $z = 10$ μm as depicted in Figure 4.5. Since the velocity profile near the wall was linear, a linear regression fit of the local velocity profile was imposed to find the zero-intercept, or the

cell surface location. Performing a linear regression fit of the local velocity profile at every *x* and *y* location yielded the cell surface topography for the entire field-of-view.

In addition to cell surface topography, shear stress was calculated for each *x* and *y* vector location using the slope, *du/dz*, of the linear regression fit of the local velocity profile found at each *x* and *y* location. Once *du/dz* was calculated for every *x* and *y* vector location in the field-of-view, shear stress was calculated using

$$\tau = \mu \frac{\partial u}{\partial z} \tag{4.1}$$

where τ is shear stress, μ is the dynamic viscosity of the working fluid, and *du/dz* is the gradient of the velocity profile.

As a preliminary method to demonstrate topography measurements, a non-confluent endothelial cell culture was subjected to a shear stress of 20 dyne/cm^2.

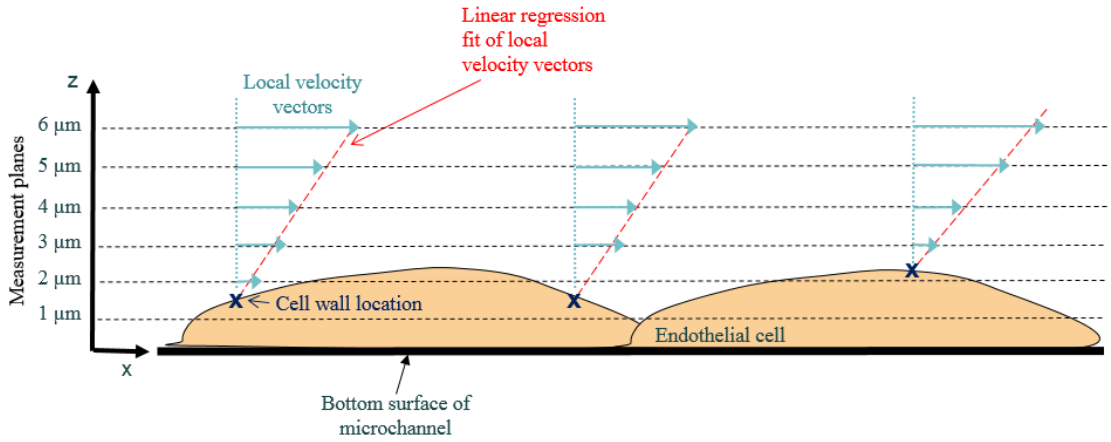

Figure 4.5: Illustration of the velocity vectors, measurement planes, and the linear regression fit used to calculate cell surface topography for sample *x* and *y* vector locations. Note that the illustration does not depict the actual number of measurement planes and is not drawn to scale.

Although the cells underwent necrosis due to phototoxicity, the perimeter of the cells was visually distinguishable during measurements. The cell surface contours computed for these cells are overlaid on an image of the cells as shown in Figure 4.6. Notice that the *x-y* positioning of the topography surface contours aligns with the location of the cell perimeters seen in the underlying image. In addition, the highest cell surface contours for each cell lie directly over the nucleus of the cell which is shown by a white-colored, circular feature on the cell. Furthermore, the cell heights found for this experiment were similar to cell height measurements found in literature using atomic force microscopy (1.8 ± 0.7 μm) [43].

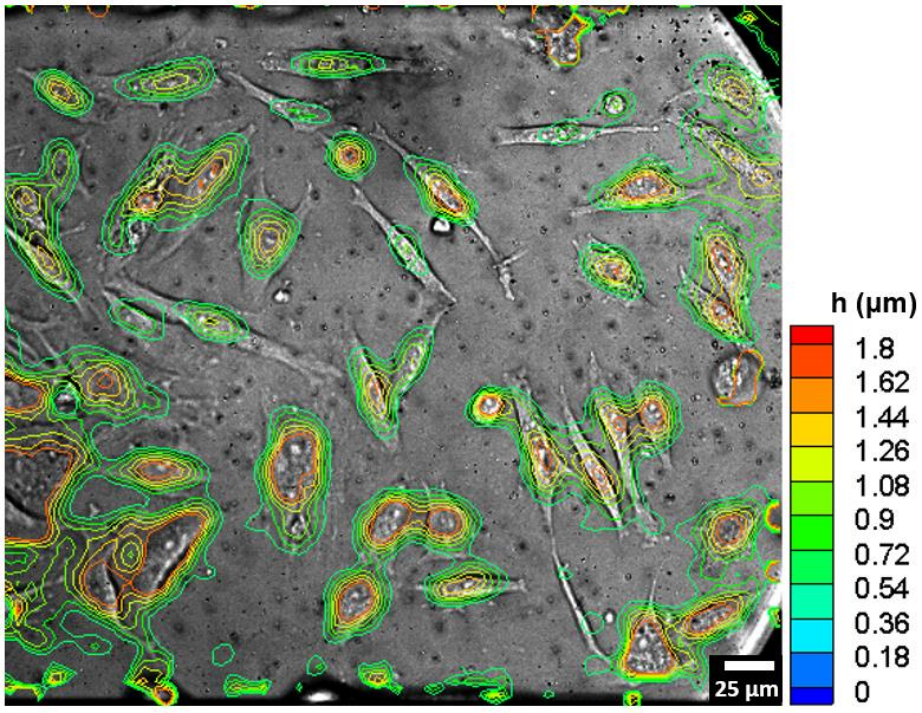

Figure 4.6: Cell surface contours computed for a non-confluent layer of necrotic bovine aortic endothelial cells for the 18th hour while subjected to an applied shear stress of 20 dynes/cm^2. The measurements were used to demonstrate the experimental methods used to compute cell surface height.

4.3.4 Pressure

Local pressure variations due to flow have not been widely studied due to experimental limitations including the ability to make measurements non-invasively. This study introduced a method to quantify local pressure variations around cells without disturbing the flow field or the cells. Although the method has not been validated, previous studies utilizing similar methods for calculating pressure have been validated with numerical modeling [52]. Therefore, pressure quantifications in this study serve as a reasonable approximation.

Pressure was calculated using an in-house MATLAB algorithm that computed a two-dimensional pressure field using a two-dimensional velocity field. Since a velocity field was computed at each measurement plane, a corresponding pressure field was able to be calculated. Given a velocity field for any given measurement place, the pressure program first solved the *x*-component of the two-dimensional Navier-Stokes equations for the streamwise pressure gradient. The pressure field was then determined by integrating the streamwise pressure gradient. The *x*-component was used for pressure calculations because the streamwise velocity fields, *u*, were able to be tilt-corrected using the algorithm mentioned in section 4.3.2, but the transverse velocity field, *v*, was not able to be tilt-corrected. Using the in-house algorithm, the velocity fields computed for each measurement plane at a given time step were analyzed using the in-house pressure code and the pressure field corresponding to each measurement plane was computed. The measurement plane closest to the endothelial cell surface without intersecting it was used to analyze pressure. This plane was chosen to limit interference in the pressure calculation due to solid object boundaries, *i.e.,* cells.

Despite using measurement planes entirely in the flow, there was still uncertainty in the pressure calculations due to the measurements plane's proximity to the cell boundaries. These wall-induced uncertainties arise because the uncertainty in velocity measurements increases near these interfaces due to the poor imaging quality at cell boundaries. The uncertainty in the pressure field can be seen in Figure 4.7(b).

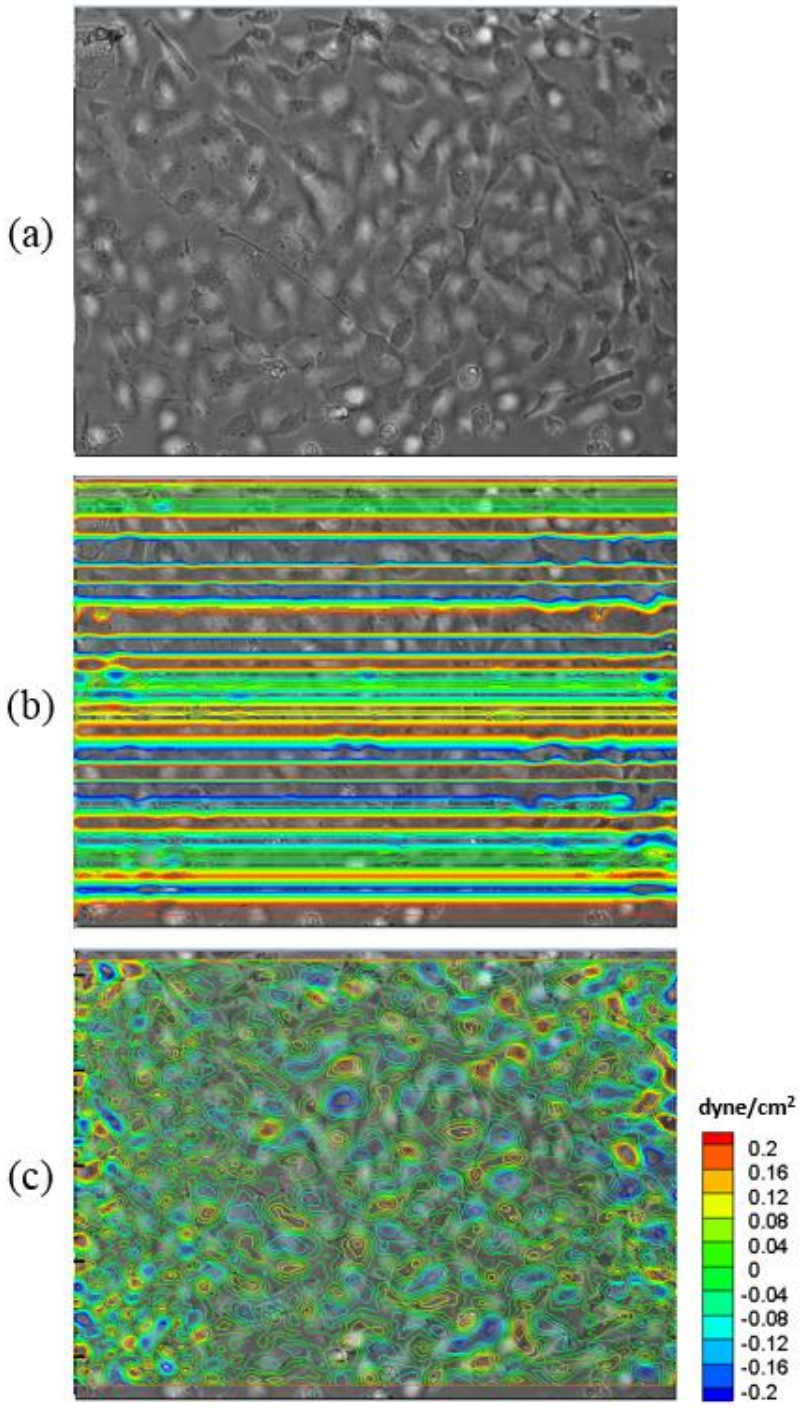

Figure 4.7: An image of BAOEC's (a) and the corresponding pressure contour plot prior to accounting for uncertainty in the pressure data (b). After applying several low-frequency polynomial filters to the pressure information in (b), the resulting pressure contour plot is shown in (c). Pressure quantifications were for confluent endothelial cells cultured on glass at the 0^{th} hour time step while subjected to an applied shear stress of 10 dynes/cm^2.

To account for uncertainty, low-wavenumber polynomials were used to filter each *y* location. Since integration paths were in the streamwise direction for each *y* location, uncertainty accumulated in the streamwise direction only. Figure 4.8 shows an unaltered pressure trace streamwise across the field-of-view for a sample *y* location. Notice the gradual decrease and then increase in the pressure trace between vector locations 45 and 110. This is an example of uncertainty accumulating in the streamwise direction during integrations. In order to account for the accumulated uncertainty in the pressure trace, a low-frequency polynomial needed to account for the gradual decline and incline of the pressure trace without removing the local fluctuations in pressure. This was done by calculating an average spline considering the maxima and minima of the pressure trace as shown in Figure 4.8. Then, the average spline was subtracted from the original pressure trace which resulted in an altered pressure trace for a given *y* location as shown in Figure 4.9. Subtracting the pressure trace not only accounted for uncertainty in the integration, but also accounted for the initial assumption that $p = 0$ at the very left-hand side of the image when integrating dp/dx from left-to-right. Applying this method for every row (*y* location) in the field-of-view resulted in the pressure field as shown in Figure 4.7(c).

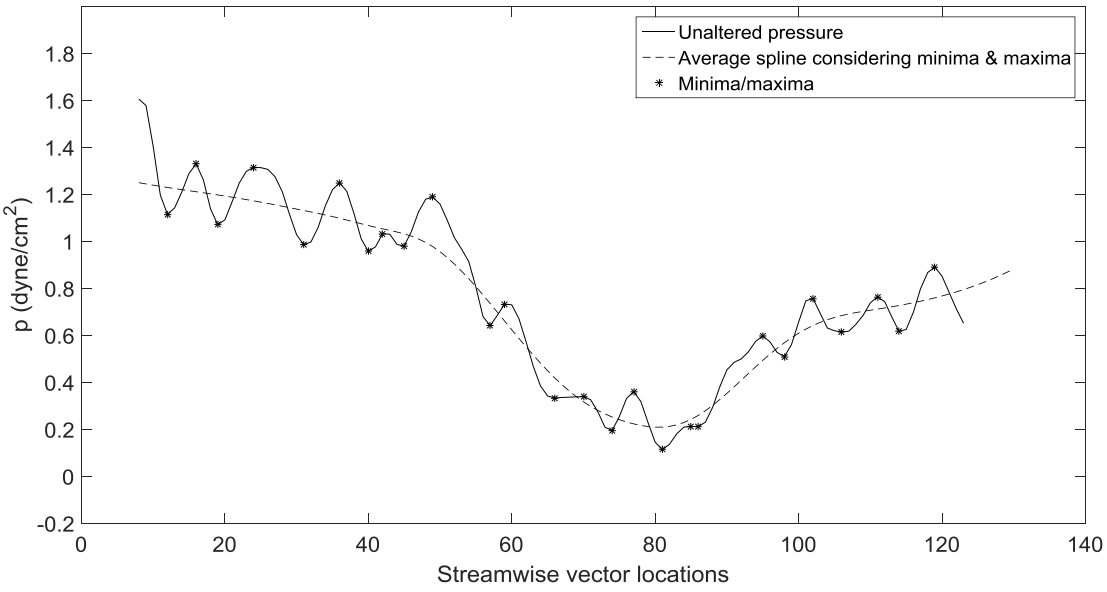

Figure 4.8: Unaltered pressure trace streamwise across the field-of-view for a sample *y* location in an unaltered pressure field. Minima and maxima were used to calculate an average spline that represented the uncertainty present in the pressure trace.

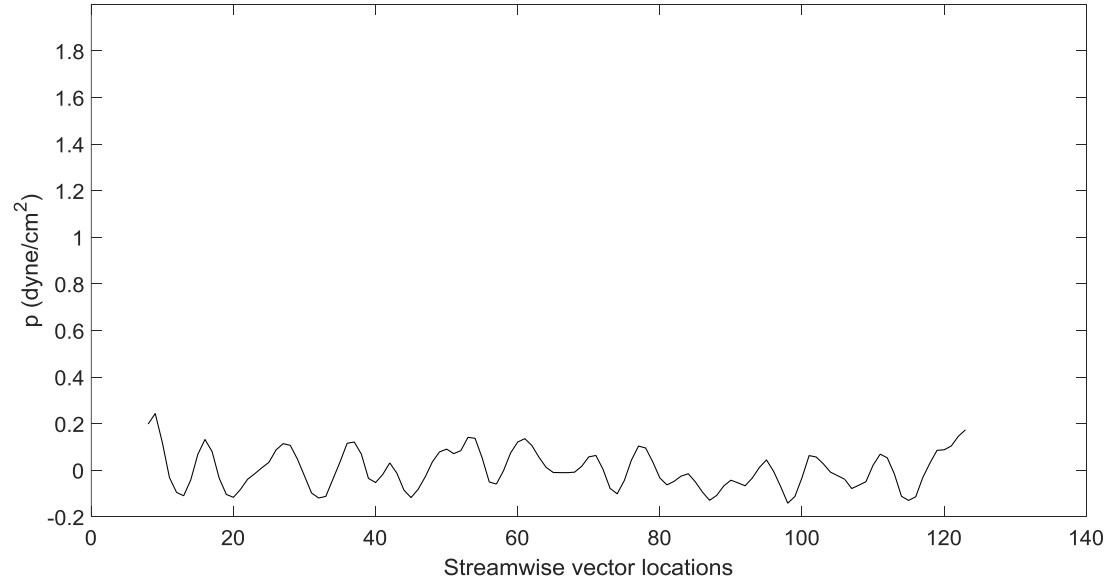

Figure 4.9: Altered pressure trace streamwise across the field-of-view for a given *y* location.

4.3.5 Cell orientation

Endothelial cell orientation was measured by implementing edge detection and region analysis algorithms from the Image Processing Toolbox in MATLAB. The perimeter of endothelial cells could be identified using the difference in contrast between a cell's boundary and the channel bottom. The orientation of each detected cell was determined by measuring the angle in degrees between the major axis with respect to the streamwise direction, or *x* direction. The angle of orientation is defined as positive in the counter-clockwise direction. Figure 4.10 shows a raw image of endothelial cells and the corresponding cell areas and major axis detected using the cell perimeter and orientation algorithms.

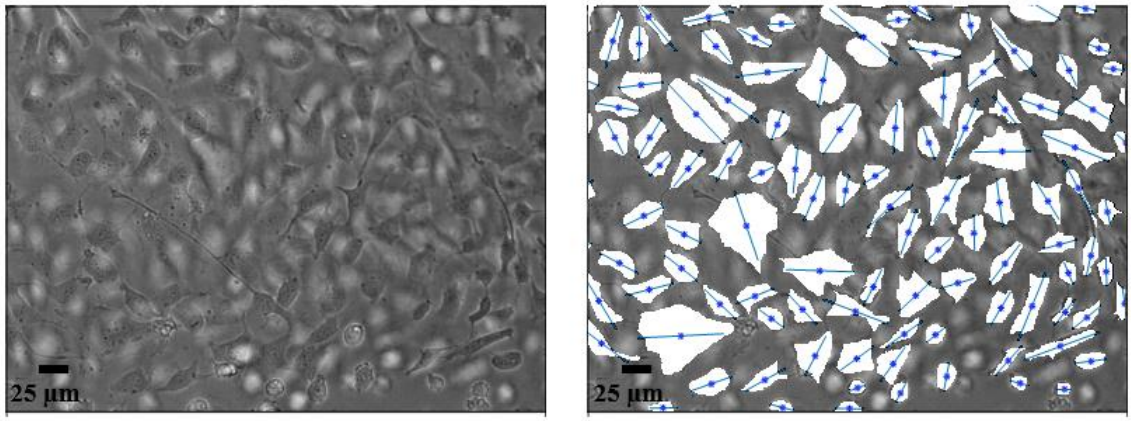

Figure 4.10: Raw brightfield image of confluent endothelial cells (a) and individual cell areas detected are filled in with white and the major axis of orientation is shown in blue (b). Flow is from left to right.

4.3.6 Averaged variations in topography, shear stress, and pressure

In order to observe changes in topography, shear stress, and pressure during a flow experiment, contour plots for each quantification were computed as shown in Figure 4.12. Although contour plots and three-dimensional surface plots are helpful to visualize data for a single data set, it is difficult to visually compare multiple data sets using these plots because isometric views in surface plots and coloring in contour plots make it difficult to compare data. For this reason, an ensemble average of the variations in topography, shear stress, and pressure along the streamwise centerline or the spanwise centerline of individual cells was computed using the information from the contour plots. The streamwise and spanwise locations with respect to an individual cell are shown in Figure 4.11. Notice that L is the streamwise length and W is the spanwise length of the endothelial cell with respect to the flow direction. These lengths are used because past studies have found that most variations in shear and cell morphology occur with respect to the direction of flow. This method allowed temporal and spatial variations in topography, shear stress, and pressure along the endothelial cell to be visualized on the same plot for multiple time steps and flow cases.

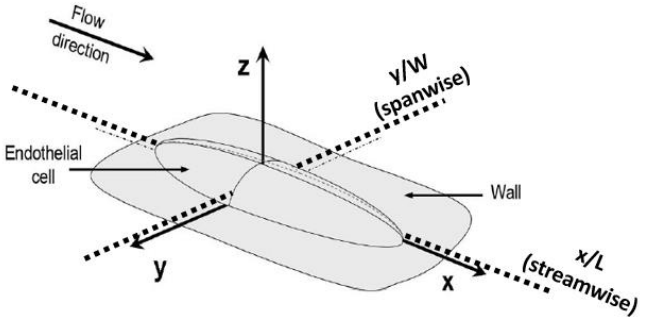

Figure 4.11: Schematic depicting the streamwise and spanwise location for cell topography, shear stress, and pressure variations in this study. Flow is along the *x*-axis, or in the streamwise direction.

In order to calculate the ensemble averages for topography, shear stress, and pressure, the MATLAB algorithm that was used to find cell perimeters like those shown in Figure 4.10 (b) was used to determine the location of individual cells. Then, the topography contour plot like the one shown in Figure 4.12 was used to determine the location of the maximum cell height for each cell identified in the previous step. Next, the streamwise length along the maximum cell height of each cell was determined by finding the upstream and downstream cell boundaries in the streamwise direction along the location of the maximum cell height. Since this dimension varied for individual cells, the streamwise location of a cell, x, was normalized by the streamwise length, L, along the location of the maximum cell height for each cell. Similarly for the spanwise direction, the spanwise location of a cell, y, was normalized by the spanwise length, W, along the location of the maximum cell height for each cell. Then, topography, shear stress, and pressure variations along the streamwise locations of 15 cells were averaged. The ensemble averages for shear stress and pressure were then normalized by the maximum shear stress at the 0^{th} hour for each flow case so that shear stress and pressure variations could be compared.

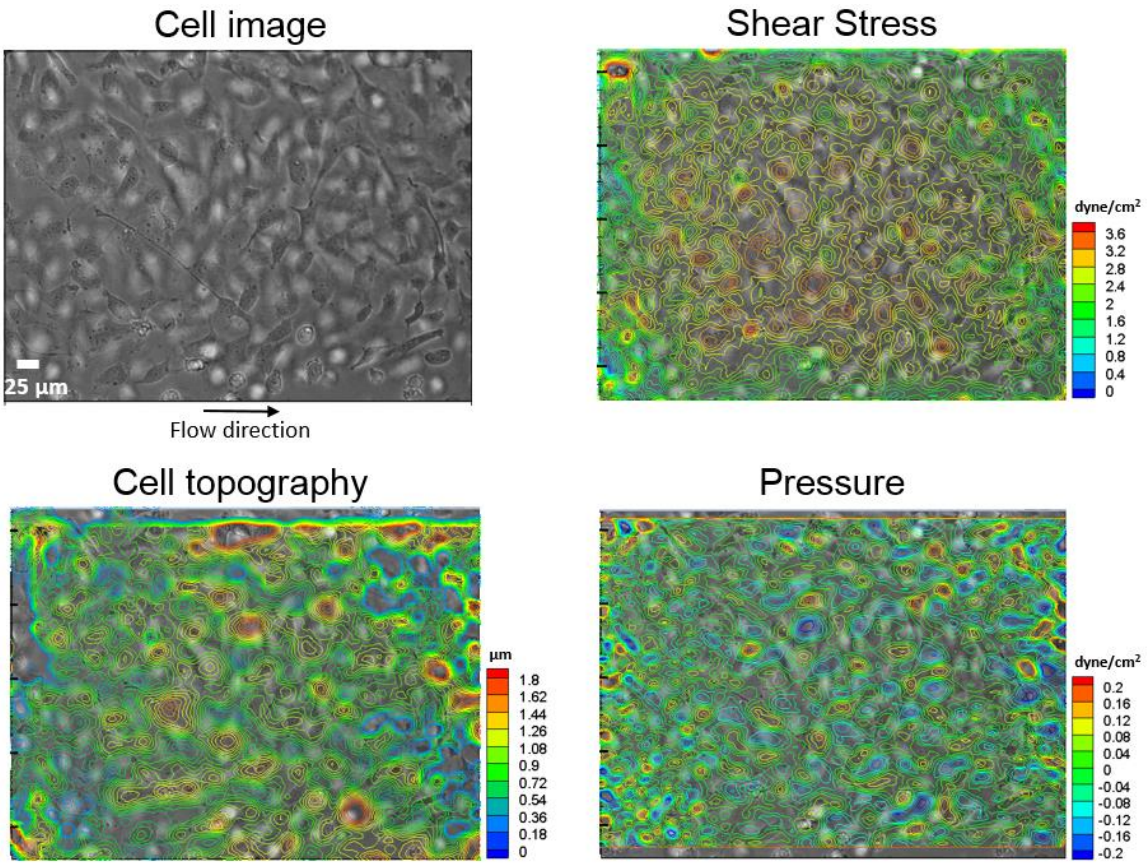

Figure 4.12: An image of confluent BAOEC's and the corresponding shear stress, cell topography, and pressure contour plots used to compute ensemble averages for each quantification. Measurements were for confluent endothelial cells cultured on glass at the 0^{th} hour time step while subjected to an applied shear stress of 10 dynes/cm^2. Flow is from left to right.

Examples of the ensemble averages for cell topography, shear stress, and pressure can be seen in Figure 4.13 in which the average topography (a), average shear stress (b), and average pressure profile (c) for the 0^{th} and 18^{th} hour time steps of a confluent layer of endothelial cells cultured on glass and subjected to an applied shear stress of 10 dyne/cm^2 are shown. The solid line indicates the mean quantification for the 0^{th} hour time step and the dotted line indicates the mean quantification for the 18^{th} hour time step. As shown in

Figure 4.13(b) and (c), the mean variations in shear stress and pressure are normalized by the maximum shear stress for a given shear rate. This allows comparisons to be made between time steps and also between mean shear stress and pressure variations.

Statistical analysis of these results was conducted using the Statistical Analysis Toolbox in MATLAB. Statistical significance was evaluated using an unpaired two-sample t-test at a significance level of 0.05. Quantifications are compared with respect to the standard error of the mean (± SE).

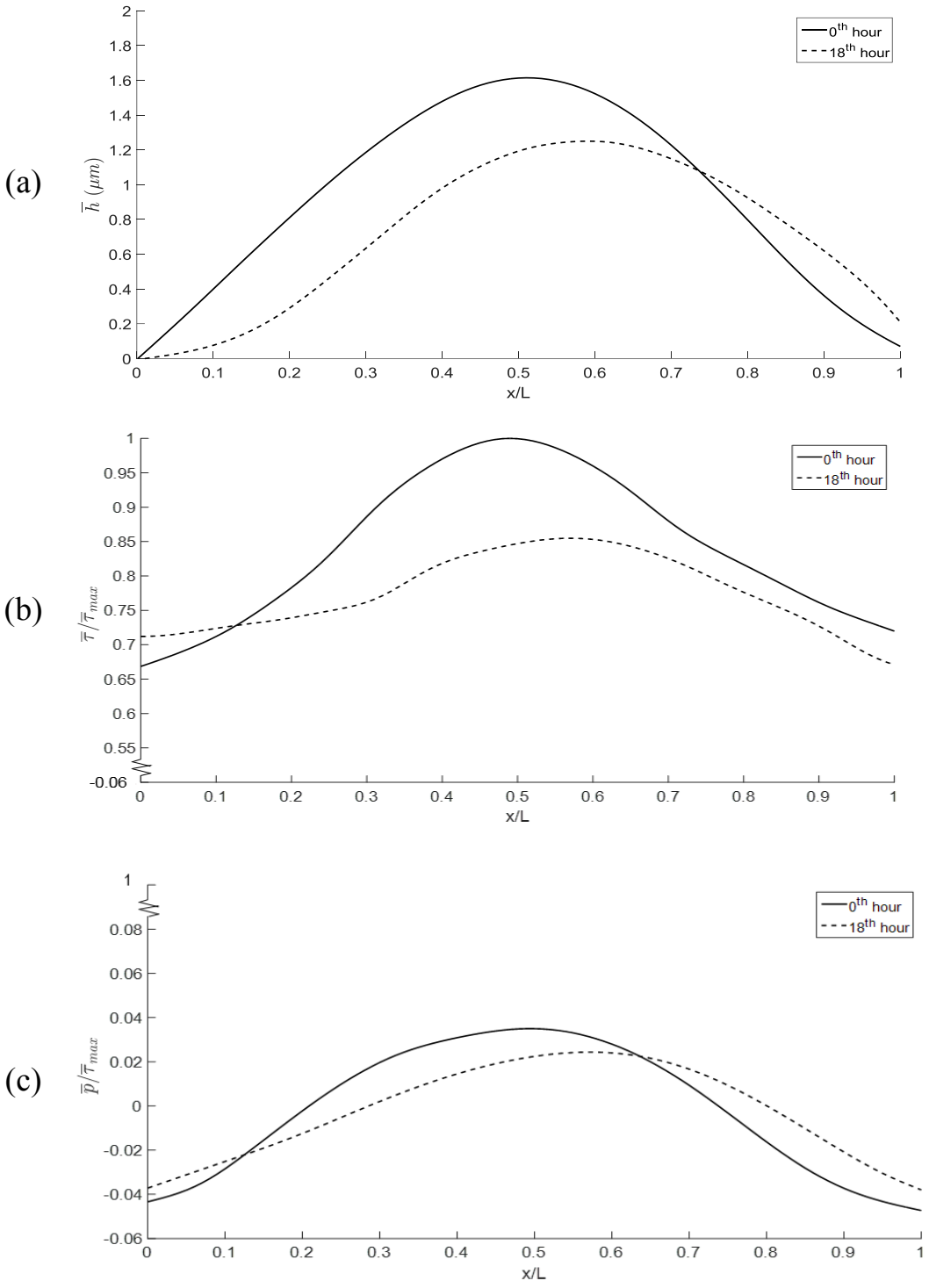

Figure 4.13: Average cell surface height (a), normalized average shear stress (b), and normalized average pressure (c) variations at the 0th and 18th hour time steps for a confluent layer of endothelial cells cultured on glass and subjected to a shear stress of 10 dyne/cm^2. Flow is from left to right.

4.3.7 Temporal evolution of endothelial cell shape

Using the method described in the previous sub-section, the mean cell height along the streamwise centerline passing through the maximum cell height was computed for each time step (0^{th}, 3^{rd}, 6^{th}, 9^{th}, 12^{th}, 15^{th} and 18^{th} hour) during flow experiments. Figure 4.14 shows the average cell topography profile computed for each time step for a confluent layer of endothelial cells cultured on glass and subjected to an applied shear stress of 10 dyne/cm^2. Using this method of data visualization, the average cell topography can be visualized for each time step in a flow experiment. As shown in Figure 4.14, the maximum average cell height decreased by 23% after 18 hours of applied flow.

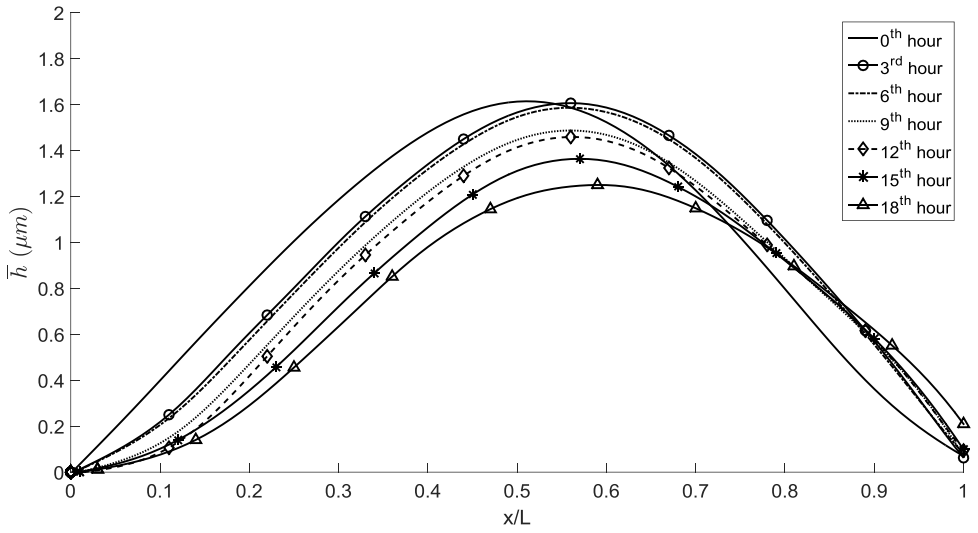

Figure 4.14: Average cell surface height along the normalized streamwise cell position for the 0^{th}, 3^{rd}, 6^{th}, 9^{th}, 12^{th}, 15^{th}, and 18^{th} hour time steps for a confluent layer of endothelial cells cultured on glass and subjected to a shear stress of 10 dyne/cm^2. Flow is from left to right.

By using the data measurement approach in Figure 4.14, temporal variations in cell height could be analyzed by comparing the maximum cell surface height of each average cell topography profile at each time step. Figure 4.15 shows the change in maximum average cell height for confluent endothelial cells cultured on glass while subjected to applied shear stresses of 5, 10, and 20 dyne/cm^2 for 18 hours. Notice that the mean cell thickness decreases with time.

In addition to maximum cell height, the streamwise locations of the average maximum cell heights were analyzed and presented in Figure 4.16. As shown, the streamwise location of the maximum cell height makes a dramatic shift downstream in the first three hours after the shear is applied. After the third hour, the streamwise location of the maximum cell height no longer changes much with time. Note that the cells do, however, continue to decrease in thickness after the third hour. It is important to note that although changes and relationships are visually observed in the figures presented in this study, not all relationships are statistically significant but those that are will be reported as so.

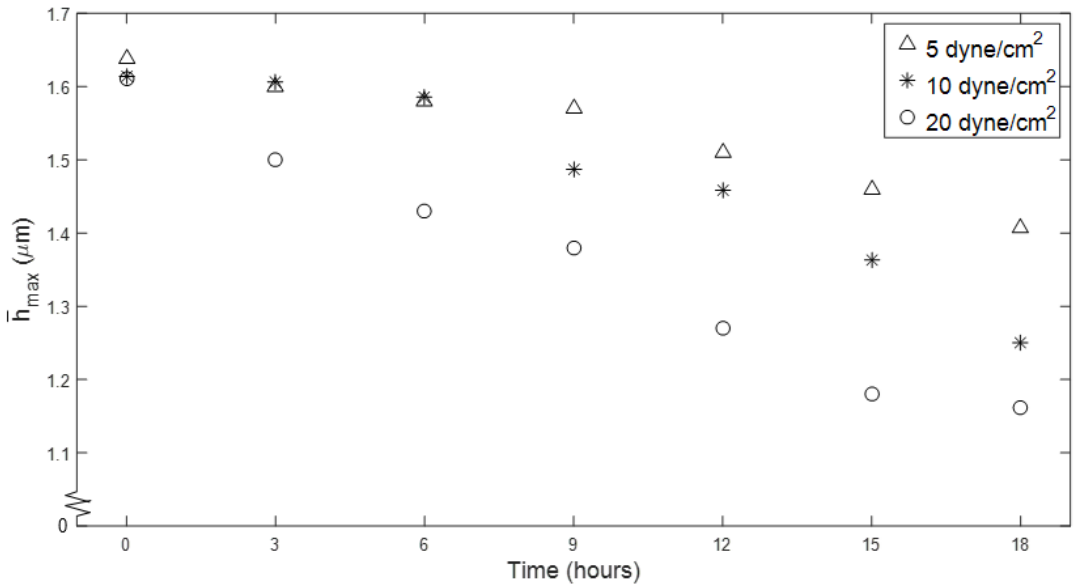

Figure 4.15: Maximum cell surface height measured at the 0th, 3rd, 6th, 9th, 12th, 15th, and 18th hour time steps for confluent layers of endothelial cells cultured on glass at applied shear stresses of 5, 10, and 20 dyne/cm^2. Flow is from left to right.

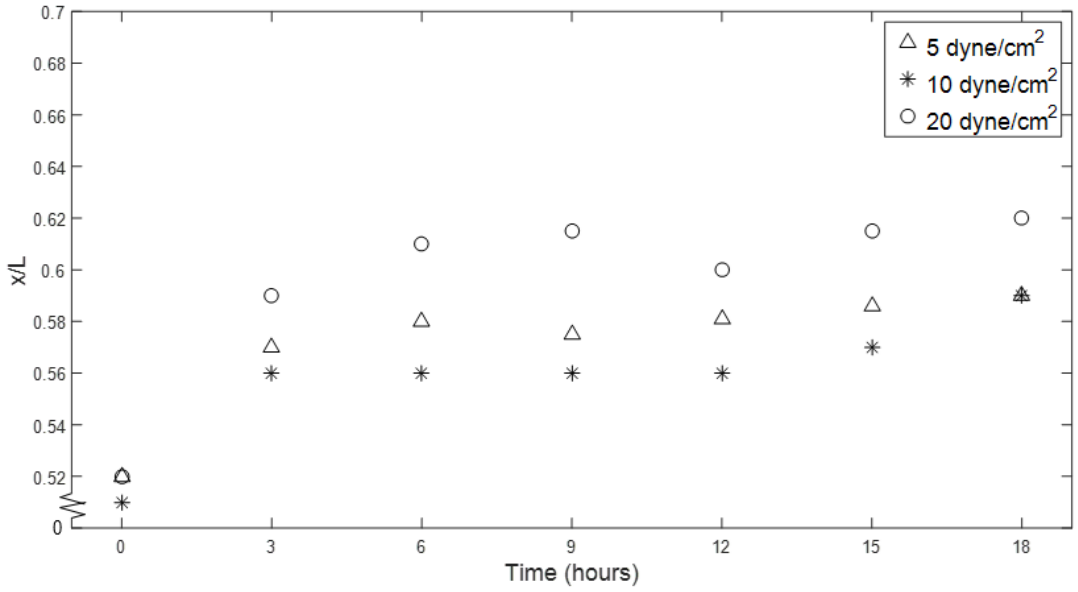

Figure 4.16: The normalized streamwise location of maximum cell height measured at the 0th, 3rd, 6th, 9th, 12th, 15th, and 18th hour time steps for confluent layers of endothelial cells cultured on glass at applied shear stresses of 5, 10, and 20 dyne/cm^2. Flow is from left to right.

CHAPTER 5

RESULTS AND DISCUSSION

The goal of this study was to develop a methodology to investigate the evolution of cardiovascular diseases on the cellular and sub-cellular level. The specific task for this phase of the investigation was to conduct μPTV experiments on living, confluent endothelial cells subjected to steady shear flow in order to measure cell morphology, shear stress, and pressure distributions. Studies were successfully conducted on confluent endothelial cells cultured on both untreated glass and fibronectin-coated glass to assess the contribution of an underlying matrix to cellular responses during shear flow. In addition, studies were successfully conducted with both normal endothelial cells and necrotic endothelial cells in order to investigate the endothelial mechanics of different cellular conditions present during cardiovascular diseases. The results of each characteristic experiment are presented and discussed in the subsequent sections.

5.1 Steady flow over endothelial cells cultured on glass

Steady flow experiments were performed on living, confluent endothelial cells cultured on untreated glass. The cells were cultured in microchannels and subjected to three different shear stresses, 5, 10, and 20 dyne/cm^2, for 18 hours. Cell surface topography, shear stress, and pressure were computed using the methods detailed in section 4.3.

5.1.1 Topography measurements

The key findings of the cell topography analysis for flow experiments at 5, 10, and 20 dyne/cm^2 are shown in Figure 5.1, Figure 5.2, and Figure 5.3, respectively. The variation of the average cell surface thickness is shown with respect to normalized

streamwise position along the cell. The solid line depicts the mean cell height at the 0^{th} hour and the dotted line depicts the mean cell height at the 18^{th} hour. The streamwise cell location and the average cell height were computed as described in section 4.3.6. Although the average cell surface thickness was calculated every three hours during the course of each 18-hour flow experiment as previously shown in Figure 4.14, results are shown for the 0^{th} hour and 18^{th} hour time steps only.

Using the results in Figure 5.1 - Figure 5.3, the differential of the maximum cell surface height between the 0^{th} and 18^{th} hour time steps could be computed for each flow experiment. The change in maximum average cell surface height from the 0^{th} hour to the 18^{th} hour time step for flow experiments at 5, 10, and 20 dyne/cm^2 were -0.23 ± 0.15 μm, -0.36 ± 0.15 μm, and -0.45 ± 0.15 μm, respectively. There was a statistically significant reduction in the maximum mean cell height after 18 hours of applied flow at 20 dyne/cm^2 ($t(28) = 2.10$, $p < 0.05$). However, there was not a statistically significant reduction in the maximum mean cell height after 18 hours of applied flow at 5 or 10 dyne/cm^2. This relationship is discussed in further detail in subsequent sections discussing shear stress and pressure distributions.

In addition, the differential of the streamwise location of the maximum cell height between the 0^{th} and 18^{th} hour time steps was computed using Figure 5.1 - Figure 5.3. The changes in the streamwise location of the maximum cell surface height from the 0^{th} hour to the 18^{th} hour time step for flow experiments at 5, 10, and 20 dyne/cm^2 were +0.07 ± 0.02, +0.08 ± 0.02, and +0.10 ± 0.02, respectively. There was a statistically significant downstream shift in the streamwise location of the maximum mean cell height from the 0^{th} hour to the 18^{th} hour for applied flows at 5 dyne/cm^2 ($t(28) = 2.43$, $p < 0.05$), 10

dyne/cm^2 ($t(28) = 2.77$, $p < 0.05$), and 20 dyne/cm^2 ($t(28) = 3.47$, $p < 0.05$). A comparison of the streamwise cell topography for all shear rates at the 0th and 18th hour is shown in Figure 5.4. As mentioned previously, this relationship is discussed further in subsequent sections discussing shear stress and pressure distributions.

For each applied shear rate, the streamwise cell topography decreased on the upstream side of the cell after 18 hours of applied flow. This was consistent with findings from Ohashi *et al.* that observed this same upstream morphology change using AFM on sheared cells [53]. The sheared cell heights found in this study (1.2 ± 0.15 μm) were more closely related with Ohashi *et al.* (1.2 ± 0.4 μm) than Barbee *et al*. (1.8 ± 0.7 μm) [43, 53]. Although, both studies observed a 45+% decrease in cell height for endothelial cells subjected to flow. This was higher than the highest percent reduction in cell height for this study which was 28% for cells subjected to 20 dyne/cm^2. However, a similar study by Sato *et al.* found that BAOECs did not significantly change height after 6 or 24 hours of applied flow [54]. The subject of cell height reduction under shear flow remains controversial.

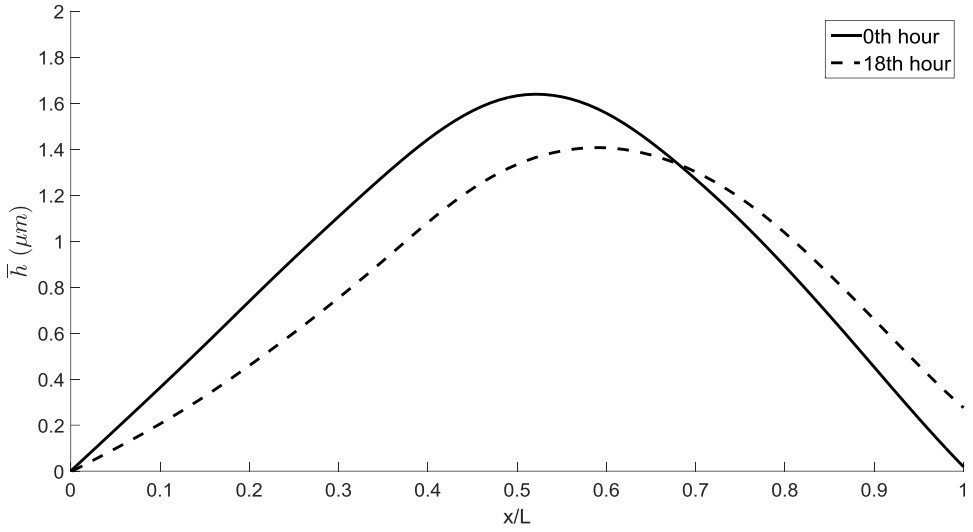

Figure 5.1: Average cell surface height variations along the normalized streamwise cell length at the 0th and 18th hour time steps for a confluent layer of endothelial cells cultured on glass and subjected to a shear stress of 5 dyne/cm^2. Flow is from left to right.

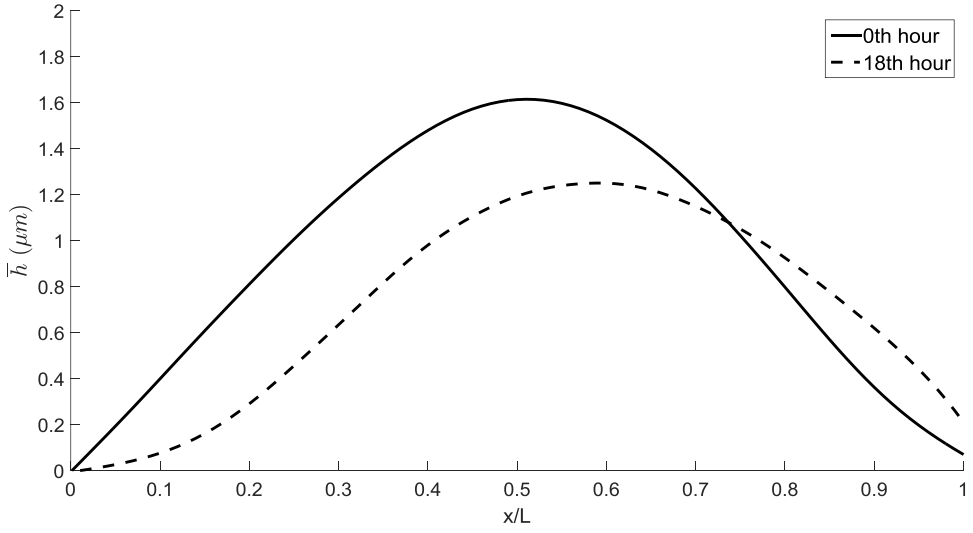

Figure 5.2: Average cell surface height variations along the normalized streamwise cell length at the 0th and 18th hour time steps for a confluent layer of endothelial cells cultured on glass and subjected to a shear stress of 10 dyne/cm^2. Flow is from left to right.

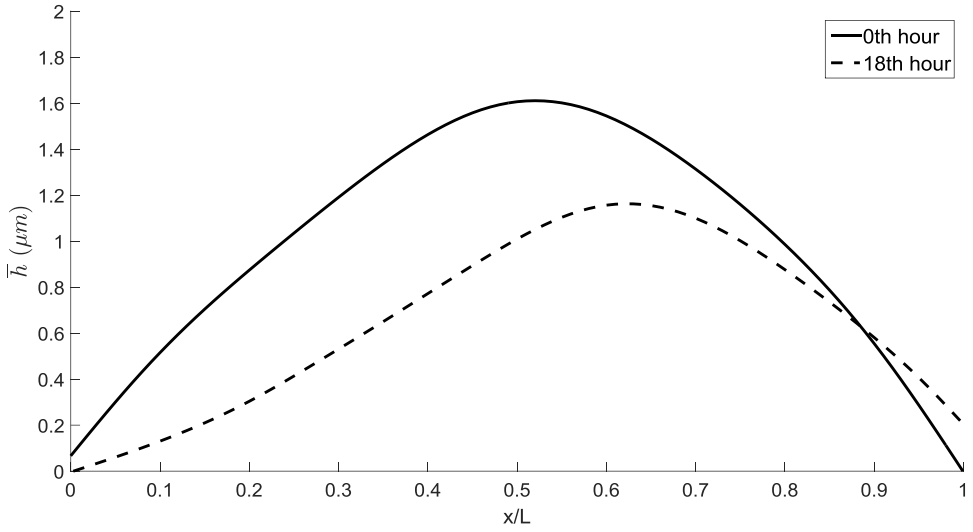

Figure 5.3: Average cell surface height variations along the normalized streamwise cell length at the 0th and 18th hour time steps for a confluent layer of endothelial cells cultured on glass and subjected to a shear stress of 20 dyne/cm^2. Flow is from left to right.

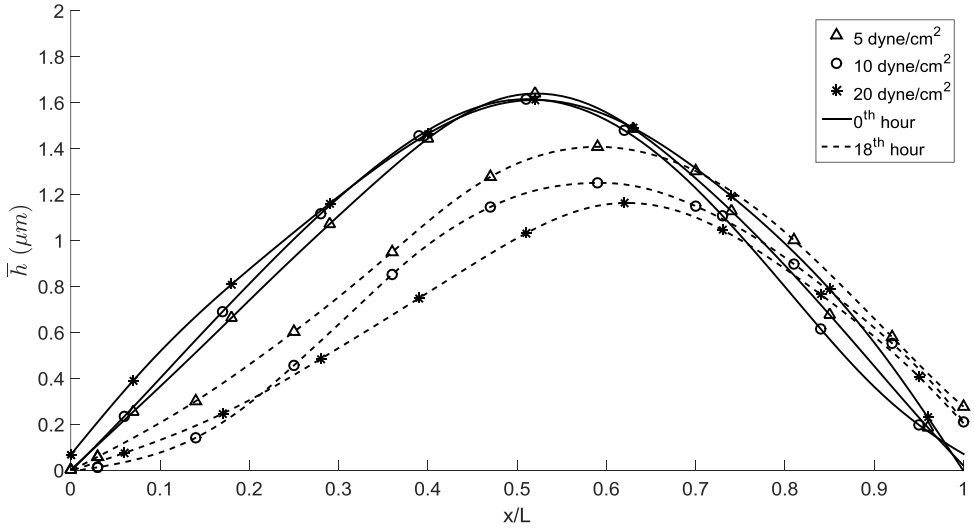

Figure 5.4: Average cell surface height variations along the normalized streamwise cell length at the 0th and 18th hour time steps for a confluent layer of endothelial cells cultured on glass at applied shear stresses of 5, 10, and 20 dyne/cm^2. Flow is from left to right.

In addition to streamwise variations in topography, spanwise variations in topography were also computed for flow experiments at 5, 10, and 20 dyne/cm^2 and are shown in Figure 5.5, Figure 5.6, and Figure 5.7, respectively. The variation in the average cell surface thickness is shown with respect to normalized spanwise position along the cell. The solid line depicts the mean cell height at the 0th hour and the dotted line depicts the mean cell height at the 18th hour. The spanwise cell location and the average cell height were computed as described in section 4.3.6.

The maximum cell height of the spanwise topography was the same as the maximum cell height of the streamwise topography for each applied shear stress. This was expected because streamwise and spanwise variations were taken with respect to the location of the maximum cell height. Notice that the cell height decreased near the center of the cell and increased towards the edges of the cell in the spanwise topography after 18 hours of applied flow. When assessing the assumption of a fixed volume cell, the decrease in the area considering the streamwise topography is approximately similar to the increase in area for spanwise topography after applied flow. This is consistent with findings that cells will retain a fixed volume during morphology change unless there is a change in the osmotic balance of the cell due to the transport of ions [55-56]. However, an ion imbalance would affect the integrity of the cell overtime which was not the case for this study. In addition, these results indicated cell reshaping which is a mechanism of minimizing drag and reducing the total force acting on a cell's nuclei [56].

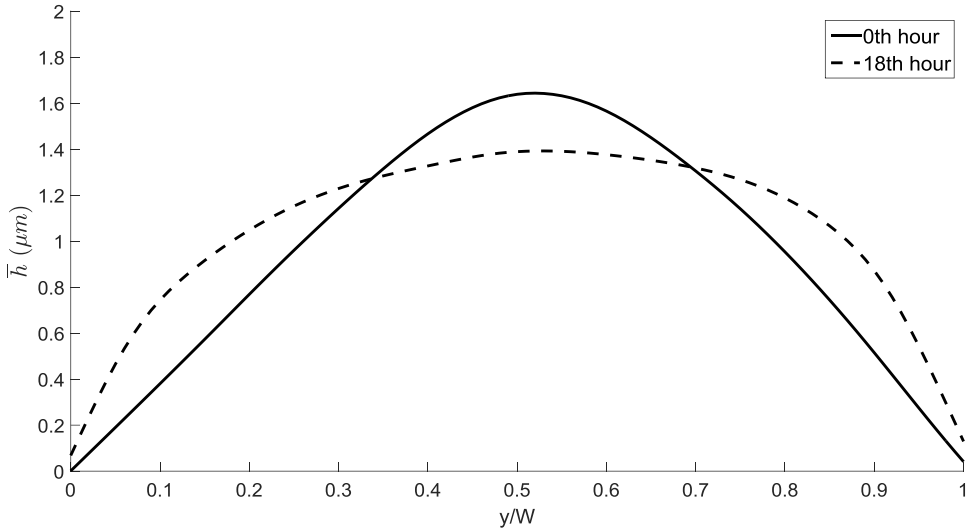

Figure 5.5: Average cell surface height variations along the normalized spanwise cell length at the 0th and 18th hour time steps for a confluent layer of endothelial cells cultured on glass and subjected to a shear stress of 5 dyne/cm^2. Flow direction is normal to the image.

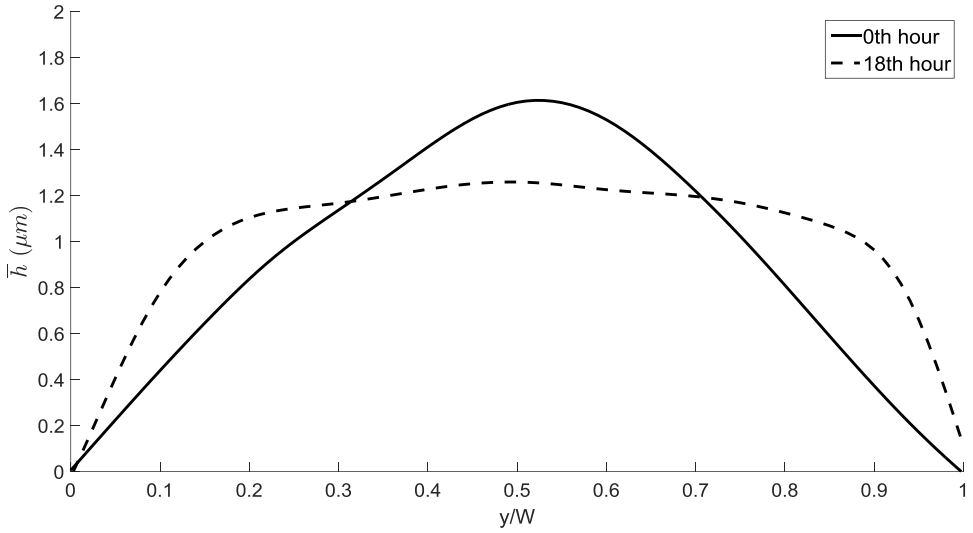

Figure 5.6: Average cell surface height variations along the normalized spanwise cell length at the 0th and 18th hour time steps for a confluent layer of endothelial cells cultured on glass and subjected to a shear stress of 10 dyne/cm^2. Flow direction is normal to the image.

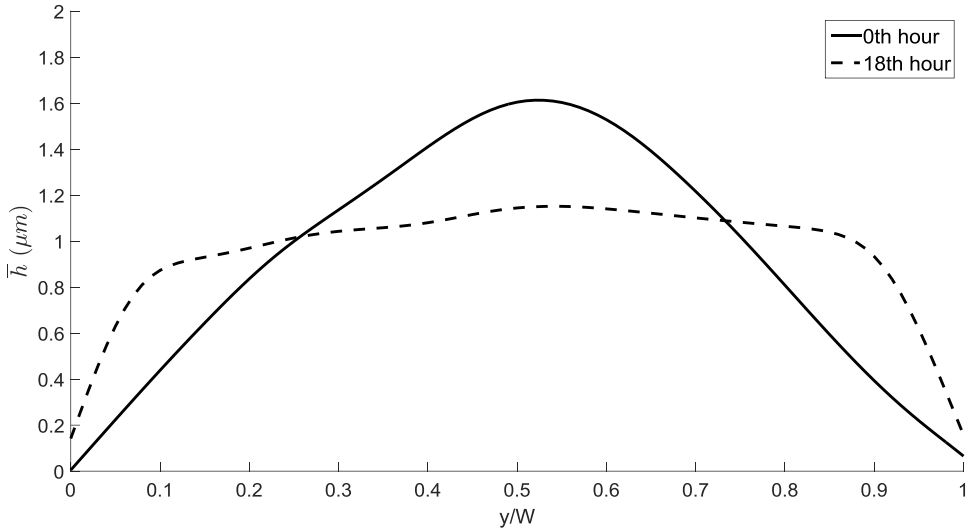

Figure 5.7: Average cell surface height variations along the normalized spanwise cell length at the 0th and 18th hour time steps for a confluent layer of endothelial cells cultured on glass and subjected to a shear stress of 20 dyne/cm^2. Flow direction is normal to the image.

5.1.2 Shear stress measurements

The key findings of the shear stress analysis for flow experiments at 5, 10, and 20 dyne/cm^2 are shown in Figure 5.8, Figure 5.9, and Figure 5.10, respectively. These figures show the variation in average shear stress with respect to normalized streamwise position along the cell. The solid line depicts the mean shear stress at the 0th hour and the dotted line depicts the mean shear stress at the 18th hour. The streamwise cell location and the average shear stress variations were computed as described in section 4.3.6.

Using the results in Figure 5.8 - Figure 5.10, the differential of the maximum shear stress between the 0th and 18th hour time steps were computed for each flow experiment. The changes in maximum average shear stress from the 0th hour to the 18th hour time step for flow experiments at 5, 10, and 20 dyne/cm^2 were -0.30 ± 0.21

dyne/cm^2, -0.48 ± 0.21 dyne/cm^2, and -0.61 ± 0.21 dyne/cm^2, respectively. There was a statistically significant reduction in the maximum mean shear stress after 18 hours of applied flow at 20 dyne/cm^2 ($t(28) = 2.09$, $p < 0.05$). In this regard, there was statistically significant reduction in cell height and shear stress at 20 dyne/cm^2. This was consistent with findings by Ohashi *et al.* that found a decrease in shear stress with a decrease in cell height for the same applied shear rate [53]. However, for this study, there was not a statistically significant reduction in the maximum mean shear stress after 18 hours of applied flow at 5 or 10 dyne/cm^2. Although studies by Barbee *et al.* found a decrease in cell height and shear stress, flow experiments were conducted at 12 dyne/cm^2 [43].

Furthermore, the differential of the streamwise location of the maximum shear stress between the 0th and 18th hour time steps was computed using Figure 5.8 - Figure 5.10. The changes in the streamwise location of the maximum shear stress from the 0th hour to the 18th hour time step for flow experiments at 5, 10, and 20 dyne/cm^2 were +0.07 ± 0.02, +0.08 ± 0.02, and +0.10 ± 0.02, respectively. There was a statistically significant downstream shift in the streamwise location of the maximum mean shear stress from the 0th hour to the 18th hour for applied flows at 5 dyne/cm^2 ($t(28) = 2.43$, $p < 0.05$), 10 dyne/cm^2 ($t(28) = 2.78$, $p < 0.05$), and 20 dyne/cm^2 ($t(28) = 3.44$, $p < 0.05$). A comparison of the streamwise shear stress variations for all shear rates at the 0th and 18th hour is shown in Figure 5.11. Furthermore, the location of the maximum shear stress was approximately centered at the location of the maximum cell height for all shear rates indicating that the shear stress was related to the streamwise cell height, as mentioned previously. This relationship between location of maximum shear stress and location of maximum cell height was consistent with several studies [29, 43, 53, 57].

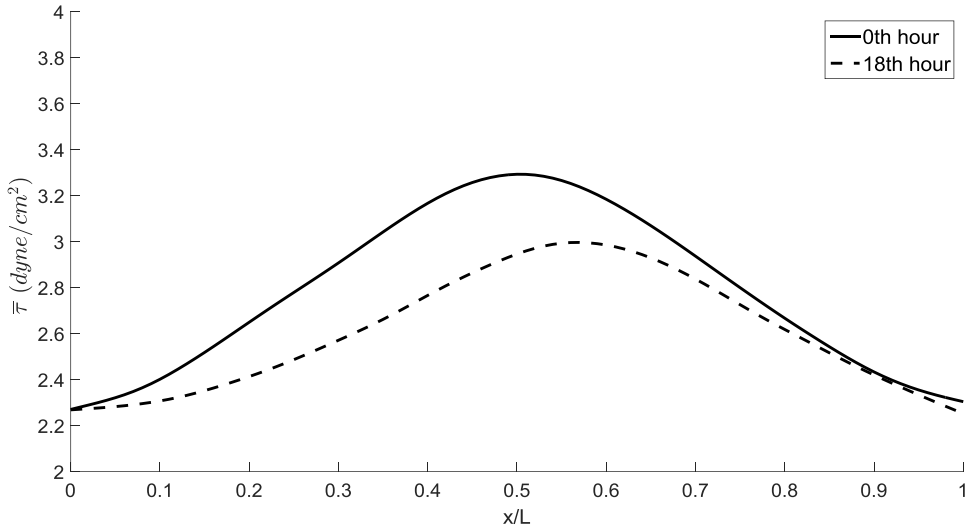

Figure 5.8: Average shear stress variations along the normalized streamwise cell length at the 0th and 18th hour time steps for a confluent layer of endothelial cells cultured on glass and subjected to a shear stress of 5 dyne/cm^2. Flow is from left to right.

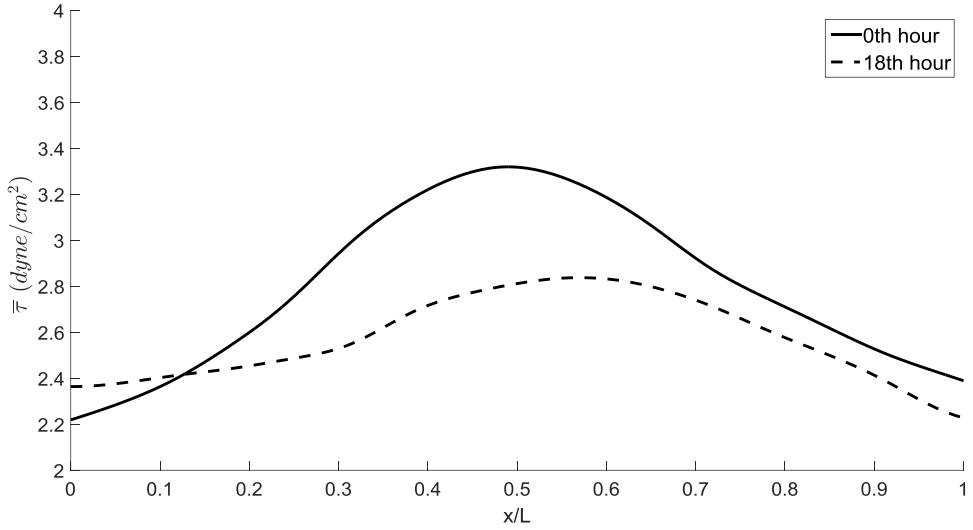

Figure 5.9: Average shear stress variations along the normalized streamwise cell length at the 0th and 18th hour time steps for a confluent layer of endothelial cells cultured on glass and subjected to a shear stress of 10 dyne/cm^2. Flow is from left to right.

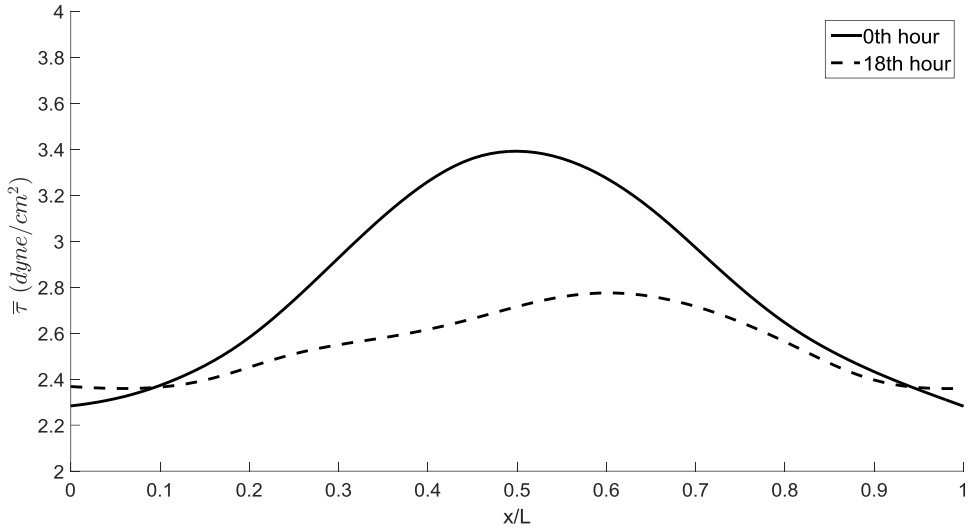

Figure 5.10: Average shear stress variations along the normalized streamwise cell length at the 0th and 18th hour time steps for a confluent layer of endothelial cells cultured on glass and subjected to a shear stress of 20 dyne/cm^2. Flow is from left to right.

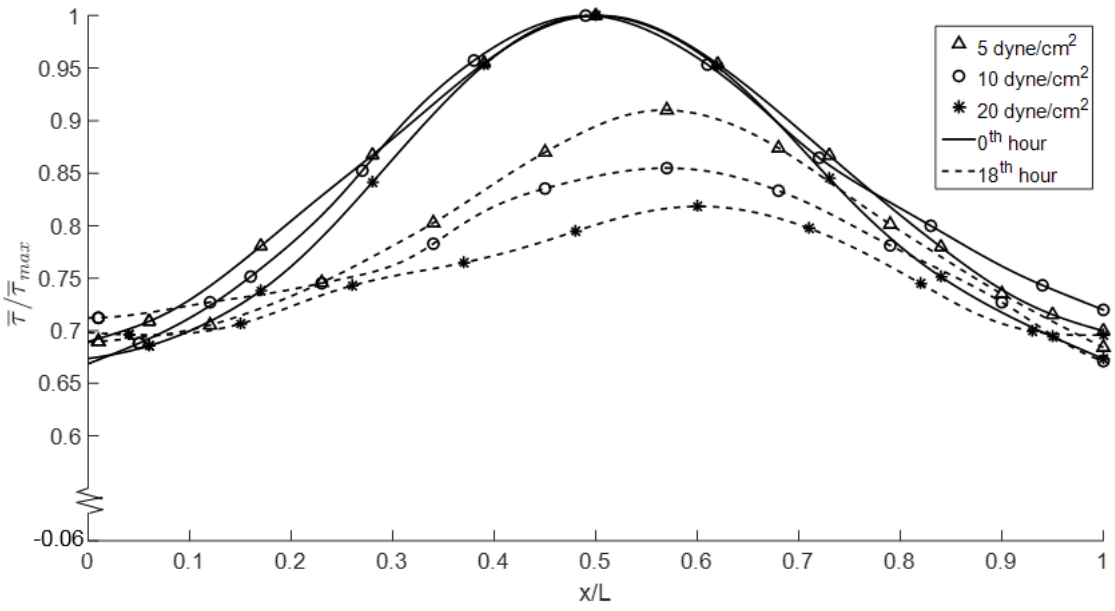

Figure 5.11: Normalized average shear stress variations along the normalized streamwise cell length at the 0th and 18th hour time steps for a confluent layer of endothelial cells cultured on glass at applied shear stresses of 5, 10 and 20 dyne/cm^2. Flow is from left to right.

5.1.3 Pressure measurements

The key findings of the pressure analysis for flow experiments at 5, 10, and 20 dyne/cm^2 are shown in Figure 5.12, Figure 5.13, and Figure 5.14, respectively. These figures show the variation in average pressure with respect to normalized streamwise position along the cell. The streamwise cell location and the average pressure variations were computed as described in section 4.3.6.

Using the results in Figure 5.12 - Figure 5.14, the differential of the maximum pressure between the 0th time step and 18th hour time step was computed for each flow experiment. The changes in the maximum average pressure from the 0th hour to the 18th hour time step for flow experiments at 5, 10, and 20 dyne/cm^2 were -0.02 ± 0.02 dyne/cm^2, -0.03 ± 0.02 dyne/cm^2, and -0.06 ± 0.02 dyne/cm^2, respectively. There was a statistically significant reduction in the maximum mean pressure after 18 hours of applied flow at 20 dyne/cm^2 ($t(28) = 2.10$, $p < 0.05$). However, there was not a statistically significant reduction in the maximum mean pressure after 18 hours of applied flow at 5 or 10 dyne/cm^2.

Additionally, the differential of the streamwise location of the maximum pressure between the 0th and 18th hour time steps was computed using Figure 5.12 - Figure 5.14. The changes in the streamwise location of the maximum pressure from the 0th hour to the 18th hour time step for flow experiments at 5, 10, and 20 dyne/cm^2 were +0.07 ± 0.02, +0.08 ± 0.02, and +0.10 ± 0.02, respectively. There was a statistically significant downstream shift in the streamwise location of the maximum mean pressure from the 0th hour to the 18th hour for applied flows at 5 dyne/cm^2 ($t(28) = 2.42$, $p < 0.05$), 10 dyne/cm^2 ($t(28) = 2.76$, $p < 0.05$), and 20 dyne/cm^2 ($t(28) = 3.47$, $p < 0.05$). A

comparison of the streamwise pressure variations for all shear rates at the 0th and 18th hour is shown in Figure 5.15. Furthermore, the location of the maximum pressure was approximately centered at the location of the maximum cell height and the location of maximum shear stress indicating a relationship between the local shear stress, pressure, and streamwise cell height. This is also another potential indicator that endothelial cells could be altering their morphology to reduce hemodynamic loading.

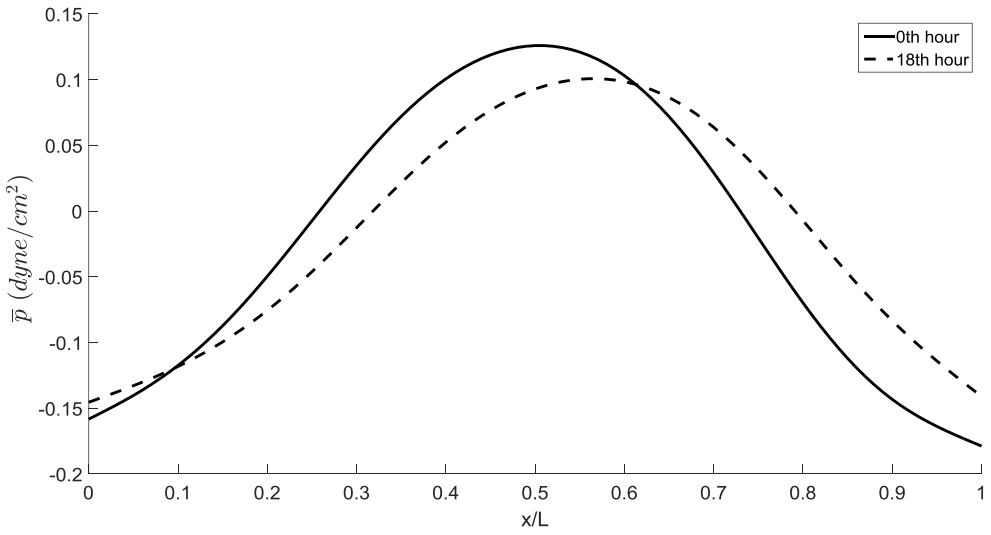

Figure 5.12: Average pressure variations along the normalized streamwise cell length at the 0th and 18th hour time steps for a confluent layer of endothelial cells cultured on glass and subjected to a shear stress of 5 dyne/cm^2. Flow is from left to right.

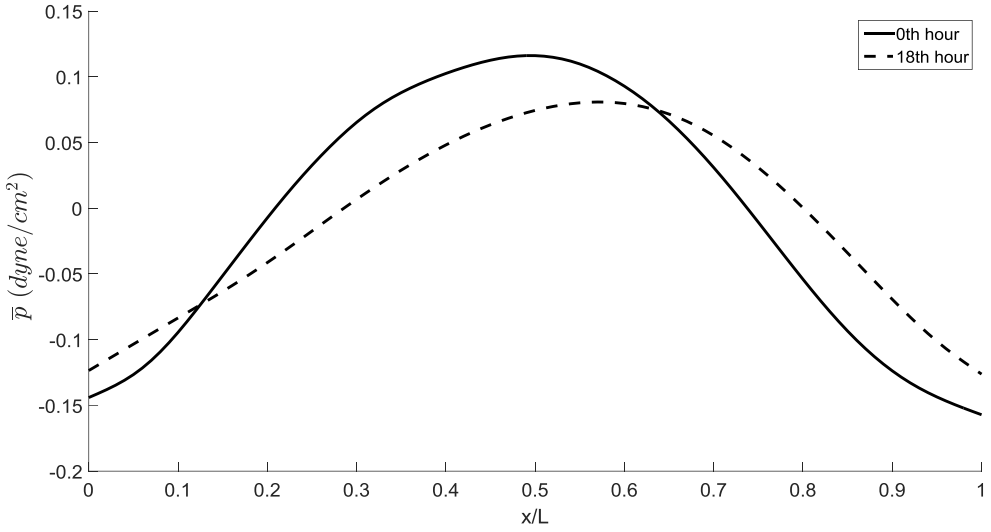

Figure 5.13: Average pressure variations along the normalized streamwise cell length at the 0th and 18th hour time steps for a confluent layer of endothelial cells cultured on glass and subjected to a shear stress of 10 dyne/cm^2. Flow is from left to right.

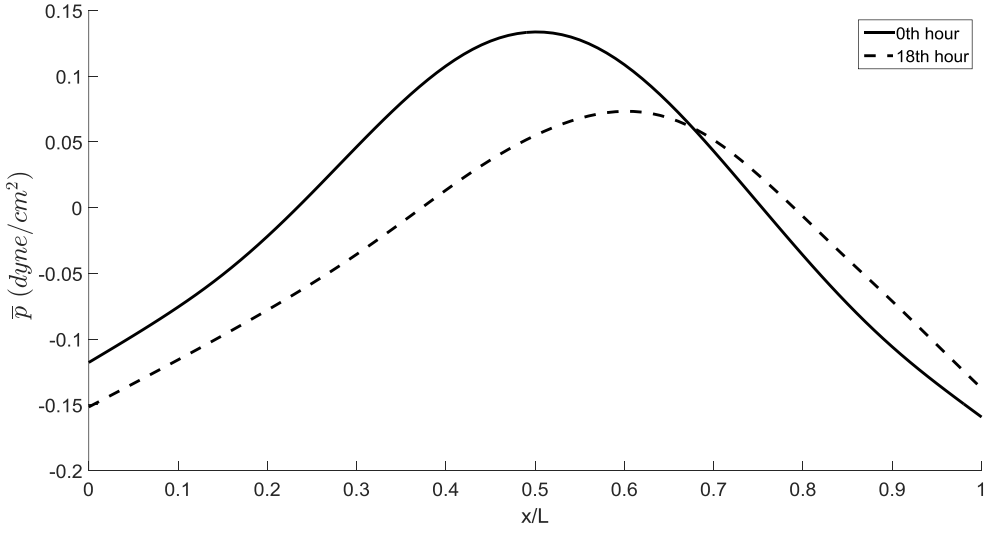

Figure 5.14: Average pressure variations along the normalized streamwise cell length at the 0th and 18th hour time steps for a confluent layer of endothelial cells cultured on glass and subjected to a shear stress of 20 dyne/cm^2. Flow is from left to right.

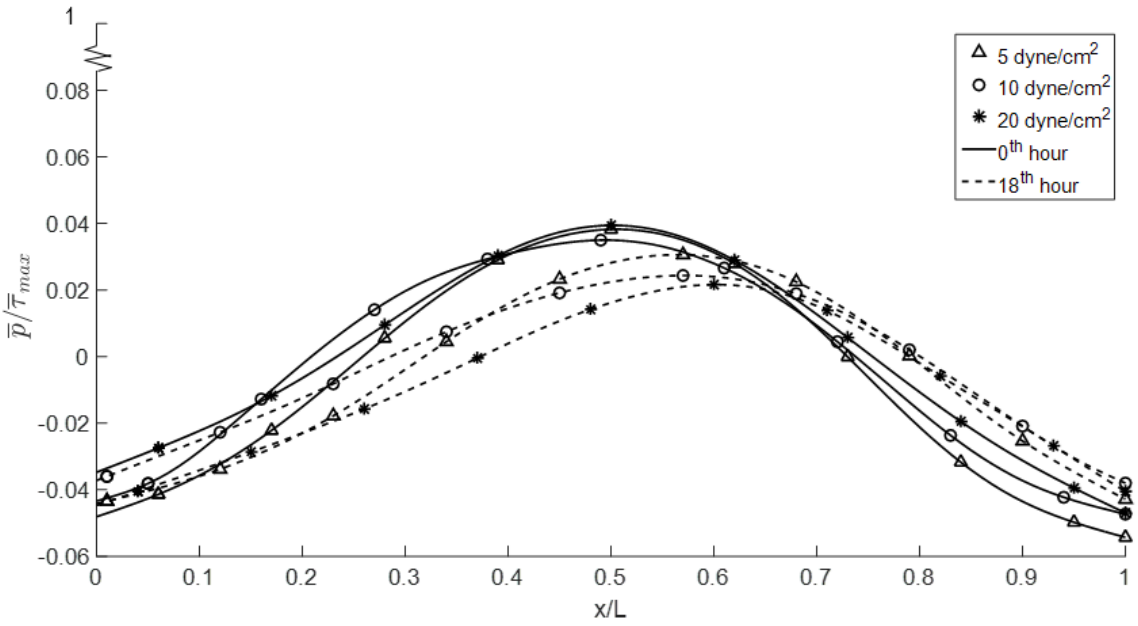

Figure 5.15: Normalized average pressure variations along the normalized streamwise cell length at the 0th and 18th hour time steps for a confluent layer of endothelial cells cultured on glass at applied shear stresses of 5, 10, and 20 dyne/cm^2. Flow is from left to right.

5.2 Steady flow over endothelial cells cultured on fibronectin

Steady flow experiments were performed on living, confluent endothelial cells cultured on fibronectin. The cells were cultured in fibronectin-coated microchannels and subjected to two different shear stresses (5 and 20 dyne/cm^2) for 18 hours. Cell surface topography, shear stress, and pressure were computed using the methods detailed in section 4.3.

5.2.1 Topography measurements

The key findings of the cell surface topography analysis for flow experiments at 5 and 20 dyne/cm^2 are shown in Figure 5.16 and Figure 5.17, respectively. These figures show the variation in the average cell surface thickness with respect to normalized

streamwise position along the cell. The streamwise cell location and the average cell surface profile were computed as described in section 4.3.6.

Using the results in Figure 5.16 and Figure 5.17, the differential of the maximum cell surface height between the 0^{th} and 18^{th} hour time steps was computed for each flow experiment. The changes in maximum average cell surface height from the 0^{th} hour to the 18^{th} hour time step for flow experiments at 5 and 20 dyne/cm^2 were -0.26 ± 0.15 μm and -0.44 ± 0.15 μm, respectively. There was a statistically significant reduction in the maximum mean cell height after 18 hours of applied flow at 20 dyne/cm^2 ($t(28) = 2.11$, $p < 0.05$). However, there was not a statistically significant reduction in the maximum mean cell height after 18 hours of applied flow at 5 dyne/cm^2.

In addition, the differential of the streamwise location of the maximum cell surface height between the 0^{th} and 18^{th} hour time steps was computed using Figure 5.16 and Figure 5.17. The change in the streamwise location of the maximum cell surface height from the 0^{th} hour to the 18^{th} hour time step for flow experiments at 5 and 20 dyne/cm^2 were +0.06 ± 0.02 and +0.09 ± 0.02, respectively. There was a statistically significant downstream shift in the streamwise location of the maximum mean cell height from the 0^{th} hour to the 18^{th} hour for applied flows at 5 dyne/cm^2 ($t(28) = 2.08$, $p < 0.05$), and 20 dyne/cm^2 ($t(28) = 3.12$, $p < 0.05$). A comparison of the streamwise cell topography for all shear rates at the 0^{th} and 18^{th} hour is shown in Figure 5.18. Similar to the untreated glass experiments, the cell topography at 20 dyne/cm^2 exhibits properties of cells trying to achieve minimum drag formations.

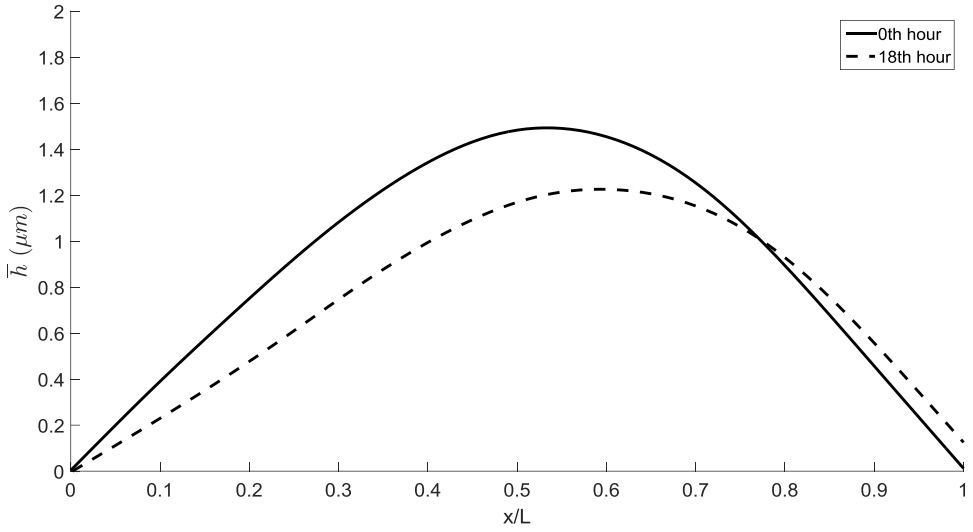

Figure 5.16: Average cell surface height variations along the normalized streamwise cell length at the 0th and 18th hour time steps for a confluent layer of endothelial cells cultured on fibronectin and subjected to a shear stress of 5 dyne/cm^2. Flow is from left to right.

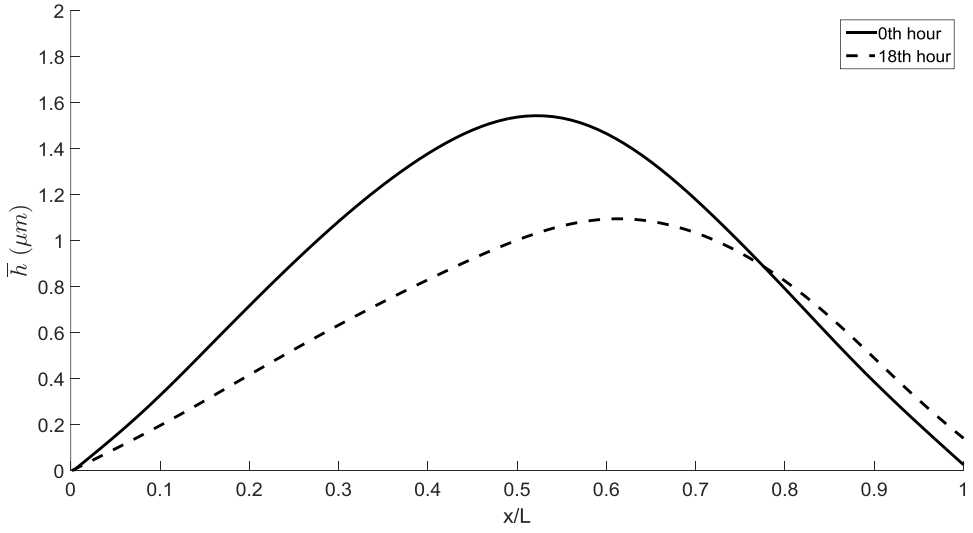

Figure 5.17: Average cell surface height variations along the normalized streamwise cell length at the 0th and 18th hour time steps for a confluent layer of endothelial cells cultured on fibronectin and subjected to a shear stress of 20 dyne/cm^2. Flow is from left to right.

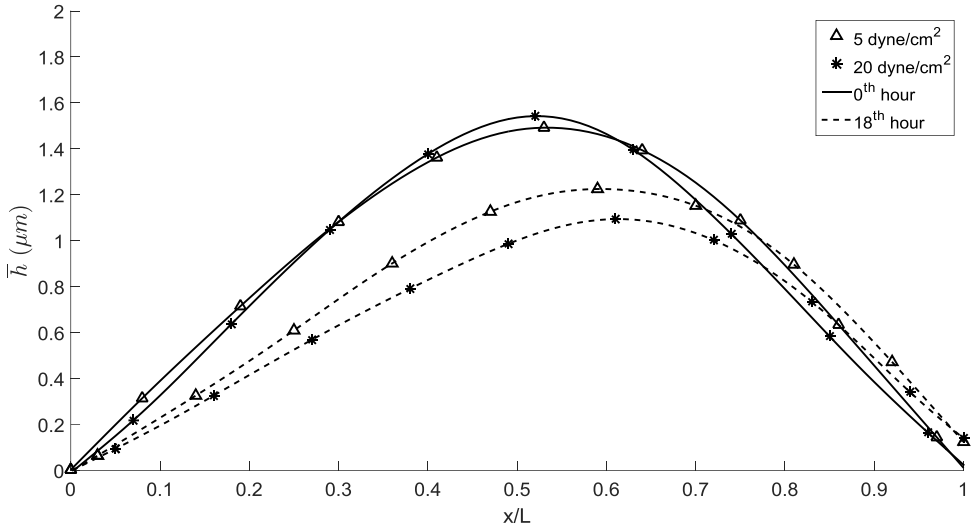

Figure 5.18: Average cell surface height variations along the normalized streamwise cell length at the 0th and 18th hour time steps for a confluent layer of endothelial cells cultured on fibronectin and subjected to shear stresses of 5 and 20 dyne/cm^2. Flow is from left to right.

5.2.2 Shear stress measurements

The key findings of the shear stress analysis for flow experiments at 5 and 20 dyne/cm^2 are shown in Figure 5.19 and Figure 5.20, respectively. These figures show the variation in the average shear stress with respect to normalized streamwise position along the cell. The streamwise cell location and the average shear stress profile were computed as described in section 4.3.6.

Using the results in Figure 5.19 and Figure 5.20, the differential of the maximum shear stress between the 0th and 18th hour time steps was computed for each flow experiment. The changes in maximum average shear stress from the 0th hour to the 18th hour time step for flow experiments at 5 and 20 dyne/cm^2 were -0.24 ± 0.2 dyne/cm^2 and -0.62 ± 0.2 dyne/cm^2, respectively. There was a statistically significant reduction in the

maximum mean shear stress after 18 hours of applied flow at 20 dyne/cm^2 ($t(28) = 2.11$, $p < 0.05$). In this regard, there was statistically significant reduction in cell height and shear stress at 20 dyne/cm^2 for cell cultures on fibronectin. However, there was not a statistically significant reduction in the maximum mean shear stress after 18 hours of applied flow at 5 dyne/cm^2.

In addition, the differential of the streamwise location of the maximum shear stress between the 0th and 18th hour time steps was computed using Figure 5.19 and Figure 5.20. The changes in the streamwise location of the maximum shear stress from the 0th hour to the 18th hour time step for flow experiments at 5 and 20 dyne/cm^2 were $+0.07 \pm 0.02$ and $+0.09 \pm 0.02$, respectively. There was a statistically significant downstream shift in the streamwise location of the maximum mean shear stress from the 0th hour to the 18th hour for applied flows at 5 dyne/cm^2 ($t(28) = 2.09$, $p < 0.05$) and 20 dyne/cm^2 ($t(28) = 3.11$, $p < 0.05$). A comparison of the streamwise shear stress variations for all shear rates at the 0th and 18th hour is shown in Figure 5.21. Furthermore, the location of the maximum shear stress was approximately centered at the location of the maximum cell height for all shear rates indicating that the shear stress was related to the streamwise cell height, as mentioned previously.

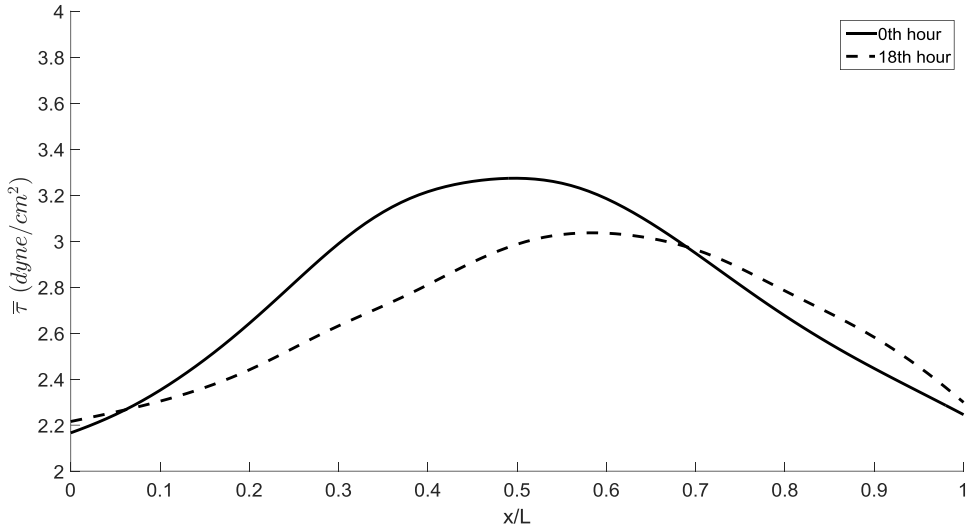

Figure 5.19: Average shear stress variations along the normalized streamwise cell length at the 0th and 18th hour time steps for a confluent layer of endothelial cells cultured on fibronectin and subjected to a shear stress of 5 dyne/cm^2. Flow is from left to right.

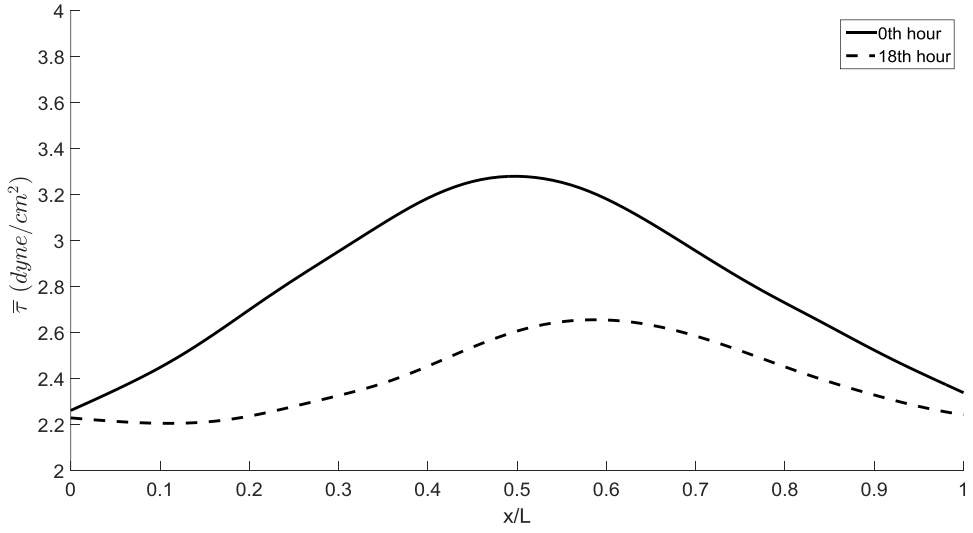

Figure 5.20: Average shear stress variations along the normalized streamwise cell length at the 0th and 18th hour time steps for a confluent layer of endothelial cells cultured on fibronectin and subjected to a shear stress of 20 dyne/cm^2. Flow is from left to right.

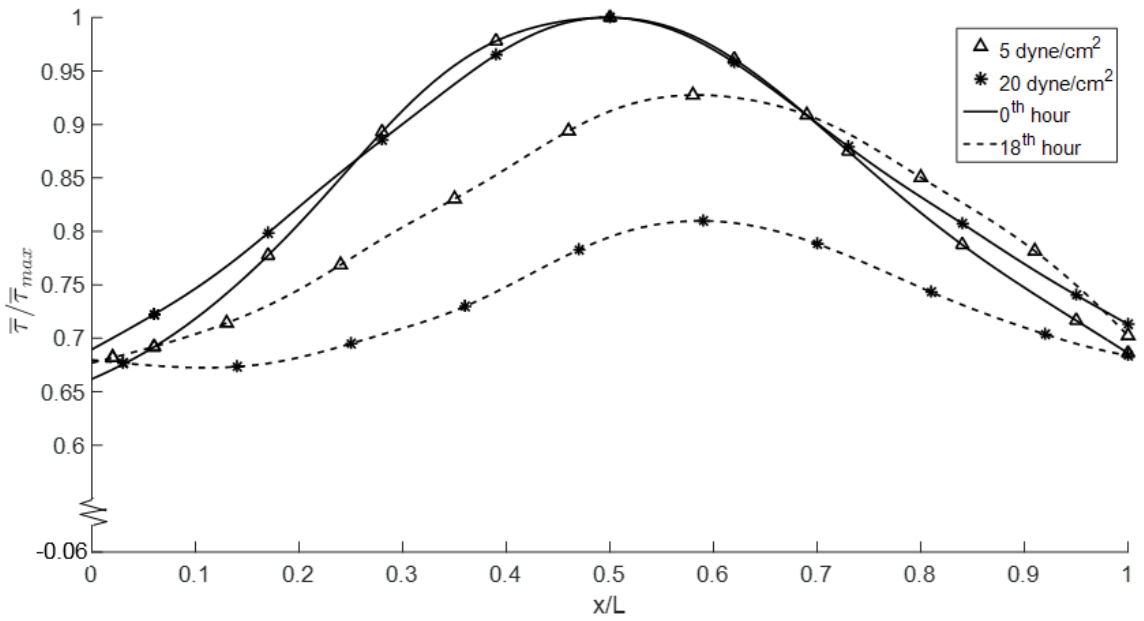

Figure 5.21: Normalized average shear stress variations along the normalized streamwise cell length at the 0th and 18th hour time steps for a confluent layer of endothelial cells cultured on fibronectin and subjected to shear stresses of 5 and 20 dyne/cm^2. Flow is from left to right.

5.2.3 Pressure measurements

The key findings of the pressure analysis for flow experiments at 5 and 20 dyne/cm^2 are shown in Figure 5.22 and Figure 5.23, respectively. These figures show the variation in the average pressure with respect to normalized streamwise position along the cell. The streamwise cell location and the average pressure variations were computed as described in section 4.3.6.

Using the results in Figure 5.22 and Figure 5.23, the differential of the maximum pressure between the 0th and 18th hour time steps was computed for each flow experiment. The changes in maximum average pressure from the 0th hour time step to the 18th hour time step for flow experiments at 5 and 20 dyne/cm^2 were -0.02 ± 0.02

dyne/cm^2 and -0.05 ± 0.02 dyne/cm^2, respectively. There was a statistically significant reduction in the maximum mean pressure after 18 hours of applied flow at 20 dyne/cm^2 ($t(28) = 2.10$, $p < 0.05$). However, there was not a statistically significant reduction in the maximum mean pressure after 18 hours of applied flow at 5 dyne/cm^2.

In addition, the differential of the streamwise location of the maximum pressure between the 0th and 18th hour time steps was computed using Figure 5.22 and Figure 5.23. The changes in the streamwise location of the maximum pressure from the 0th hour to the 18th hour time step for flow experiments at 5 and 20 dyne/cm^2 were +0.06 ± 0.02 and +0.09 ± 0.02, respectively. There was a statistically significant downstream shift in the streamwise location of the maximum mean pressure from the 0th hour to the 18th hour for applied flows at 5 dyne/cm^2 ($t(28) = 2.42$, $p < 0.05$) and 20 dyne/cm^2 ($t(28) = 3.47$, $p < 0.05$). Similar to the untreated glass experiments, the location of the maximum pressure was approximately centered at the location of the maximum cell height and the location of maximum shear stress indicating a relationship between the local shear stress, pressure, and streamwise cell height.

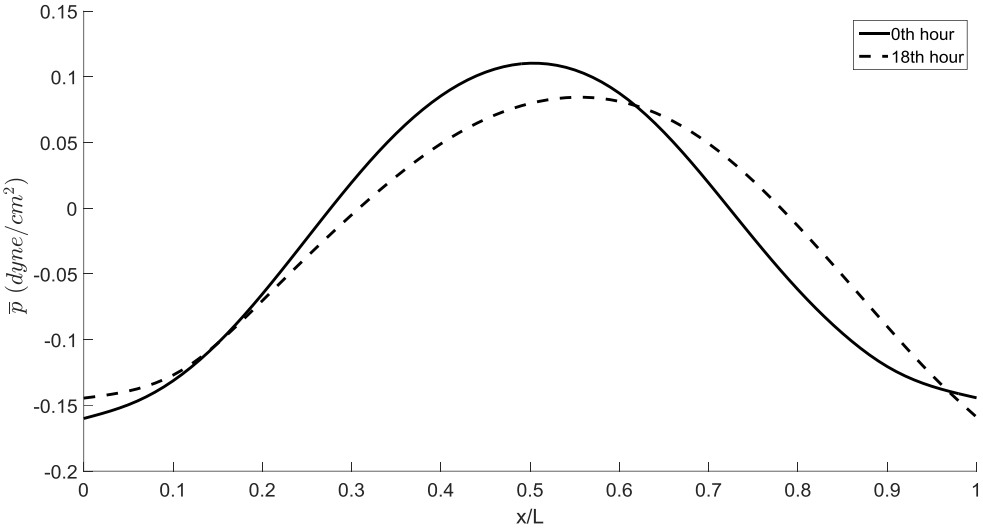

Figure 5.22: Average pressure variations along the normalized streamwise cell length at the 0th and 18th hour time steps for a confluent layer of endothelial cells cultured on fibronectin and subjected to a shear stress of 5 dyne/cm^2. Flow is from left to right.

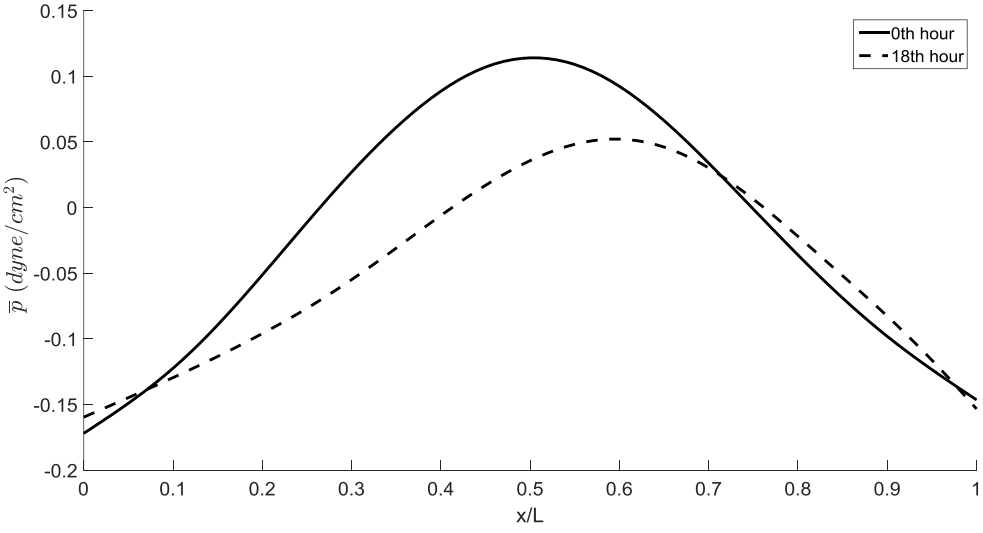

Figure 5.23: Average pressure variations along the normalized streamwise cell length at the 0th and 18th hour time steps for a confluent layer of endothelial cells cultured on fibronectin and subjected to a shear stress of 20 dyne/cm^2. Flow is from left to right.

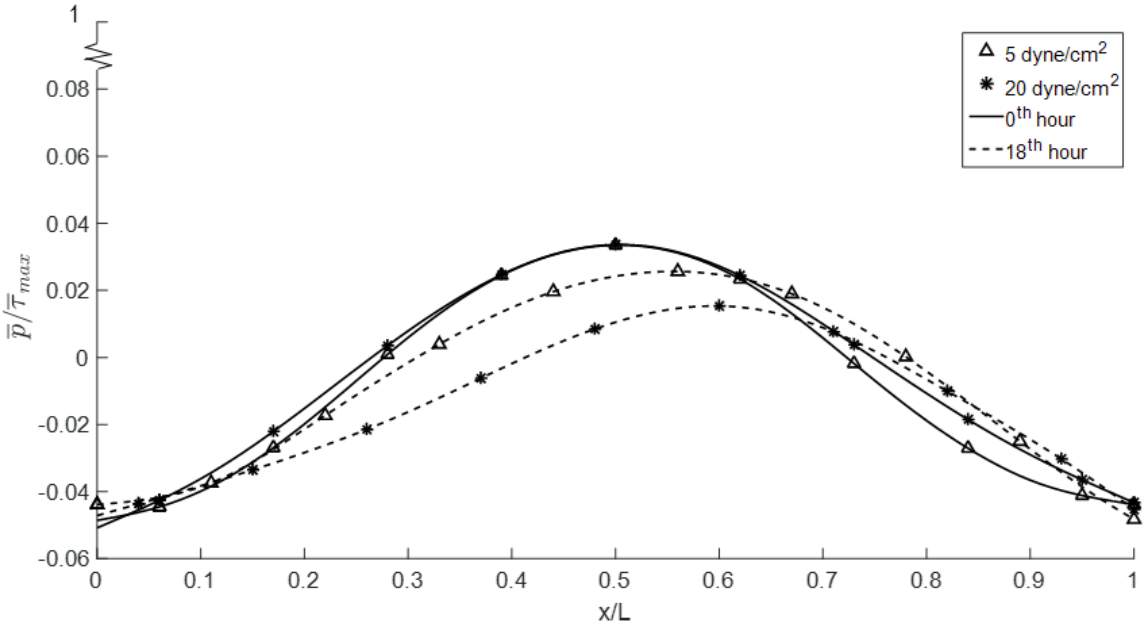

Figure 5.24: Normalized average pressure variations along the normalized streamwise cell length at the 0th and 18th hour time steps for a confluent layer of endothelial cells cultured on fibronectin and subjected to shear stresses of 5 and 20 dyne/cm^2. Flow is from left to right.

5.3 Normal cell experiments discussion

Cell surface topography, shear stress, and pressure key findings can be compared for normal endothelial cell experiments by analyzing information from the average cell height, shear stress, and pressure variations computed in sections 5.1-5.2. The change in the streamwise location of the maximum average value, $\Delta(x/L)_{max}$, and the change in the maximum value, Δmax, from the 0th hour to the 18th hour for untreated glass and fibronectin-coated experiments are shown in Table 5.1 for comparison.

For glass and fibronectin-coated experiments at 5, 10, and 20 dyne/cm^2, $(x/L)_{max}$ of topography, shear stress, and pressure variations increased after 18 hours of applied flow. However, there was only a statistically significant reduction in maximum

topography, maximum shear stress, and maximum pressure when subjected to 20 dyne/cm^2. This could indicate that the cell nucleus does not decrease its height to reduce drag until the applied shear rate is higher than 10 dyne/cm^2.

Given the statistical significance of the results, μPTV measurement is a reliable investigative tool for flow experiments over living cells. Compared to AFM, these experimental methods allow *in-situ* measurements over living cells during flow so that it is possible to observe temporal and spatial changes in cell morphology and hemodynamic forces. With that said, the relationships between the applied shear stress, cell surface topography, local shear stress, and local pressure are similar for glass and fibronectin-coated experiments. Due to the relationships between the hemodynamic forces and endothelial cell morphology found in this study, both should be quantified and taken into account while conducting living cell experiments with or without culture substrates.

Table 5.1: Cell topography, shear stress, and pressure variations comparison of the change in the normalized streamwise location of maximum value, $\Delta(x/L)_{max}$, and the change in the maximum value, Δmax, for fibronectin and non-fibronectin flow experiments on confluent endothelial cells.

	Applied shear stress	**Quantification**	$\Delta(x/L)_{max}$	Δmax
Glass	5 dyne/cm^2	Topography	+0.07	-0.23 μm
		Shear stress	+0.07	-0.30 dyne/cm^2
		Pressure	+0.07	-0.02 dyne/cm^2
	10 dyne/cm^2	Topography	+0.08	-0.36 μm
		Shear stress	+0.08	-0.48 dyne/cm^2
		Pressure	+0.08	-0.03 dyne/cm^2
	20 dyne/cm^2	Topography	+0.10	-0.45 μm
		Shear stress	+0.10	-0.61 dyne/cm^2
		Pressure	+0.10	-0.06 dyne/cm^2
Fibronectin	5 dyne/cm^2	Topography	+0.06	-0.26 μm
		Shear stress	+0.07	-0.24 dyne/cm^2
		Pressure	+0.06	-0.02 dyne/cm^2
	20 dyne/cm^2	Topography	+0.09	-0.44 μm
		Shear stress	+0.09	-0.62 dyne/cm^2
		Pressure	+0.09	-0.05 dyne/cm^2

5.4 Steady flow over necrotic endothelial cells cultured on glass

Steady flow experiments were performed on necrotic, confluent endothelial cells cultured on untreated glass. The cells were subjected to three different shear stresses (5, 10, and 20 dyne/cm^2) for 18 hours and underwent necrosis due to the working fluid having a lower pH (6.7) than desired by endothelial cells (7.4).

5.4.1 Topography measurements

Cell topography results for necrotic endothelial cell experiments were computed differently than the normal endothelial cell experiments because necrotic endothelial cells were unable to remain adhered to the microchannel and moved out of the field-of-view during the flow experiments. Therefore, measurements over specific individual cells could not be assessed during time steps. Despite cell movement, changes in cell surface topography during a flow experiment could still be observed by quantifying the cell surface heights considering the endothelial cells present in the field-of-view. The key findings of the cell surface topography analysis for necrotic flow experiments at an applied shear stress of 5, 10, and 20 dyne/cm^2 are shown in Figure 5.25, Figure 5.26, and Figure 5.27, respectively. These figures show the percent of data locations that are associated with specific cell heights considering the cell height quantifications for the entire field-of-view at the 0th hour and 18th hour time steps. The average cell surface height considering every data location is shown by a vertical line with the average height value noted.

Using the results in Figure 5.25 - Figure 5.27, the differential of the average maximum cell surface height for the field-of-view between the 0th and 18th hour time steps could be computed for each flow experiment. The change in average cell surface height from the 0th hour to the 18th hour time step for flow experiments at 5, 10, and 20 dyne/cm^2 were +0.28 ± 0.01 μm, +0.24 ± 0.01 μm, and +0.05 ± 0.01 μm, respectively. These differentials showed that the magnitude of applied shear stress is related with an increase in average cell surface height after 18 hours of applied steady flow. Notice that this is opposite for healthy endothelial cell experiments where the average maximum cell

surface height decreased after 18 hours of applied flow. These findings are consistent with previous literature indicating that cell surface height increases when cells undergo necrosis [25].

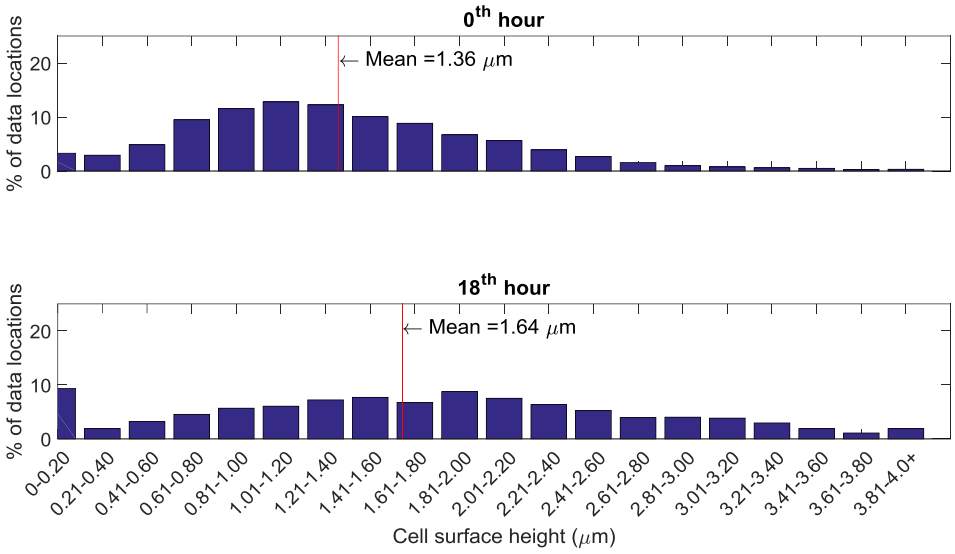

Figure 5.25: Cell surface topography results for necrotic, steady flow experiments at an applied shear stress of 5 dyne/cm^2. The percent of data locations that are associated with specific cell surface heights considering the measurements for the entire field-of-view at the 0th hour and 18th hour time steps are shown.

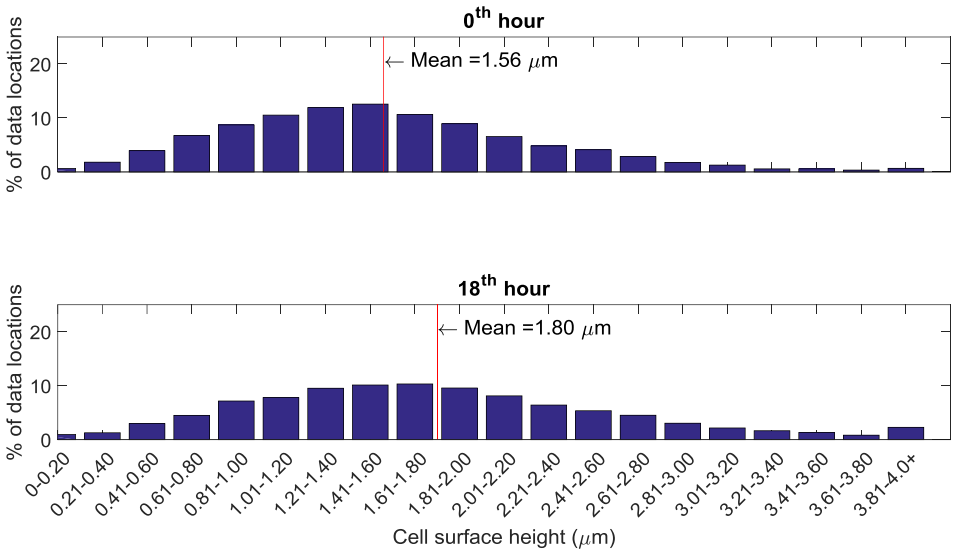

Figure 5.26: Cell surface topography results for necrotic, steady flow experiments at an applied shear stress of 10 dyne/cm^2. The percent of data locations that are associated with specific cell surface heights considering the measurements for the entire field-of-view at the 0th hour and 18th hour time steps are shown.

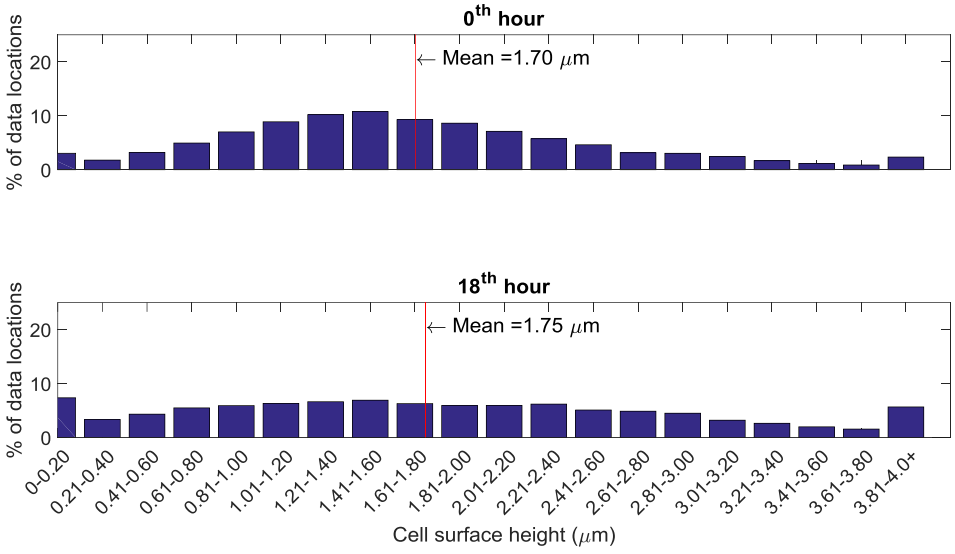

Figure 5.27: Cell surface topography results for necrotic, steady flow experiments at an applied shear stress of 20 dyne/cm^2. The percent of data locations that are associated with specific cell surface heights considering the measurements for the entire field-of-view at the 0th hour and 18th hour time steps are shown.

5.5 Cell orientation: healthy versus necrotic endothelial cells

Endothelial cell orientation was measured by implementing edge detection algorithms and analyzing region properties as discussed in section 4.3.5. Figure 5.28 shows the results of the cell orientation analysis for normal (healthy) cells and necrotic cells at the 0^{th} and 18^{th} hour time step for an applied shear stress of 20 dyne/cm^2. The orientation of each detected cell was determined by measuring the angle in degrees between the major axis with respect to the streamwise direction, or *x* direction. The angle of orientation is defined as positive in the counter-clockwise direction.

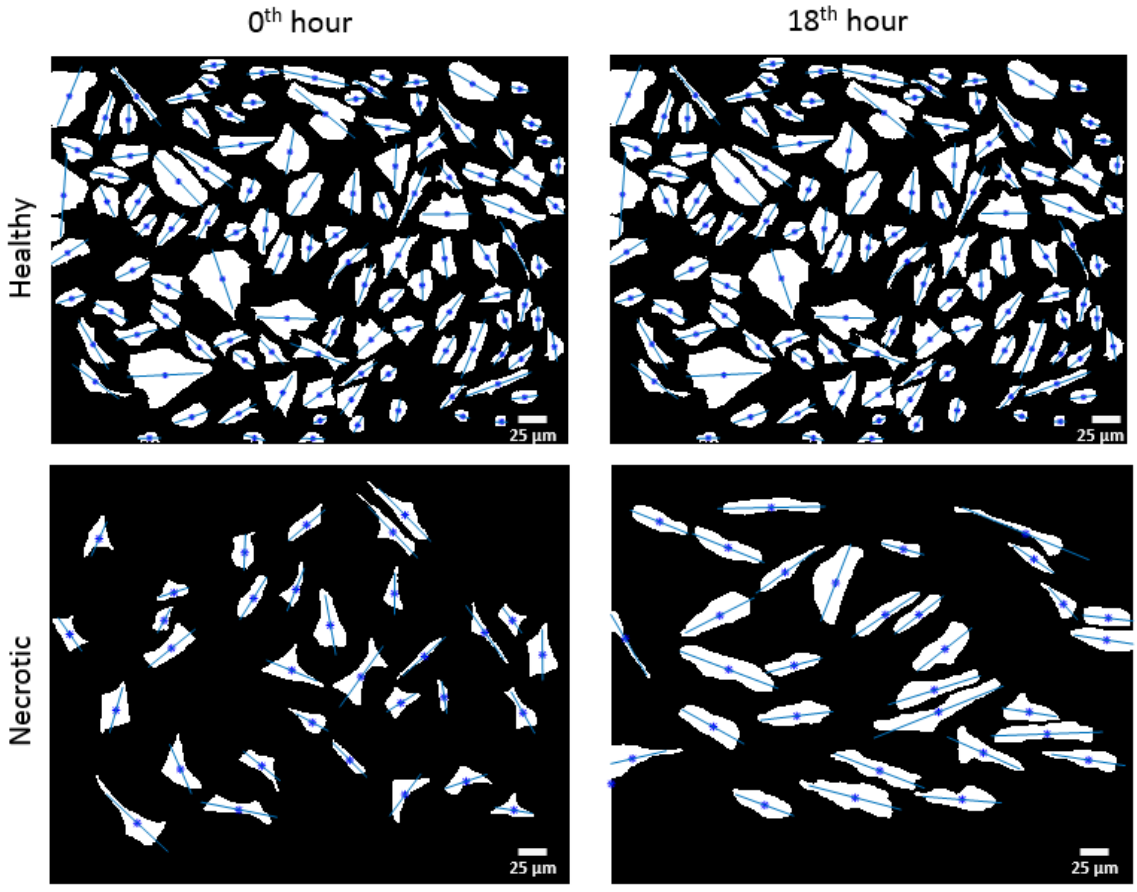

Figure 5.28: Individual cell areas detected are filled in with white and the major axis of orientation is shown in blue for healthy and necrotic endothelial cell flow experiments at the 0^{th} and 18^{th} hour time steps for an applied shear stress of 20 dyne/cm^2. Flow is from left to right.

Utilizing the results shown in Figure 5.28, the percentage of the total number of cells corresponding to specific angles of orientation for healthy and necrotic flow experiments at an applied shear stress of 20 dyne/cm^2 during the 0th and 18th hour time steps are shown in Figure 5.29 and Figure 5.30, respectively. Notice that between the 0th and 18th hour, healthy endothelial cells did not change orientation but necrotic cells shifted their position towards alignment in the streamwise direction as shown in Figure 5.30. It should be noted that since necrotic endothelial cells did not stay in the field-of-view during the experiment, it is possible that only cells directed in the streamwise direction remained purely due to the applied flow not forcing those cells out of the field-of-view. Although the average cell heights for necrotic endothelial cells found in this study provide some insight into their behavior, future experiments analyzing individual cells could provide more detailed information regarding morphological changes due to an applied shear stress.

In addition to the alignment of necrotic cells, the cell alignment of healthy cells found in this study was contrary to several studies that found healthy endothelial cells align with the flow direction when subjected to comparable shear rates [32, 43, 44]. Although, it should be noted that not all studies observed in literature have been consistent in their findings on the behavior of bovine aortic endothelial cells under shear flow. Certain studies have indicated a change in cell orientation starting at 3 hours while other studies did not observe a change in cell morphology after 24 hours of applied flow [37, 58, 59]. For this study, it is unknown why the cells did not align with the flow direction. For this reason, it would be beneficial to fluorescently tag focal adhesion sites so that we can better understand cell motility in future studies. Despite this, the

orientation of healthy and necrotic endothelial cells can be effectively measured using μPTV experimental methods and provides further information regarding the cell morphology of varying cellular conditions present in cardiovascular diseases.

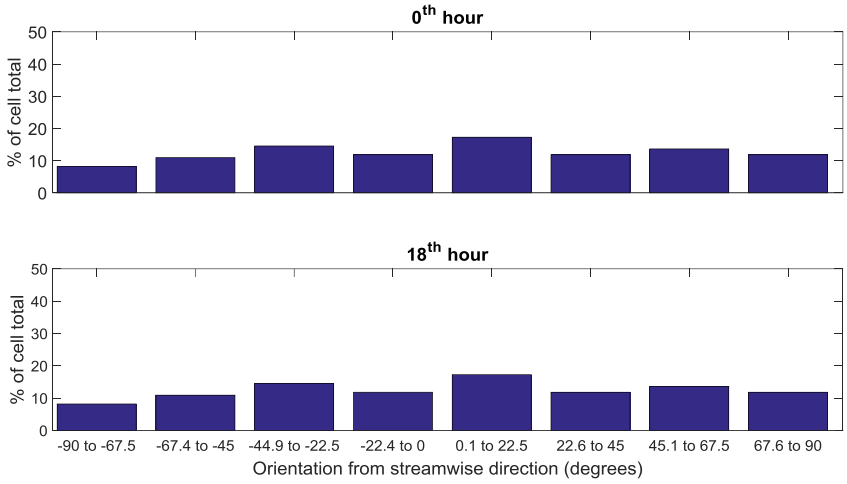

Figure 5.29: Cell orientation results for healthy, steady flow experiments at an applied shear stress of 20 dyne/cm^2. Results show the percentage of the total number of cells corresponding to specific angles of orientation for the 0th and 18th hour time steps. Angles are in degrees and defined between the major axis with respect to the streamwise direction, or *x* direction. The orientation is defined as positive in the counter-clockwise direction.

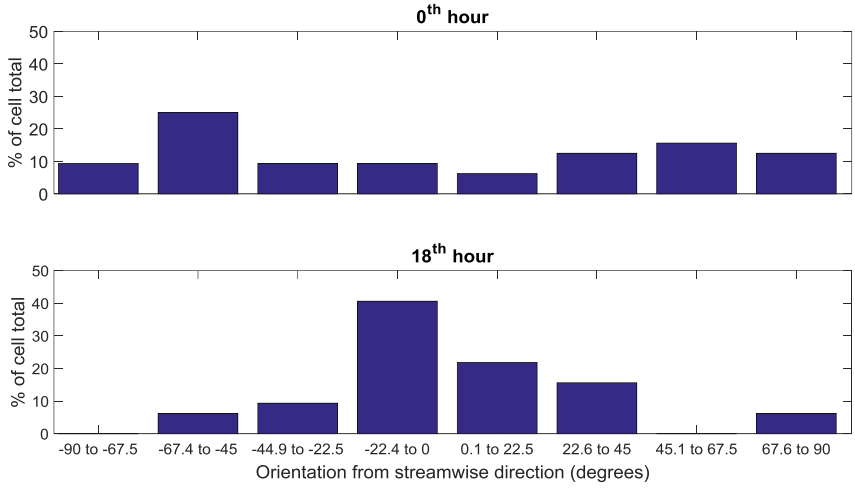

Figure 5.30: Cell orientation results for necrotic, steady flow experiments at an applied shear stress of 20 dyne/cm^2. Results show the percentage of the total number of cells corresponding to specific angles of orientation for the 0th and 18th hour time steps. Angles are in degrees and defined between the major axis with respect to the streamwise direction, or *x* direction. The orientation is defined as positive in the counter-clockwise direction.

CHAPTER 6

CONCLUSIONS

In this study, cell topography, shear stress, and/or pressure quantifications were made for normal endothelial cells cultured on glass, normal endothelial cells cultured on fibronectin, and necrotic endothelial cells cultured on glass. The findings made from these quantifications are summarized as,

1. There was a statistically significant reduction in the maximum mean cell height, shear stress, and pressure after 18 hours of applied flow at 20 dyne/cm^2 for cells cultured on untreated glass and fibronectin.
2. There was a statistically significant downstream shift in the streamwise location of the maximum mean cell height, shear stress, and pressure from the 0th hour to the 18th hour for applied flows at 5, 10, and 20 dyne/cm^2.
3. Cell orientation does not change after 18 hours of applied steady flow for normal endothelial cells cultured on glass or fibronectin while subjected to an applied shear rate of 5, 10, or 20 dyne/cm^2.

From the findings in this study, the major conclusions are summarized as,

1. This study demonstrated the ability to make *in-situ* quantifications of fluid forces and endothelial mechanics using μPTV techniques and fluid mechanics principles.
2. There is a three-dimensional change in cell morphology as a result of applied shear stress.
3. Cell morphology is directly related to local variations in fluid loading, *i.e.*, shear stress and pressure.

Furthermore, these experiments demonstrated that μPTV is a promising technique for *in-situ* quantification of fluid forces and endothelial mechanics for varying endothelium conditions. With this technique, future experiments introducing pulsatile flow, LDL, and fluorescence microscopy can investigate different stages of atherosclerosis while simultaneously quantifying the mechanical and biological responses of endothelial cells.

REFERENCES

[1] "Cardiovascular Disease Statistics," Johns Hopkins Medicine, 2015. [Online]. Available: http://www.hopkinsmedicine.org/healthlibrary/conditions/cardiovascular_diseases/cardiovascular_disease_statistics_85,P00243/. [Accessed 8 March 2016].

[2] D. McDonald, Blood Flow in Arteries, London: Edward Arnold, 1960.

[3] "Disease Statistics," National Heart, Lung, and Blood Institute, 2012.

[4] Merriam-Webster Dictionary, Springfield: Merriam-Webster, 2000.

[5] "Atherosclerosis," NHS Choices, 2014. [Online]. Available: http://www.nhs.uk/conditions/atherosclerosis/Pages/Introduction.aspx. [Accessed March 2016].

[6] M. DeBakey, G. Lawrie and D. Glaeser, "Patterns of atherosclerosis and their surgical significance," *Annals of Surgery*, vol. 201, pp. 115-131, 1985.

[7] D. Ku, D. Giddens, C. Zarins and S. Glagov, "Pulsatile flow and atherosclerosis in the human carotid bifurcation: positive correlation between plaque location and low and oscillating shear stress," *Arteriosclerosis*, vol. 5, pp. 293-302, 1985.

[8] J. Tarbell, "Mass transport in arteries and the localization of atherosclerosis," *Annu Rev Biomed Eng*, pp. 79-118, 2003.

[9] C. Caro, "Discovery of the Role of Wall Shear in Atherosclerosis," *Arterio, Thromb, and Vasc Bio,* vol. 29, pp. 158-161, 2009.

[10] L. Cancel, A. Fitting and J. Tarbell, "In vitro study of LDL transport under pressurized (convective) conditions," *Am J Phsiol Heart Circ Physiol,* pp. H126-H132, 2007.

[11] U. Olgac, V. Kurtcuoglu and D. Poulikakos, "Computational modeling of coupled blood-wall mass transport of LDL: effects of local shear stress," *Am J Physiol Heart Circ Physiol.,* vol. 294, no. 2, pp. H909-H919, 14 December 2007.

[12] N. Sun, N. B. Wood, A. D. Hughes, S. Thom and X. Xu, "Effects of transmural pressure and wall shear stress on LDL accumulation in the arterial wall: a numerical study using a multilayered model," *Am J Physiol Hear Circ Physiol,* pp. 292: H3148-H3157, 2007.

[13] J. M. Tarbell, "Shear stress and the endothelial transport barrier," *Cardio Res,* pp. 320-330, 2010.

[14] N. Yang and K. Vafai, "Modeling of low-density lipoprotein (LDL) transport in the artery - effects of hypertension," *Int J Heat Mass Transf,* pp. 49: 850-867, 2006.

[15] L. Nielson, "Transfer of low-density lipoproteins (LDL) transport in the artery - effects of hypertension," *Atherosclerosis,* vol. 123, pp. 1-15, 1996.

[16] R. Ross, "Atherosclerosis - An Inflammatory Disease," *New England J Med,* vol. 340, pp. 115-126, 1999.

[17] S. Roll, J. Müller-Nordhorn, T. Keil, H. Scholz, D. Eidt, W. Greiner and S. Willich, "Dacron vs. PTFE as Bypass Materials in Peripheral Vascular Surgery -- Systematic Review and Meta-analysis," Medscape, 2009.

[18] H. Tamai, P. Berger, Tsuchikane, "Frequency and time course of reocclusion and restenosis in coronary artery occlusions after balloon angioplasty versus Wiktor stent implantation: results from the Mayo-Japan Investigation for Chronic Total Occlusion (MAJIC) trial.," *Am Heart J,* vol. 3, no. 147, p. E9, 2004.

[19] S. Greenwald and C. Berry, "Improving vascular grafts: the importance of mechanical and hemodynamic properties," *J Pathol,* vol. 190, pp. 292-299, 2000.

[20] T. Salam, A. Lumsden, W. Suggs and D. Ku, "Low shear stress promotes intimal hyperplasia thickening," *J Vasc Invest,* vol. 2, no. 1, pp. 12-22, 1996.

[21] D. Wootton and D. Ku, "Fluid mechanics of vascular systems, diseases, and thrombosis," *Annu Rev Biomed Eng'g,* vol. 1, pp. 299-329, 1999.

[22] S. Glagov, C. Zarins, D. Giddens and D. Ku, "Hemodynamics and atherosclerosis: insights and perspectives gained from studies of human arteries," *Arch Pathol Lab Med,* vol. 112, pp. 1018-1031, 1988.

[23] J. Tarbell, Z. Shi, J. Dunn and H. Jo, "Fluid Mechanics, Arterial Disease, and Gene Expression," *Annu Rev Fluid Mech,* vol. 46, pp. 591-614, 2014.

[24] J. Tarbell, "Wallace H. Coulter Laboratory," 2016. [Online]. Available: http://bme.ccny.cuny.edu/faculty/jtarbell/SMC%20images.htm. [Accessed August 2014].

[25] C. M. Leong, "In Vitro Measurements of Flow Over Endothelial Cells," ProQuest, Ann Arbor, 2008.

[26] J. Humphrey, Cardiovascular Solid Mechanics, New York: Springer-Verlag, 2002.

[27] P. Davies, "Flow-mediated endothelial mechanotransduction," *Physiol Rev,* vol. 75, pp. 519-560, 1995.

[28] R. Satcher, S. Bussolari, M. Gimbrone Jr. and C. Dewey Jr., "The distribution of fluid forces on model arterial endothelium using computational fluid dynamics," *J Biomech Eng,* vol. 114, no. 3, pp. 309-316, 1992.

[29] K. Barbee, T. Mundel, R. Lal and Davies, "Subcellular distribution of shear stress at the surface of flow-aligned and nonaligned endothelial monolayers," *Am J Physiol,* vol. 268, pp. H1765-H1772, 1995.

[30] P. Wache, X. Wang, G. Maurice, M. Lucius and J. Stoltz, "Numerical computation of mechanical deformation of a modeled endothelial cell," *C R Acad Sci Paris, Serie II b, Biomechanique,* vol. 328, no. 8, pp. 633-638, 2000.

[31] A. Vorhees, G. Nackman and T. Wei, "Experiments show importance of flow-induced pressure on endothelial cell shape and alignment," *Proc Royal Soc A,* vol. 463, pp. 1409-1419, 2007.

[32] J. Flaherty, J. Pierce, V. Ferrans, D. Patel, W. Tucker and D. Fry, "Endothelial nuclear patterns in the canine arterial tree with particular reference to hemodynamic events," *Circ Res,* vol. 30, pp. 23-33, 1972.

[33] R. Neren, M. Levesque and J. Cornhill, "Vascular endothelial morphology as an indicator of the pattern of blood flow," *J Biomech Eng,* vol. 103, pp. 172-176, 1981.

[34] C. Dewey Jr., S. Bussolari, M. Gimbrone Jr. and P. Davies, "The dynamic response of vascular endothelial cells to fluid shear stress," *J Biomech Eng,* vol. 103, pp. 177-185, 1981.

[35] M. Sato, M. Levesque and R. Merem, "Micropipette aspiration of cultured bovine aortic endothelial cells exposed to shear stress," *Arteriosclerosis,* vol. 3, no. 7, pp. 276-86, 1987.

[36] A. Malek and S. Izumo, "Mechanism of endothelial cell shape change and cytoskeletal remodeling in response to fluid shear stress," *Journal of Cell Science,* vol. 109, pp. 713-726, 1996.

[37] C. Galbraith, R. Skalak and S. Chien, "Shear stress induces spatial reorganization of the endothelial cell cytoskeleton," *Cell Motil Cytoskeleton,* vol. 40, no. 4, pp. 317-330, 1998.

[38] P. Davies, A. Remuzzi, E. Gordon, C. Dewey Jr. and M. Gimbrone Jr., "Turbulent fluid shear stress induces vascular endothelial cell turnover in vitro," *Proc Natl Acad Sci,* vol. 83, no. 7, pp. 2114-2117, 1986.

[39] G. Helmlinger, R. Geiger, S. Schreck and R. Nerem, "Effects of pulsatile flow on cultured vascular endothelial cell morphology," *J Biomech Eng*, vol. 113, pp. 123-131, 1991.

[40] S. Liu and Y. Fung, "Dependence of arterial remodeling on locally altered blood pressure," *ASMA Bioengineering Division,* vol. 29, pp. 59-60, 1995.

[41] S. Liu, M. Yen and Y. Fung, "On measuring the third dimension of cultured endothelial cells in shear flow," *Proc Natl Acad Sci,* vol. 19, no. 91, pp. 8782-8786, 1994.

[42] P. Davies, K. Barbee, M. Volin, A. Robotewskyj, J. Chen, L. Joseph, M. Griem, M. Wernick, E. Jacobs, C. Polacek, N. DePaola and A. Barakat, "Spatial

relationships in early signaling events of flow-mediated endothelial mechanotransduction," *Annu Rev Physiol,* vol. 59, pp. 527-549, 1997.

[43] K. Barbee, P. Davies and R. Lal, "Shear stress-induced reorganization of the surface topography of living endothelial cells imaged by atomic force microscopy," *Circ Res,* vol. 74, pp. 163-171, 1994.

[44] K. Barbee, T. Mundel, R. Lal and P. Davies, "Subcellular distribution of shear stress at the surface of slow-aligned and nonaligned endothelial monolayers," *Am J Physiol,* vol. 268, pp. H1765-H1772, 1995.

[45] S. Liu, M. Yen and Y. Fung, "On measuring the third dimension of cultured endothelial cells in shear flow," *Proc Natl Acad Sci,* vol. 91, no. 19, pp. 8782-8786, 1994.

[46] Fluxion Biosciences Inc., *BioFlux 1000z User Guide,* San Francisco, CA.

[47] Nikon, "Depth of Field and Depth of Focus," [Online]. Available: http://www.microscopyu.com/articles/formulas/formulasfielddepth.html. [Accessed 24 March 2016].

[48] B. M. Gumbiner, "Cell Adhesion: The Molecular Basis of Tissue Architecture and Morphogenesis," *Cell Press,* vol. 84, no. 3, pp. 345-357, 2000.

[49] C. Baquey, Biomechanical Transport Processes, New York City: Springer, 2014.

[50] J. Westerweel, "Efficient detection of spurious vectors in particle image velocimetry data," *Experimental Fluids,* vol. 16, pp. 236-247, 1994.

[51] K. Barbee, P. Davies and R. Lal, "Shear stress-induced reorganization of the surface topography of living endothelial cells imaged by atomic force microscopy," *Circulation Research,* vol. 1, pp. 163-71, Jan 1994.

[52] J. Dabiri, S. Bose, B. Gemmel, S. Colin and J. Costello, "An algorithm to estimate unsteady and quasi-steady pressure fields from velocity field measurements," *J Experimental Biology,* vol. 217, pp. 331-336, 2014.

[53] T. Ohashi, H. Sugawara, T. Matsumoto and M. Sato, "Surface topography measurement and intracellular stress analysis of cultured endothelial cells exposed to fluid shear stress," *JSME,* vol. 43, no. 4, pp. 780-786, 2000.

[54] M. Sato, K. Nagayama, N. Kataoka, M. Sasaki and K. Hane, "Local Mechanical Properties Measured by Atomic Force Microscopy for Cultured Endothelial Cells Exposed to Shear Stress," *J. Biomech,* vol. 33, pp. 127-135, 2000.

[55] C. Chung and B. Min, Fluid dynamic effects on endothelial cell morphology, Sapporo: Hokkaido University, 1998, p. 170.

[56] A. Hazel and T. Pedley, "Vascular endothelial cells minimize the total force on their nuclei," *Biophys. J.,* vol. 78, pp. 47-54, 2000.

[57] T. Pham, S. Maenz, C. Ludecke, C. Schmerbauch, U. Settmacher, K. Jandt, J. Bossert and J. Zanow, "Quantitative characterization of endothelial cell

morphologies depending on shear stress in different blood vessels of domestic pigs using a focused ion beam and high resolution scanning electron microscopy (FIB-SEM)," *Tissue and Cell,* vol. 47, no. 2, pp. 205-212, 2015.

[58] M. Levesque and R. Nerem, "The elongation and orientation of cultured endothelial cells in response to shear stress," *J Biomech Eng,* vol. 107, no. 4, pp. 341-347, 1985.

[59] A. Malek and S. Izumo, "Mechanism of endothelial cell shape change and cytoskeletal remodeling in response to fluid shear stress," *J Cell Sci,* vol. 109, pp. 713-726, 1996.

[60] P. Davies, T. Mundel and K. Barbee, "A mechanism for heterogeneous endothelial responses to flow in vivo and in vitro," *J. Biomechanics,* vol. 28, pp. 1553-1560, 1995.

[61] S. Liu, M. Yen and Y. Fung, "On measuring the third dimension of cultured endothelial cells in shear flow," *Proc. Natl. Acad. Sci.,* vol. 91, no. 19, pp. 8782-8786, 1994.

APPENDIX A

CELL CULTURE AND EQUIPMENT PROTOCOL

All experiments require cell culturing before and after cell insertion into the microchannel. This section details the steps to culture endothelial cells and set up equipment for flow experiment.

A.1 Culturing BAOEC's

The first step in preparation for the experiment is to culture bovine aortic endothelial cells.

A.1.1 Materials

- Endothelial basal media with growth factors
- Culturing solutions
- 70% isopropanol

A.1.2 Equipment

- Laminar fume hood
- CO_2 incubator at 37°C
- Water bath at 37°C
- Pipettes
- Marker pen
- Tissue culture (TC) dishes
- Sterile gloves

A.1.3 Procedure

1. If cells are frozen, it will take about 10 days to thaw and culture before they are ready.
2. A detailed protocol for culturing, sub-culturing, counting, and cryopreserving endothelial cells can be found in [25].
3. Culture 4 x (100 x 20) mm culture dishes of BAOEC's to confluency.
4. Remove endothelial basal media (EBM) and culturing solutions from fridge. Warm to room temperature. Use a warming bath if needed.
5. Take 4 x (100 x 20) mm culture dishes from incubator.
6. Aspirate EBM.
7. Add 2-3 mL of HBSS (PBS).
8. Aspirate PBS.
9. Add 2.5-3 mL of Trypsin.
10. Incubate until cells detach from tissue culture (TC) dish – no longer than 3 minutes. Do not tap on plate or disturb cells – this could affect their viability! Check TC dish on microscope to see that cells are no longer attached to TC dish.
11. Add 7-8 mL of TNS or media. Draw in and out with pipette then put into 15 mL vial.
12. Centrifuge at 200 g for 5 minutes. Make sure to balance weight in centrifuge.
13. Put 6 mL of EBM each into 4 - 100 x 20 mm TC dishes. Label dishes with Name, Date, and Cell type.
14. Take vial from centrifuge and see that pellet has formed on the bottom. Aspirate solution from vial without aspirating the cells.

15. Add 12 mL of EBM to vial and draw EBM in and out with pipette to ensure mixing.
16. Put 4 mL into each of the 4 TC dishes previously prepared with EBM.
17. Incubate for ~3 days or until 4 x (100 x 20mm) TC dishes (55 cm^2 surface area) of cells are ~100% confluent.

A.2 Coating microchannels (Day #1)

A.2.1 Materials

- Endothelial basal media with growth factors
- Culturing solutions
- 70% isopropanol
- Fibronectin

A.2.2 Equipment

- Laminar fume hood
- CO_2 incubator at 37°C
- Water bath at 37°C
- Pipettes
- BioFlux™ system
- Sterile gloves

A.2.3 Procedure

1. Take culturing solutions out of fridge (EBM, HBSS, trypsin, TNS, and D-PBS) and put on counter to warm.

2. Put 10 mL of EBM in a vial and 8 mL D-PBS in a vial. Warm solutions briefly by swirling in water bath.
3. Check confluency of cells in tissue culture dishes. Note down confluency.
4. Turn BioFlux™ computer on. Turn on all power switches on BioFlux™ equipment.
5. Attach 24-well place pressure interface to the BioFlux™ pump.
6. Select "Manual" and then select "EBM" from the "Fluid" drop down menu of the BioFlux™ software.
7. Turn microscope bulb on by clicking "Multi-dimensional Acquisition" in the BioFlux™ software and then raising the "Wavelength" to 2 and then clicking between "TRITC" and "Brightfield" options.
8. Use 24-well plate. Place plastic cover that comes with plate over one-half of plate if only using one-half of plate.
9. Add 0.3 mL of EBM to each outlet well of interest to prime channels.
10. Disinfect pressure interface by wiping with 70% isopropyl.
11. Run system from outlet to inlet well at 3-5 dynes/cm^2 for 3 minutes.
12. Aspirate excess solution in inlet and outlet wells to innermost punch out. Always aspirate inner wells with 200 µL pipette.
13. Make 1.250 mL of 100 µg/mL fibronectin solution by combining 1.125 mL D-PBS and 125 µL of 1 mg/mL fibronectin. Mix thoroughly. DO NOT AGITATE. Store solution at 2-6 ºC in dark. (This is enough solution for 8 channels.)
14. Add 150 µL of fibronectin solution to each outlet well of interest.

15. Run system with flow from outlet well to inlet well at 2-3 dynes/cm^2 until outer punch-out of inlet well is almost filled.
16. Place plate in laminar flow hood and let fibronectin adhere to channel for 1 hour.
17. After 1 hour, put culturing solutions in water bath.
18. Aspirate fibronectin solution from outlet and inlet wells.
19. Fill each aspirated outlet well with 0.5 mL of D-PBS (warmed).
20. Run BioFlux™ system with flow from outlet well to inlet well at 5 dynes/cm^2 for 10 minutes.
21. Bring plate to incubator and then continue to preparing cells steps in the subsequent section.

A.3 Preparing and counting cells (Day #1)

A.3.1 Materials

- Endothelial basal media with growth factors
- 70% isopropanol
- Trypan blue

A.3.2 Equipment

- Laminar fume hood
- Water bath at 37°C
- Pipettes
- Tissue culture dishes
- Sterile gloves

- Countess

A.3.3 Procedure

1. Using centrifuge, spin down 3 x 100% confluent 100 x 20 mm dishes at 200 g for 5 minutes. (Save 4th dish in case more cells are needed in channels and also to reseed cells in new dishes.)
2. Re-suspend each dish in 330 µL of EBM. If plate isn't confluent, use less media. Use a 1000 µL pipette when re-suspending so that cells are not damaged by smaller pipettes. 3 TC dishes is enough for 1 x BioFlux™ plate and, if no 4th TC dish, use about 80 µL for splitting cells into 3 TC dishes for future experiments.
3. If needed, re-seed 20 µL of 200 µL cell suspension in 2-3 new tissue culture dishes (for future experiments).
4. Draw 20 µL of re-suspended cells/EBM solution and combine with 20 µL of Trypan blue. Inject the 40 µL mixture into cell counter slide and use the Countess cell counter to count cells. Should be >7.6 x 10^6 cells/mL.
5. Note cell concentration & viability.
6. If the cell concentration is not high enough, spin down cells again and re-suspend the cells in less EBM and recount.
7. Bring the re-suspended solution to the BioFlux™ system. Make sure the cell solution is mixed thoroughly and cells have been counted.

A.4 Seeding endothelial cells in the BioFlux™ plate (Day #1)

A.4.1 Materials

- Endothelial basal media with growth factors

- Culturing solutions
- 70% isopropanol
- BioFlux™ plate

A.4.2 Equipment

- Laminar fume hood
- CO_2 incubator at 37°C
- Water bath at 37°C
- Pipettes
- Tissue culture dishes
- Sterile gloves
- BioFlux™ system

A.4.3 Procedure

1. Tip BioFlux™ plate slightly and slowly aspirate D-PBS from the outer part of each outlet well with 200 µL pipette.
2. We are trying to balance the amount liquid in the inlet/outlet wells before the cells are introduced: put 50 µL of media in each of the inlet wells. There will be 100 µL of cell solution in the outlet well.
3. Swirl tip around inner punch out of BioFlux™ plate to ensure no bubbles have accumulated.
4. Ensure cells are mixed in vial using 1 mL pipette. Add 100 µL of cell suspension into each outlet well of interest. Again, swirl tip to ensure no bubbles are on the bottom of the well.

5. Turn on BioFlux™ at 2 dyne/cm^2 for 3-5 seconds to bring cells into channels (*pumping outlet well to inlet well*).
6. Incubate the plate for 2 hours at 37°C in 5.0% CO_2 to allow the cells to adhere to the channel.
7. Defrost a vial of FBS, and prepare CO_2 independent media (For 1 channel (4 days' worth), need 16+ mL of media total (8 mL CO_2 independent media and 8 mL EBM). See below for supplemental amounts:
    - ~8 mL CO_2 independent media =6.91 mL CO_2 independent media + 181 µL GlutaMax + 908 µL FBS
    - ~32 mL CO_2 independent media =27.6 mL CO_2 independent media + 724 µL GlutaMax + 3.63 mL FBS
    - ~48 mL CO_2 independent media =41.4 mL CO_2 independent media + 1.09 mL Unscrew lid of CO_2 independent media vial slightly, and put in incubator to warm.
8. Check the cells in the BioFlux™ plate after 2 hours to see how they are adhering.
9. Take image of cells for reference.
10. Slowly aspirate excess cell media in outlet wells. Add 2 mL of fresh media solution (50% CO_2 independent media/50% EBM) to each inlet well.
11. Optional: apply small amount of shear to inlet wells to ensure the initiation of gravity flow.
12. Incubate BioFlux™ plate with cells for 24 hours.

A.5 Checking for confluency and replenishing media (Day #2-5)

A.5.1 Materials

- Endothelial basal media with growth factors
- CO_2 independent media solution
- 70% isopropanol
- Microscope

A.5.2 Equipment

- Laminar fume hood
- CO_2 incubator at 37°C
- Water bath at 37°C
- Pipettes
- Marker pen
- Tissue culture dishes
- Sterile gloves

A.5.3 Procedure

1. Warm EBM in incubator with cap unscrewed so media is pre-conditioned with CO_2.
2. Bring BioFlux™ plate with cells to microscope.
3. Check for confluency. If close to 100% confluent, proceed to next section.
4. If not confluent, take pictures of channels, aspirate media in wells and replenish each inlet well with fresh 2mL of 50% CO_2 independent media/50% EBM solution and continue to incubate for another 24 hours.

5. Check to make sure gravity flow is occurring by observing that liquid from the inlet wells made it to the outlet well.

A.6 Experiment day (100% confluency reached)

A.6.1 Materials

- Endothelial basal media with growth factors
- 70% isopropanol
- Fluorescent particles (1 μm diameter)

A.6.2 Equipment

- Laminar fume hood
- CO_2 incubator at 37°C
- Water bath at 37°C
- Pipettes
- Tissue culture dishes
- Sterile gloves
- >1 TB WD Hard Drive for data
- MIRO M310 camera
- Laptop for camera & data acquisition
- BioFlux™ system

A.6.3 Procedure

1. Defrost FBS.

2. Prepare CO_2 independent media. Start out by making 48 mL of this solution. (Each inlet well holds 3 mL). See below for supplemental amounts:
    - ~48 mL CO_2 independent media =41.4 mL CO_2 independent media + 1.09 mL GlutaMax + 5.45 mL FBS
3. Warm CO_2 independent media solution in water bath at 37°C. Do not warm in incubator as this could cause the pH to change.
4. Turn on BioFlux™ camera, equipment, & computer.
5. Select "Manual" mode and "EBM" selection in BioFlux™ software.
6. Switch to 10X objective. Switch to filter 1 on microscope.
7. Be sure the correct 24-well pressure interface is attached and outlet tubing is attached to the pressure interface and draining to a waste container.
8. Retrieve BioFlux™ plate with cells from incubator.
9. Disinfect pressure interface by wiping with 70% isopropyl.
10. Place BioFlux™ plate on stage with pressure interface for stability when moving stage.
11. Set the origin for the BioFlux™ system at the center of the "0" above channel 1. See BioFlux™ manual for more detailed instructions.
12. Use a piece of paper to mark the horizontal & vertical position of the screen. Use this for future reference when setting the origin as a check.
13. Save several locations in the BioFlux™ system that look suitable for data collection (with respect to the origin).
14. Note down 2 locations for data acquisition.

15. Take pictures of each of these locations with the BioFlux™ camera. Use screenshot if necessary. *Do this with 10x and 20x objectives.
16. Bring BioFlux™ plate back to incubator. Always disinfect BioFlux™ plate's lid before placing back on plate.
17. Set up Miro M310 camera, computer, and hard drive for data collection. (See subsequent section)
18. Switch to 40X objective. Be sure correction ring of microscope objective is on 0.18.
19. Retrieve seeding particles with gloves and thoroughly roll bottle of seeding particles (1 µm diam.) to ensure particles do not clump.
20. Mix 15 mL of particle/CO_2 independent media solution in a separate vial. (Always use a seeding concentration of 1 drop of particles/3 mL of media). Swirl thoroughly (do not agitate) to ensure mixing particles.
21. In fume hood, add 3 mL of particle solution to one inlet well for each channel and 3 mL of non-particle solution to the other inlet well. Note down which well has which solution. **Each well can only run for 2.88 hours with 3 mL volumes at 10 dynes/cm^2 and only 1.44 hours while running at 20 dynes/cm^2*.
22. NOTE: If running two different shear stresses on opposite sides of the plate, add particle solution to opposite inlet wells.
23. After adding solution to wells, check to see if there are any bubbles in the punch-out of the wells. Carefully move a pipette tip around the walls of the inner punch-out of the inlet wells to remove any bubbles.
24. Disinfect pressure interface and place BioFlux™ plate on stage.

25. Select the origin for the BioFlux™ system on the software.
26. Click CSR on camera software.
27. Take a picture of the cells at each saved location for topography reference. Remember, only 1 location can be used for data because the cells cannot be under the microscope light for long periods of time.

A.7 Data acquisition

A.7.1 Materials

- 70% isopropanol

A.7.2 Equipment

- MIRO M310 camera
- Laptop for camera & data acquisition
- BioFlux™ system
- >1 TB WD Hard Drive for data
- Sterile gloves

A.7.3 Procedure

1. Input correct gain (~5) in camera software and place light intensity at 40% of maximum.
2. Click first saved location for data collection and use the middle of the image to focus your z-plane.
3. Click CSR on camera software before taking a picture.
4. Run BioFlux™ at 1 dyne/cm^2 and introduce non-particle media first.

5. After a few seconds, introduce particles at 1 dyne/cm^2.
6. Turn off the flow in the non-particle channel.
7. Check seeding density and adjust particle density if needed.
8. Focus z-position for first plane and note down position. Be sure to focus the z-plane AFTER turning the particle flow on in case the plate shifts when switching pumps.
9. Take data at each z-position needed.
10. Recalibrate z-location every time in order to ensure the objective is focusing on the bottom of the channel. Do this by bringing the focal plane below the bottom of the channel and then move upwards to the top of the channel.
11. Turn off microscope lamp and room light when able. Put napkin over side of plate not in use while taking data in order to block light.
12. After first recording, increase shear by 2.25 dyne/cm^2 every 30 seconds until applied shear of interest is reached.
13. Take data at a 3 dyne/cm^2 to allow longer exposure times and thus lower intensity light.
14. Change out media every 2 hours & 40 minutes (max) while running at 10 dyne/cm^2, every 1 hour & 20 minutes while running at 20 dyne/cm^2, and 5 hours & 20 minutes while running at 5 dyne/cm^2 (linear relationship for other shear rates).

A.8 Setting up the MIRO M310 camera for data acquisition

A.8.1 Equipment

- MIRO M310 camera
- Laptop for camera & data acquisition
- BioFlux™ system
- >1 TB WD Hard Drive for data
- Sterile gloves

A.8.2 Procedure

1. Turn on camera computer.
2. Connect the Ethernet cable and power cord to the camera.
3. Turn the camera's switch to "ON".
4. Open the PCC 2.2 software on the computer.
5. Click "Live" tab, then select the camera for use on the drop down menu: 13130.
6. Find the flow channel of interest using the Nikon Ti-S Microscope and 40X objective.
7. Adjust the camera so the channel walls are horizontal on the image shown on the PCC 2.2 display. Use a resolution of 960 x 720.
8. Use the microscope focus to the find what is possibly the bottom of the channel. Note the coordinates from the BioFlux™ system for this position and the resolution of the microscope.
9. Open the "Cine Settings" tab on the right to specify settings.
10. Push CSR – take a current session reference. If image is yellow, right click on area of the image that you know is white and click "White balance".

11. Continue to define settings under “Cine Settings”:
    - Image Range & Trigger Pos.: Drag all the way to the left (green bar). If drag cursor to the left (green bar), all images will be taken after clicking “Trigger”. If drag cursor to the right (red bar), then the number of images taken before clicking “Trigger” will be saved.
12. Open “Advanced Settings” tab to further define settings:
    - Don’t click exposure in PIV
    - Burst count: 2 (for image pairs in PIV)
    - Burst Period: Δt within an image pair
13. Take Data: Click “Capture”, and then click “Trigger”. (Blinking red light means the camera is recording.)
14. Go to “Play” after recording. Verify images are satisfactory for PIV (particle displacement, density, lighting, etc.). Go to “Play Speed & Options” tab to adjust playback. Click “Play each image” for best playback.
15. Click “Save”, then “Save as Cine Raw” (this is faster than tiffs). Make sure to only save 1-6000 images or it will save the total amount of images in the camera’s memory. Do not add the border data at this time.

A.9 To convert cines to TIFFS:

A.9.1 Equipment

- Laptop for camera & data acquisition
- >1 TB WD Hard Drive for data

A.9.2 Procedure

1. Open PCC 2.2 program.
2. Click icon on top left screen with label “Batch Convert Files”.
3. Open .cine file of your choice.
4. Click on “Play” tab and identify which image number is the first image of the pair for saving and then click “Save cine” at bottom.
5. Click save as “TIFF”. Bit depth: 48.
6. Click “User Defined” from “Mark in, Mark out” drop down menu – specify number of images to save depending on first image of pair (ex: 1-2000)
7. Click image borders and specify all the data to be displayed on image: absolute time, image number, exposure, burst period, etc.)
8. Then specify the file name as “image_+5” (this specifies number of digits after underscore). Be sure no previous settings have changed once this is typed.
9. Save to hard drive.